OROGRAPHIC PRECIPITATION: A MESOSCALE MODELING PERSPECTIVE

John M. Papineau

Roger A. Pielke Sr., Adviser
NSF Grant No. ATM-9306754

Colorado State University

DEPARTMENT OF ATMOSPHERIC SCIENCE

PAPER NO. 658

OROGRAPHIC PRECIPITATION: A MESOSCALE MODELING PERSPECTIVE

John M. Papineau

Department of Atmospheric Science
Colorado State University
Fort Collins, Colorado
Summer 1998

Atmospheric Science Paper No. 658

ABSTRACT

OROGRAPHIC PRECIPITATION: A MESOSCALE MODELING PERSPECTIVE

This study demonstrates the utility of the Regional Atmospheric Modeling System (RAMS) in analyzing the distribution of precipitation along Alaska's Kenai Peninsula during the September 19-21, 1995 heavy precipitation and flood event. The model generated heavy precipitation over the coastal mountains, with lighter amounts at both lower elevations and to the lee of the windward barrier. The model precipitation was in reasonably good agreement with the limited set of observations.

Included in this study are series of simulations that are designed to test the models sensitivity to initial values of wind speed, wind direction, moisture, and atmospheric stability. The results show that the areal and vertical distribution of model generated precipitation is quite sensitive to realistic perturbations in the initial fields, primarily as a result of the change in the vertical velocity structure of the model atmosphere.

It is apparent that since most mountainous regions are also data sparse, initializing a model is a serious challenge. Large uncertainty in initial conditions as well as the highly non-linear nature of the precipitation process, necessitates an ensemble approach to quantitative precipitation forecasting (QPF). Using 15 six hour model simulations an ensemble QPF is generated. The results indicate an order of magnitude variance in precipitation over the mountains, using perturbations that are within observational uncertainty.

Since mesoscale models have adjustable grids, it is important to understand the relationship between grid interval, terrain resolution and model generated precipitation.

Findings from this study suggest that as the grid interval decreases from 15 km to 10 km, precipitation increased by 33%. A further decrease in grid interval from 10 km to 5 km increased precipitation by an additional 26%. This grid interval dependency is in part due to changes in terrain height and slope angles in conjunction with the increased density of grid points. This dependency is also a function of energy propagation across a finite-difference grid.

John M. Papineau
Department of Atmospheric Science
Colorado State University
Fort Collins, Colorado 80523
Summer 1998

ACKNOWLEDGMENTS

I would like to express my gratitude to my advisor Dr. Roger Pielke Sr. for his direction and support of this study, also to my committee members: Drs. William Cotton, Richard Johnson, Tom Mckee, and Jorge Ramirez. There is no way in the world I could have finished this modeling experiment without the help of many past and present students and researchers in the Pielke and Cotton groups at CSU. Many thanks to Dr. Ligia Bernardet, Tom Chase, Dr. Pier Luigi Vidale, Joe Eastman, and Drs Glen Liston, Peter Olsson, Jerry Harrington, Jason Nachamkin, Robert Walko. I also had the support of the office staff who tracked down miscellaneous journal articles and performed various mundane tasks for me: Dallas McDonald, Tara Pielke, and James Cizek. Major credit to my wife Judy who supported me through much of my college life and who did not give up on me in the lean years. I also want to give acknowledgment to the fruitful discussions on various topics of mountain meteorology while climbing, skiing and backpacking with both John Forsythe and Chris Cochran. Thanks to the Alaska Region of the National Weather Service for the use of their computer resources.

TABLE OF CONTENTS

LIST OF FIGURES

LIST OF TABLES

Chapter 1

LITERATURE REVIEW

1.1-Introduction

For over a hundred years scientists have been observing and studying the distribution of precipitation in mountainous terrain (Barry 1992). Much of this early work took place in the Alps and Britain, but during the second-half of the 20th century many of the Earth's large mountain ranges have been the site of some type of orographic precipitation investigation ALPEX (Hantel *et al* 1984), PYREX (Georgelin *et al* 1994), SALPEX (Wratt *et al* 1996). Before the advent of computers, there were a number of analytical studies that focused on the dynamics of airflow in mountainous terrain (Scorer 1949, 1953, Long 1953), specifically on the generation of mountain waves in a stratified atmosphere. From these studies the complex nature of airflow in and around elevated topography was evident, however their application to orographic precipitation was limited due to the exclusion of microphysics. Over the past 30 years numerical models have allowed researchers to explore the problem to a greater extent, essentially linking dynamics with microphysics.

As a result of all this work, a number of points regarding orographic precipitation are widely accepted:

1. Precipitation increases with altitude to some height (varies from storm to storm), then decreases at higher elevations, (more in summer than winter). This represents a coupling between dynamics which supplies the moisture and the microphysics which determines the type and local distribution of the precipitation (Barry 1992, Alpert 1986).

2. Climatic zone (continental versus maritime), season (Summer versus Winter), terrain configuration (isolated mountain versus multiple peaks and valleys), storm type, as well as

mountain height and slope; determine the nature of orographic precipitation (Rauber 1992, Katzfey 1995, Barry 1992).

3. In cases where moist thermal convection is **not** important, precipitation is enhanced over mountainous terrain. Some type of synoptic or mesoscale disturbance advects moisture into the area (Pedgley 1970, Browning 1980, Hill *et al* 1981).

4. Terrain induced gravity waves (mountain waves), potential instability, movement of frontal zones, and blocking dictate the amount and areal distribution of precipitation (Hobbs *et al* 1975, Browning 1980, Bruintjes *et al* 1994).

Despite advances in our understanding of orographic precipitation in recent years, there are still a number of gaps in that understanding. One of the primary challenges in mountain meteorology in general is the lack of observed data. In most mountainous regions meteorological instruments are co-located with places of human habitation which of course tend to be in valley bottoms, hence there is a serious lack of data at higher elevations. Data void regions create two problems. The first is that it makes the initialization of numerical models difficult at best, and secondly, it limits the verification of not only model output but also that of radar and satellite data, causing the modeler and operational meteorologist to work in a vacuum. It is these same data void mountains that are of the greatest hydrologic interest in both the short term (flash floods) and the long term (storage in the form of snow and ice).

Some of the topics that need to be addressed with regard to stratiform precipitation are:

* What are the controlling parameters on the vertical and horizontal distribution of precipitation in complex terrain?
* What is the scale of interaction: How important is local topography (fine scale) in determining the distribution of precipitation? On the one hand there are studies that show that small isolated hills or fine-scale features enhance precipitation (Bergeron 1960, Alpert and Shafir 1991), while other researchers (Pedgley 1970, Dore *et al* 1992) suggest that precipitation patterns do not closely follow fine-scale topography.
* What are the limitations and sensitivities of numerical models to heavy precipitation events?

There are a number of reviews on the subject of airflow in mountainous terrain (Smith 1979,1989), cloud dynamics and microphysical processes (Cotton & Anthes 1989, Banta 1990), as well as mountain weather and climate (Barry 1992).

A number of different atmospheric processes have been identified as mechanisms for the generation or enhancement of orographic precipitation. Smith (1982,1989) identifies a number of these processes: 1) Smooth forced ascent; 2) Bergeron: seeder-feeder cloud system; 3) Diurnally forced convection; 4) Potential instability; 5) Differential advection. Of course, nature operates across a spectrum of processes, in essence, blurring the dividing lines between classification of the various processes. In fact, several of the aforementioned processes probably operate in conjunction with each other.

Smooth forced ascent is the classic textbook example of orographic precipitation, however, as Smith (1989) points out, with typical wind speeds of 10 m s^{-1} to 30 m s^{-1}, the time for a parcel of lifted air to travel up and over a mountain barrier is much less than the time for the formation of hydrometeors, according to traditional microphysics theory. Banta (1990) suggests that for the case of warm-rain processes, there is some mounting evidence that the formation of precipitation in some orographic clouds occurs faster than current theory predicts. This is an area of ongoing research, and if it is ever verified, may be limited to a small subset of orographic flows (i.e. marine tropical systems). The majority of orographic precipitation events recorded in the literature (Hill *et al* 1981, Katzfey 1995), are associated with wide-spread precipitation that interacts with steep terrain and becomes enhanced. For most cases, it is likely that smooth forced ascent works in concert with other processes.

Bergeron in 1960 suggested a conceptual model of orographic precipitation that expands the smooth forced ascent concept. In this model there are two cloud layers, the first is the low-level cloud that forms due to upslope flow (feeder cloud), the mid-level cloud generally forms upstream or above the low-level cloud and produces *seeder* hydrometeors which when they fall through the *feeder* cloud grow at an accelerated rate. It has been traditionally thought that seeder clouds form independently of any terrain effects, and are a result of synpotic or mesoscale instabilities. Although more recently (Smith 1989) it has

been recognized that the seeder clouds may be influenced by downstream terrain.

Diurnally forced convection can, of course, occur in most climate regimes, and over regions with a wide spectrum of surface characteristics. Mountains act as elevated heat sources, especially in drier mid-latitude climates. Thermals produced over the higher slopes are important source regions for thunderstorm development. Even though thermals are generated over steep terrain, hydrometeor formation and any subsequent precipitation maybe independent of the terrain.

According to Smith (1979), a controversy was initiated when Bonacina (1945) suggested that intense orographic rain is the result of potential instability being released. Douglas and Glasspoole (1947) countered with evidence from a number of heavy rain events that occurred over Britain, suggesting that simple orographic lifting of conditionally stable air could account for the observed precipitation rates, without relying on potential instability. In the following years a number of studies using both observations and models came out in support of each process. There has been no clear defeat of either mechanism, since both can be valid under the proper atmospheric conditions.

Smith (1982) proposed a type of mountain blocking scenario he called differential advection. In this model the blocking of low-level air by a mountain causes approaching cold air to override warm air, in turn producing an unstable layer upstream of the mountain. It is thought that the small-scale embedded convection might enhance precipitation upstream of the mountain and on its windward slopes. There is some observational evidence (Hobbs *et al* 1975, Marwitz 1980) that supports this model, how often it occurs and to what extent it enhances precipitation is not well known.

This review consists of three parts: 1. An overview of dynamical processes in or around complex terrain, including gravity waves, blocking and potential instability. 2. Observations of orographic precipitation 3. Modeling of orographic precipitation by two and three dimensional models.

1.2-Dynamics of airflow in complex terrain

Gravity Waves: There is an extensive body of literature on the subject of terrain forced gravity waves (i.e. mountain waves), Smith (1979) and Durran (1986) provide comprehensive overviews, with Clark & Peltier (1977), Klemp & Lilly (1978), Pierrehumbert (1984), Olafsson & Bougeault (1996) providing numerical modeling results, while Baines and Hoinka (1985) use the results from a wave tank to provide insight into this problem.

In a stable atmosphere two types of gravity waves can be generated: 1. Evanescent waves: whose amplitude decays exponentially with height; and, 2. Propagating waves that move vertically without loss of amplitude. The criteria that determines whether a wave is evanescent or propagating is the relation of the horizontal wave number (**k**) to the Scorer Parameter ($\mathbf{L}=[\mathbf{N}^2/\mathbf{U}^2]^{1/2}$). Since the Scorer Parameter is a function of the atmospheric stability and wind speed, a number of complicated wave structures are possible. For both types of waves there is a certain amount of upstream lifting as the flow approaches the barrier; this, of course, is important to the formation of orographic clouds and the possible enhancement of precipitation over mountainous terrain.

In the propagating wave case, lines of constant phase tilt upstream relative to the barrier because the frequency of the terrain forcing (**uk**, where **u** is the mean wind in a layer) is less than the natural frequency of the atmospheric oscillations ($\mathbf{uk}<\mathbf{N}$, where **N** is often referred to as the Brunt-Vaisalla frequency). For linear waves the relation: $\mathbf{uk}=\mathbf{N}\cos\phi$ determines the angle which the phase lines tilt from the vertical. Relative to the air stream, wave energy propagates upstream but is advected to the lee of the barrier by the mean wind. Relative to the barrier, the wave propagates vertically and downstream (Smith 1979).

Downstream of the barrier gravity waves can: 1. Create a series of updraft-downdraft couplets. 2. Steepen and form a region of wave breaking which usually leads to strong downslope winds. 3. Form trapped lee waves. In general, these lee-side waves produce areas in the lower and mid-atmosphere of descending motion, which increases evaporation and often creates a precipitation shadow. There is some scale dependency to these processes, hills or small mountains exert less forcing on gravity wave generation than large mountains for the

same atmospheric conditions. In addition to the dynamic effects, precipitation formed upwind of the crest of a hill or small mountain may be advected downstream, so that a precipitation maximum occurs on the crest or to the lee of the crest. Bruintjes *et al* (1994) point out that the downdraft regions of gravity waves can transport hydrometeors that are created aloft, down to lower regions where they may coalesce or aggregate with hydrometeors that were formed at lower levels.

Blocking:

Blocking is another upstream effect that is critical to the creation of clouds and precipitation. The most frequently used indicator for the onset of blocking is the Froude Number, which is defined in this study as: $\mathbf{Fr=u/Nh}$ where **h** is the height of the barrier. For high Froude Numbers ($\mathbf{Fr} > 1.5$-2.0), air is unrestricted in its path up and over a barrier. As the Froude Number decreases, according to Pierrehumbert & Wyman (1985), an upstream propagating disturbance causes a deceleration of low-level flow that is approaching the barrier. In this case a large percentage of the low-level flow is diverted horizontally around the barrier. In extreme cases, the flow reaches a stagnation point, where flow reversal can occur (Olafsson & Bougeault 1996). The flow above the blocked layer is diverted upward and if it impinges on the barrier, it creates vertically propagating gravity waves.

A number of studies have found different values of **Fr** for the onset of blocked flow. Using a wave tank with a radiative upper boundary, Baines & Hoinka (1985) found that stagnation occurred when $\mathbf{Fr}=0.5$, and the depth of the blocked layer was $0.5\mathbf{h}$. However, columnar wave motions were observed to propagate upstream and start the deceleration process when $\mathbf{Fr}<2.0$. Using a numerical model, Pierrhumbert & Wyman (1985) found the onset of columnar waves for $\mathbf{Fr}=1.3$, with upstream stagnation occurring at $\mathbf{Fr}=0.7$. They suggest that upstream blocking is somehow linked to wave breaking over the crest/lee of the barrier.

Smolarkiewicz & Rotunno (1990) found that the aspect ratio (β) of the barrier plays an important role in blocking. When $\beta \leq 1$ stagnation occurs first at the surface and is caused by the piling up of cooler higher density air. When $\beta \rightarrow \infty$ stagnation first occurs aloft, and is

thought to be due to the upstream propagation of columnar disturbances that are generated by wave breaking over the crest of the barrier. The authors suggest that these two processes are distinct but complementary ways of creating upstream stagnation.

Mayr and Mckee (1995) found from their study of 47 Winter blocking events in Western Colorado, that synoptic cross-barrier pressure gradients can at times negate any mountain induced blocking. They also suggest that radiation effects, namely the growth of the daytime boundary layer due to morning heating, can cause mid-level air to mix down into the blocked region creating an unblocked situation. At night, as the surface radiatively cools, the depth of the boundary layer decreases, allowing blocking to re-establish itself.

Using Bernoulli's equation as a starting point, Smith (1990) has shown that the pressure gradient between a point over a windward slope and a point far upstream at the same elevation, is critical to blocking. The pressure at the point over the slope is higher than the point upstream because of lifting above the slope creates cooler, higher density air. This replaces the earlier interpretation that blocked flow could not move up and over a barrier because the kinetic energy of the flow was less than the potential energy needed to cross the barrier. Smith's results agree with those of Smolarkiewicz and Rotunno's (1990) that the onset of stagnation is a function of the barrier's aspect ratio. Essentially deceleration results from increasing pressure along a streamline which in turn is caused by the lifting and cooling of the inflow air.

Blocking is critical to the areal distribution of precipitation because the presence of a low-level pool of cold air can enhance upstream condensation (Peterson *et al* 1991, Wesley 1991). This enhancement may or may not lead to an increase in precipitation on the windward slopes or over the barrier itself. Peterson *et al* (1991) investigated winter snowfall in the Yampa River Valley of NW Colorado, and found that the presence of a cold pool upstream of the barrier enhanced snowfall upstream of the barrier and on the windward slopes. They attribute this to the upstream lifting of moist air as it rides up and over the nose of the cold pool. For the two storms that they analyzed in detail, the cold pool acted as an extension of the mountain barrier.

Wesley (1991) studied a series of winter precipitation events along Colorado's Front Range and found that in cases where a deep cold pool was entrenched at the base of the Front Range, that areas of heavy precipitation *could* occur well upstream of the barrier. It appeared that cloud bands were forming along the eastern edge of the cold pool and were responsible for the large snowfalls in the eastern plains.

These last two examples illustrate the complexity of precipitation in or around steep terrain. It is possible that the difference whether precipitation falls out well upstream of the barrier or is enhanced upstream as well as over the barrier is due to the stability of the atmosphere above the cold pool. In the case of cloud bands, when the lapse rate is near neutral, some type of localized instability seems to be involved, while a more stable lapse rate may suggest a classical smooth forced ascent of the moist inflow.

The influence of cold pools located downstream of a barrier can be significant on wind patterns and precipitation as suggested by Lee *et al* (1989). In their modeling work they show that a cold pool located to the lee of a barrier acts as an extension of the barrier. The horizontal wind maximum shifted from the lee of the barrier when there is no cold pool, to the barrier crest when a cold pool was in place. It is not exactly clear how the precipitation would respond to this dynamic change, but it is possible that precipitation processes over the crest and to the lee of the crest would be enhanced as vertical velocities increase in response to the shift in the horizontal wind maximum.

Potential Instability:

If a layer of air is characterized by $\mathbf{d\theta e/dz < 0}$ it is considered potentially unstable. If this layer undergoes forced lifting then this instability may be realized and cumuliform clouds will form. In this hypothetical layer the upper sections, by definition, have to be drier than the lower sections during lifting. The upper section cools at the dry adiabatic lapse rate, hence is colder than the lower section, which has been cooling at the moist adiabatic lapse rate (once it reaches saturation). This most often occurs when an inversion is forced to ascend. Banta (1990) gives the example of stratus or orographic stratus being forced up the slope of a

mountain resulting in the formation of convective cloud elements embedded in a layer of stratus.

The role which potential instability (**P.I.**) plays in orographic precipitation still remains vague after a number of decades of speculation. Douglas and Glasspoole (1947) suggest it is at best a subsidiary factor, and would only be important if it occurred over a "deep layer". In the 1970's a number of field programs in Wales and SW England began to identify **P.I.** signatures in a number of heavy precipitation events (Browning *et al* 1974, Browning 1980, Hill *et al* 1981). Both radar and rawinsonde data indicated that **P.I.** was being released in some cases 100 km upstream of the first barrier, while still out over the North Atlantic. In several well documented cases by Browning *et al* (1974), **P.I.** occurred at both low and mid-levels. The exact role that **P.I.** plays in the enhancement of orographic precipitation is still not clear, but it seems to be able to precondition low-level flow by increasing the condensation rate and at mid-levels it could generate a larger number of seeder hydrometeors (Hill *et al* 1981).

The presence of convective clouds in orographic storms where thermal convection played no role is well documented (Marwitz 1980, Parsons and Hobbs 1983, Wratt et al 1996). However, besides thermal forcing and **P.I.**, a number of other mechanisms can lead to the formation of convective clouds, particularly the formation of a convergence zone upstream of a barrier and frontal lifting (Hobbs *et al* 1975). Wratt *et al* (1996) note that embedded convection has been observed by radar for a number of precipitation events along the west coast of New Zealand's South Island, which the authors attribute to the release of potential instability. Katzfey (1995b) in his modeling of three storms that occurred over the Southern Alps, concludes that for at least the cases he worked with that the overall contribution of convective precipitation was minor.

1.3-Observations

For as much as has been written about orographic precipitation, there is a general lack of published studies on the vertical and areal distribution of precipitation for individual storms, especially in the larger mountain ranges. Much of the data for individual events comes from

Wales or Southwestern England (Browning 1980, Hill *et al* 1981), however, data from the Alps and Rockies (Hjermstad 1970), is in large part based on seasonal or annual precipitation patterns. There has been some work of this nature in the Himalayas, but it deals with the highly convective monsoon season (Ageta 1976, Higuchi *et al* 1982). Barry (1992) gives the most extensive review on the subject, and from his synopsis it is apparent that the climatic regime plays a significant part in the vertical and areal distribution of orographic of precipitation. This is especially true for maritime versus continental ranges, and for tropical versus mid-latitude. It can be difficult to discern what processes apply to a given mountain range. Rauber (1991) notes that microphysical processes differ substantially between continental mountains and coastal ranges. During winter events, the latter experience more ice multiplication by rime-splintering.

Hills and small mountains:

Browning (1980) and Hill *et al* (1981) summarize observations of heavy rain events in Southern Wales and SW England. The terrain rises from sea-level to about 600 m, and could best be described as hilly. The salient points of their work are:

* More than 80% of orographic enhancement took place in the lowest 1.5 km above the terrain.
* Potential instability was common at both mid-levels and at low-levels.
* Heavy rain events were always associated with low-level winds in excess of 20 m s^{-1}, and occurred in the warm sectors of extratropical cyclones.
* The majority of these events occurred in the winter (Nov-Feb) when moisture levels were lower than during the summer, but the wind speeds were considerably higher.
* Pre-existing background rain was almost always present
* There was evidence that the areal distribution of rainfall was insensitive to small scale variations in the topography, since high rainfall rates were also measured in narrow valleys.
* Observational evidence supports the Bergeron seeder-feeder mechanism.

Passarelli and Boehme (1983) studied a number of storms over New England and concluded that even shallow orographic clouds (500 m) could account for the 20-60% increase in measured rain between the 300-500 m high hills and the coastal plains.

Larger Mountains:

In Alaska there is little historical or real time weather/climate data from stations above 1000 m, however there have been several climatological precipitation studies. Miller (1963) using data collected in the 1940's through the early 1960's, suggested that the warming trend which occurred in Southeast Alaska, caused a 400 m rise in the zone of maximum snowfall on the Juneau Icefield. Marcus and Ragle (1970) found that the annual snow accumulation in a transect across the St Elias Range, was a maximum at the relatively low elevation of 1800 m. They also found that accumulation at higher elevations was unrelated to precipitation anomalies at the Gulf of Alaska coastal town of Yakutat.

The Southern Alps of New Zealand have been the site of some comprehensive precipitation studies over the past several years. The Southern Alps is a steep maritime range that rises to 3700 m over distances of less than 70 km from the coastline. There are numerous peaks above 2500 m. Wratt et al (1996) have observed: 1. During heavy precipitation events, mountain waves are generated which produce strong lee-side surface winds. 2. Radar returns show embedded convection in many storms, and that there is strong low-level growth in the precipitation rate in the lowest 500 m of the atmosphere. Katzfey (1995a) found that for the three case studies he modeled, low-level jets with winds stronger than 20 m s^{-1} were the norm.

Henderson (1993) looked at a series of raingages that form a west to east transect across the Southern Alps. He first investigated 30 years worth of annual mean precipitation data which showed that the peak rainfall occurred some 10-20 km *upstream* of the ridge crest. Then he looked at individual heavy rain events and found that the pattern was almost identical to the 30 year totals. The result is a bit surprising, one might expect that the long term ensemble average might alter the pattern because it represents contributions from a full spectrum of storm types. It indicates just how strong the terrain forcing can be.

There is overwhelming evidence that Bergeron's seeder-feeder mechanism is valid. It probably does not operate in the text book fashion of two separate cloud entities, however the concept that an upper level cloud produces small hydrometeors that fall through a lower level cloud and washout moisture is well observed. What has been in question is whether the seeder cloud is in anyway enhanced or "affected" by the upstream topography. Browning (1980) suggested that the seeder cloud forms independently of the terrain downstream of it, usually by baroclinic ascent or potential instability. However, Bradley (1985) using a two-dimensional (2D) numerical model suggests that the upstream gravity wave induced by the terrain has some effect on the seeder cloud.

There has been a considerable amount of work in the Pacific Northwest with regard to the influence of orography on the modification of frontal rainbands (Hobbs *et al* 1975, Parsons and Hobbs 1983). The investigators found that rainbands moving onshore are modified in a variety of ways, depending on the width of the frontal zone and whether the rainbands are pre-frontal or post-frontal. The channeling of low-level from the south (generally drier air), has an important effect on the amount of precipitation that is received over the foothills of the Cascades. The presence of this low-lying air tends to lift moist pre-frontal air, so by the time the front reaches the higher mountains, cloudiness and precipitation are decreased. In general, warm-sector rainbands contributed the largest percentage of rain at coastal stations while post-frontal rainbands are the largest contributors of precipitation at stations in the foothills.

1.4-Modeling Studies

The numerical modeling of orographic precipitation began in the late 1960's. Since then a spectrum of models, ranging from two and three dimensional as well as diagnostic, all with various degrees of complexity, have been constructed. As in any field of scientific inquiry, some modeling results have been at times contradictory, while some models are too simplistic to be of any lasting scientific value.

Two-dimensional models have an obvious advantage over three-dimensional models in that computer resources are less of a requirement for the 2D models. These models

(Sarker 1966, Carruthers and Choulartun 1983, Bradley 1985, Richard *et al* 1987, Robichaud and Austin 1988, Dore *et al* 1990, 1992, Meyers and Cotton 1992), for the most part have been constructed with very limited microphysics parameterizations, meaning that the precipitation rate from mid-levels is hardwired into the model, resulting in a lack of interaction between dynamics and microphysics. The exception being the work of Meyers and Cotton (1992), who use a primitive equation model with explicit microphysics.

Bradley (1985) used a nonhydrostatic 2D model which accounted for water vapor in the lowest model layers but contained a fixed precipitation rate (seeder cloud), at a prescribed model level (around 3 km). He conducted a number of simulations using soundings from a saturated neutral atmosphere, as well as an unsaturated stable atmosphere. For topography he used the terrain of Southern Wales, and compared model results with the work of Hill *et al* (1981).

He found that for a given wind speed, the unsaturated stable atmosphere produced the *highest precipitation rates.* He also noted the sensitivity of model produced precipitation to wind speeds, especially in the 20 m s^{-1} to 30 m s^{-1} range. He attributes these two findings to mountain wave affects. However, he does not draw the distinction between a terrain forced updraft and true gravity waves. This issue will be addressed in a subsequent chapter of this study.

Bradley also discussed the role in which the release of latent heat causes a decrease in the stability of the atmosphere, and a reduction in mountain wave amplitude (Meyers and Cotton 1992, Katzfey 1995b). In order to investigate potential instability he set up two experiments in which the atmosphere experienced either a cooling or drying aloft. In both cases the condensation and precipitation rates were less than in the simulations of a unsaturated stable atmosphere. He concludes that at least for the cases reported by Browning (1980) and Hill *et al* (1981), potential instability apparently was not very significant.

Meyers and Cotton (1992) used the RAMS model to investigate the sensitivity of the models microphysics parameterization to flow over the Sierra Nevada Range. The model produced precipitation was sensitive in various degrees, to different hydrometeor species.

Over the course of their work they noted the sensitivity of the model results to the initial modeling sounding. They also found that the Coast Range had only minimal impact on the flow and precipitation generation downwind over the Sierra Nevada.

Richard *et al* (1987) also found that a rapid increase (near exponential) in precipitation enhancement rate was due to nonlinear increases in updraft velocities, which in turn were a function of nonlinear mountain waves. What their study does not specify is how these values change with changing stabilities. They also do not distinguish between a terrain forced updraft and a true gravity wave.

There have been considerably less studies that use 3D models, in large part due to the increase in computer requirements (Colton 1976, Nickerson *et al* 1986, Bruintjes *et al* 1994, Katzfey 1995a,b). One of the earliest to address orographic precipitation was Colton (1976) who constructed his model using explicit microphysics. He was able to show considerable skill in reproducing a number of heavy rain events over the Sierra Nevada Range.

Nickerson *et al* (1986) used a 3D model to investigate airflow and rainfall over SW Germany. They found that two mountainous areas that differ in height by only 150 m, but have greatly varying windward slopes, can have significantly different dynamic responses. The steeper slope generates larger ascent rates which in turn increases the condensation mixing ratio.

Using the same model as Nickerson *et al* (1986), Romero *et al* (1997) studied a heavy rain event that occurred over NE Spain. Using a Δx, Δy of 20 km they attempted to investigate the role in which orography and evaporation from the Mediterranean Sea played in this event. Their results show the importance of the orography in confining the heaviest rain to the region between the coastline and the highest summits of the Pyrenees. They note the formation of an off-shore convergence zone is due to the upstream influence of the Pyrenees. In part due to the short duration of the event (12 hours), their results indicate that evaporation in the Western Mediterranean was not a statistically significant contributor to the heavy precipitation generated over the mountains.

Bruintjes *et al* (1994) used the Clark-mesoscale model to investigate dynamical effects of flow over Northern Arizona during the passage of a winter storm. This modeling effort not only had surface data to work with but a number of aircraft flights through the storm. They make the important distinction between terrain forced updrafts and gravity waves that were produced as a result of the flow over a series of ridges. Modeling results indicated that terrain forced updrafts were on the order of 1 m s^{-1} while updrafts in gravity waves were on the order of 5 m s^{-1}. Due to the much stronger updrafts in the gravity waves, cloud liquid water content were much larger than in the terrain forced updrafts. In large part this is due to the nature of the storm's thermodynamic structure, where the atmosphere was dry from the surface to 800 mb and nearly saturated above. The implication is that in continental mountainous regions, gravity waves may have a much larger role in the vertical and areal distribution of precipitation than in maritime ranges where low-level moisture and terrain forced updrafts tend to dominate the precipitation process.

Katzfey (1995a,b) using the Division of Atmospheric Research (DAR), hydrostatic mesoscale model, investigated several heavy rain events along New Zealand's South Island. This model did not have explicit microphysics but instead used the dump bucket scheme (when the air becomes supersaturated, precipitation is generated from the excess moisture and immediately falls out of the layer of air). One of the goals of his work was to see the sensitivity of the modeled rain to the height of the orography and horizontal grid spacing. Results indicated that the 15 km grid spacing produced larger amounts of peak rain over the Southern Alps, and a stronger mountain wave, than the 30 km grid spacing experiment. However, the area-averaged rain for the 15 km run was slightly less than for the 30 km run. Katzfey attributes this to the steeper slopes and higher vertical velocities in the 15 km run, leading to increased localized low-level convergence around the steepest slopes. In another simulation, where the elevation of the Southern Alps was increased (made closer to the actual barrier height), the net effect was an increase in peak rain and a slight increase in upstream blocking. While investigating the influence of latent heat effects, Katzfey found that in and around regions of

heavy rain, low-level convergence increases when latent heating is activated in the model. With it turned off the rain maxima decreased by some 20%-25%.

RAMS has been used in a number of studies involving complex terrain, one of the first ones was Bader (1985, 1992), using an early 2D version of RAMS, he investigated boundary layer evolution over sloping terrain. Abbs and Pielke (1987) used a 3D version of the model with a horizontal grid increment of 15 km to investigate orographic effects over NE Colorado. Snook (1993) used the model with a 10 km horizontal grid increment to study winter storms over Colorado. Along similar lines Thompson (1993) used a 25 km nested grid to test the utility of RAMS as an operational forecast model. More recently, Poulos (1996) used the model to investigate the interaction of katabatic flows with lee-side mountain waves on the meso-γ scale. Due to the nature of katabatic flows that drain from steep mountain canyons, he used a nested grid with a Δx, Δy of 400 m and a Δz of 20 m near the surface. He also notes the importance of scaling the horizontal grid increment with the vertical increment in steep terrain due to the truncation error in the pressure gradient term. The higher resolution simulations of more recent years has followed the evolution of increased computer speed, and will continue to do so in the future.

1.5-Diagnostic Models

In operational weather and hydrologic forecasting, quantitative precipitation forecast (QPF) are of major interest, especially since hydrologic modeling is expanding and most of these models need QPF's as input data. Historically, due to the low resolution of NCEP models (resulting in extremely poor terrain representation in mountainous regions), there has been a need for an alternative source of QPF's. This vacuum has been partially filled by a number of diagnostic models that have shown skill in creating QPF's (Rhea 1979, Alpert and Shafir 1989, Sinclair 1994). These models advect layers of air over a given topographic barrier, where the vertical velocity is estimated using: $\mathbf{W}=\mathbf{U}\cdot\nabla\mathbf{Z}$ These models run on smaller computer platforms on the order of several minutes. They can also be constructed using almost any terrain data set, although 10-20 km is the most common horizontal grid spacing. They are also

limited to stratified storm types since condensation and subsequent precipitation is only produced by uplift.

Rhea (1979), using 13 years worth of winter precipitation data from Colorado, was able to show a strong correlation between model output and seasonal precipitation and river runoff. Alpert and Shafir (1989) found a mean error of ±8% for the simulation of annual precipitation over the Judean Hills of Israel, while for three precipitation events they modeled, the error increased to ±15%-20%.

Sinclair (1994) built a 2D diagnostic model and used it to simulate several heavy precipitation events over New Zealand's North Island. He suggests that model grid spacing of 10 km-15 km is optimal; any smaller spacing did not improve his results because the airflow over and around the fine-scale topography was not properly estimated by such a crude parameterization.

1.6-Objectives

The primary objective of this study is to determine the utility and limitations of a numerical model in estimating stratiform precipitation (rain) over a high latitude coastal mountain range. Specifically, the sensitivity of modeled precipitation to perturbations in the temperature, moisture, and wind fields will be addressed. These simulations should indicate the usefulness of a high resolution model, such as RAMS, in a region where there is a moderate to large amount of uncertainty in the data fields.

From the review in sections 1.1- 1.5 given above, it is clear that there are a number of issues that still need to be resolved. Some of the issues that will be addressed are: 1) The increase of precipitation with increasing elevation, 2) The roles which potential instability and gravity waves play in the distribution of precipitation, and; 3) How sensitive is RAMS to realistic perturbations in the initial fields? Is there any value in ensemble QPF forecasting? 4) What role does the model grid interval play in the generation of precipitation? and how is this related to the resolution of fine-scale topographic features?

Chapter two of this study consists of a RAMS simulation of the September 19-21, 1995 heavy precipitation event on Alaska's Kenai Peninsula. **Chapter three** consists of a suite of sensitivity simulations whose purpose is to show the sensitivity of the model and hopefully to some degree the real atmosphere, to small perturbations in temperature, moisture and wind fields. **Chapter four** covers futuristic ensemble QPF techniques, while **Chapter five** investigates the role which the model grid interval, and hence terrain resolution, has on the development of precipitation. Finally, **chapter six** provides a summary and conclusions.

Chapter 2

SEPTEMBER 19-21, 1995: A CASE STUDY

2.1-Introduction

On September 19,1995 the remnants of typhoon *Oscar* made landfall along Alaska's Kenai Peninsula. High freezing levels, abundant moisture and wet antecedent soils led to extensive flooding along the Kenai River and in the Seward area. There was no loss of life directly related to this event, but property damage was in excess to $30 million. The National Center for Environmental Prediction (NCEP) suite of forecast models were indicating that a major system was headed for the North Gulf Coast, more than three days in advance. However, the Quantified Precipitation Forecast (QPF), from those models turned out to be roughly an order of magnitude below the observed rainfall totals (Flood Report-ARNWS 1996).

This heavy rain event makes it an ideal storm to model since the orography of the Kenai Peninsula played a major role in the vertical and horizontal distribution of rain. However, numerical modeling in a data sparse region like Alaska is not without its own difficulties. The major limitation is a lack of data to: 1). initialize the model, and; 2). verify model output. From a scientific point of view it was fortunate that this storm came ashore over a region that has the highest density of rain gages in the state. In addition to rain gages there are surface observations from Homer and Kenai airports, rawinsonde data from Kodiak and Anchorage. In September of 1995 the WSR-88D located on the NW corner of the Kenai Peninsula was operational, however, during the event it had technical problems and was "down" for part of the time, making the radar data of limited value.

2.2-Kenai Peninsula: Geography and Topography

The Kenai Peninsula is a 200 km by 220 km landmass that is connected to the rest of the state by a 20 km wide strip of mountainous land on its NE corner (Figure 2.1). To the south lies the Gulf of Alaska, to the west the sheltered Cook Inlet, and to the east Prince William Sound. The western third of the peninsula consists of a low-lying coastal plain, dotted with numerous lakes; the major towns are Homer, Kenai, and Soldotna. This area is delineated by mountains which lie to its south and east, creating an effective rain shadow from storms that track NE across the Gulf of Alaska.

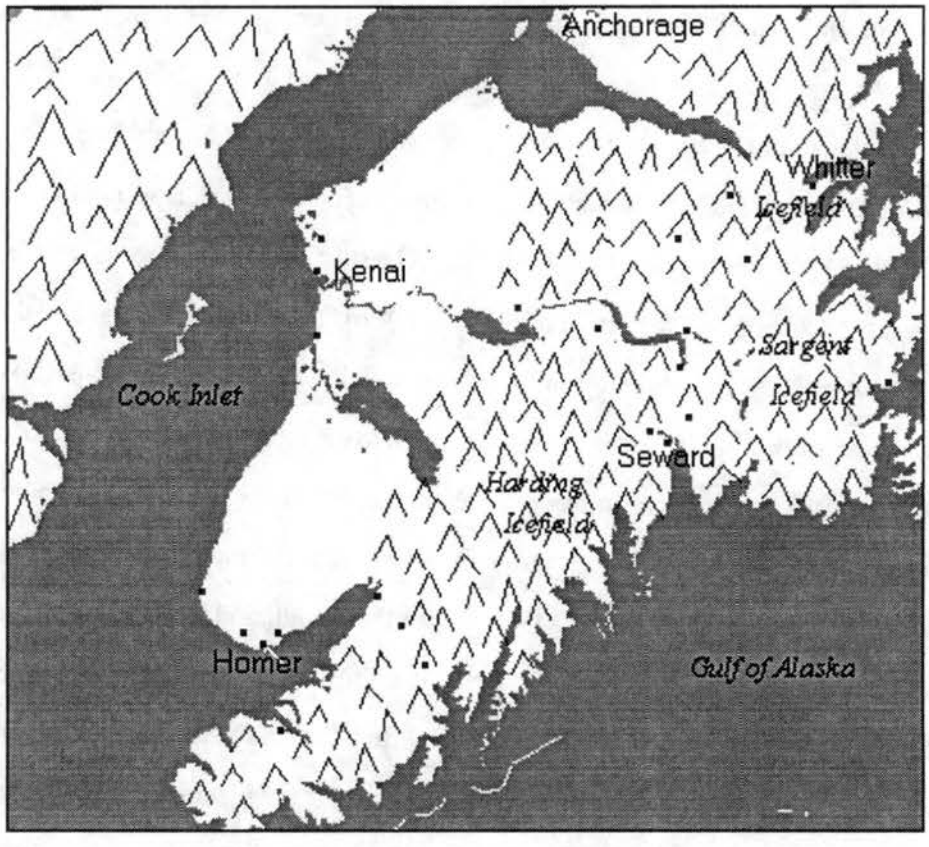

Figure 2.1: Landscape of the Kenai Peninsula

Due to the longitudinal positioning of the Aleutian Low in the North Pacific, the west coast is comparatively dry since it is located in a rain shadow with respect to moisture rich

southeastly flows. The remaining two-thirds of the peninsula can be classified as mountainous terrain, dissected by a number of deep glaciated valleys. The highest mountains are 1800 m high, but the majority of mountains fall in the 1000-1400 m range. On the southern and eastern coastlines, these mountains rise abruptly from the oceans edge, creating a formidable topographic barrier to on-shore flow. Straddling this barrier the Harding, Sargent, and Blackstone Icefields give evidence of the amount of moisture that falls out along this coastline. Numerous outlet glaciers flow down to the Gulf of Alaska, creating the fiord topography. The only population centers along the coastline are at Seward, located at the head of Resurrection Bay, and at Whittier, lying in the NW corner of Prince William Sound.

The mountains to the north and west of the coastal zone are drier, as indicated by a lack of glaciers and snowfields. Coniferous forest extends from valley bottoms to about 500 m, above which slopes are either covered by alpine vegetation or are bare.

2.3-Climate & Weather

The climate of the Kenai Peninsula is that of a high-latitude maritime mountainous region. The wettest region is along the eastern and southern coastline. The driest months on the Kenai Peninsula are April and May; the wettest September and October. Low pressure systems which move across the northern tier of the Gulf of Alaska tend to move from the SW, skirting the southern coast of the Kenai Peninsula, with secondary lows often forming in Prince William Sound. Average annual precipitation for selected sites where long-term records exist are: Whittier= 441 cm, Seward= 172 cm, Homer= 62 cm, Kenai= 49cm.

Figure 2.2 is taken from Jones and Fahl's (1994) mean annual precipitation map, for which they used precipitation as well as runoff data to generate the isohyetals. The values over mountainous terrain are estimates based on very limited data. What is of interest is the large precipitation gradients across the Kenai Peninsula.

Even though Figure 2.2 does not explicitly show strong gradients across the windward slopes on the south coast, there is some evidence that they exist. For example, outlet glaciers which flow northward from the 20-30 km wide Harding Icefield, are not as extensive as the

tidewater glaciers that flow southward. As further evidence, monthly precipitation from two gages located in the Bradley Lake Basin (40 km SE of Homer), indicates that the gage which is closest to the southern coast (at an elevation of 400 m), receives approximately 60% more rain than a gage located 9 km farther inland but 300 m higher. Some of the difference may be attributed to local topographic effects, since this second gage sits on the floor of a narrow valley. However the first gage sits just to the lee of a small pass in the mountains which has direct exposure to onshore flow.

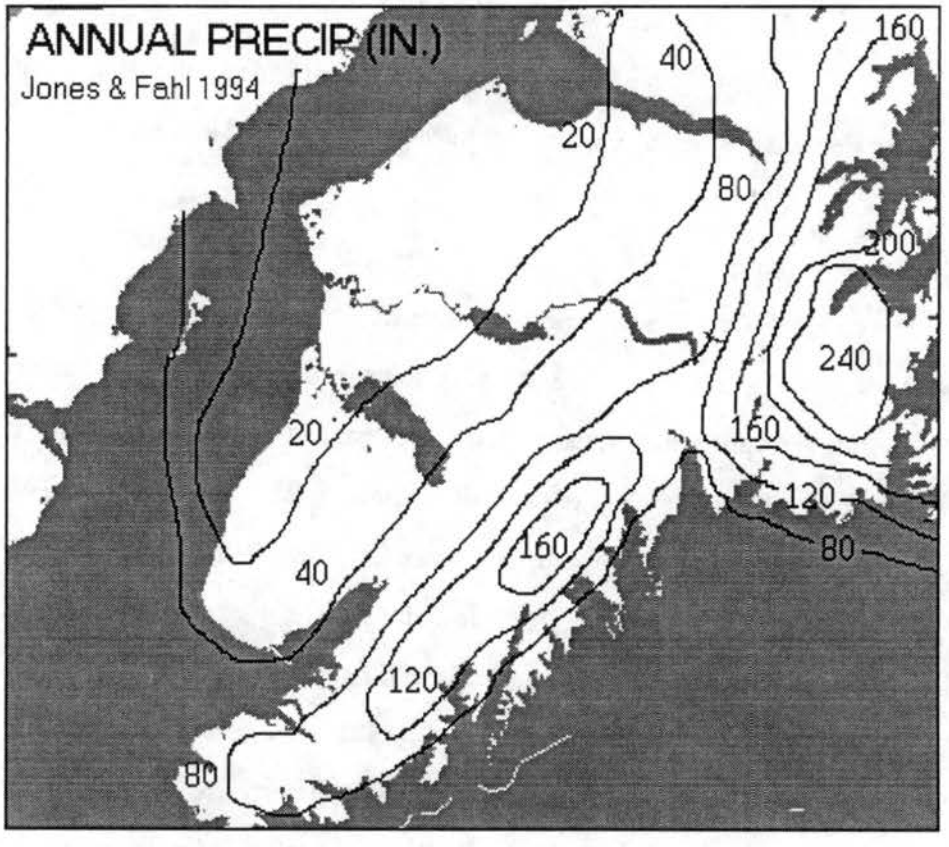

Figure 2.2: Annual mean precipitation (in), taken from Jones and Fahl (1994)

Analyzing 31 moderate to heavy rain events that occurred between 1984 and 1994, the ratio of total storm rainfall between Seward and the gage at Seward 9NW (Exit Glacier) shows that Seward received 69% of the rain that Exit Glacier recorded, but 129% of that observed at

Seward 19N (Kenai Lake). The gage at Kenai Lake is roughly 25 km due north and about a 100 m higher up the valley that extends from the head of Resurrection Bay. There is limited data but on a monthly basis it appears that the ratio between Seward and Exit Glacier approaches one. This probably indicates that Seward receives light rain more frequently than Exit Glacier, but when stronger dynamic forcing is involved, the latter is in a more favorable location, despite being situated in a narrow valley and being in a precipitation shadow for pure southerly flow.

2.4- Precipitation Gages

Data from 21 precipitation gages was used in the storm analysis; seven of these gages record data hourly, while the remaining 14 are read once per day by volunteer observers. There are a number of limitations to this "network" of gages: 1) they are composed of an assortment of four and eight inch gages, most are storage types, while the automated gages are either a weighing or tipping bucket; 2) most of the gages are not shielded; and 3) gages are predominately at low elevations. Seven gages are at elevations at or above 300 m, but only two of the seven are above 500 m. 4) the non-automated gages are read at *different* times of the day; 7 AM and 5 PM being the most common.

These limitations mean that observations are for the most part restricted to valley bottoms. In addition there are only two gages (Seward, Nuka) that are anywhere close to the southern coastline where flow with any amount of southerly component, brings the heaviest precipitation. The fact that many of the gages are read at different times means that there is a certain amount of uncertainty in the timing of precipitation at these gages. In creating the precipitation map the policy adopted in this study was to use the nearest automated gage as an indicator of the timing for the manual gages. For example, hourly data exist at both Lawing and Turnagain Pass, which are in close proximity to Grandview. At 9Z on Sept.20 Grandview reported 5.0 cm for a 24 hour total. Based on the temporal distribution of rain at the two automated gages, it is estimated that all of the 5.0 cm fell between 0Z and 9Z.

2.5- Storm Analysis

Prior to September 19th, a number of intense low pressure systems had been moving in the long wave pattern across the North Pacific; these storms brought moderate to heavy rain to Kodiak Island, Kenai Peninsula and the North Gulf Coast. By Sept.19 a high amplitude 500 mb ridge was positioned over Southeast Alaska and the Yukon Territory, which remained stationary for the next three days (Figure 2.3). By 12Z on Sept.19, an intense upper-level cut-off low pressure system was tracking NE across the Gulf of Alaska, and was located about 400 km south of the tip of the Alaska Peninsula (51N,160W). The stationary ridge over western Canada retarded the eastward movement of this storm. At the surface, a series of lows were merging along the 157° meridian (Figure 2.4). In the process ex-typhoon Oscar was continuing to move NE into the Gulf of Alaska, bringing with it copious amounts of moisture (Figure 2.5). By 12Z on Sept.19 the flow at mid and upper-levels was southeasterly and remained so for the duration of the event. Surface winds at Homer were northeasterly at the start of the simulation (0Z, Sept. 20), and by 12Z Sept.21 were easterly.

The rain first began along the southern coast line of the Kenai Peninsula on the afternoon of Sept.19. Freezing levels from the Kodiak sounding at 12Z Sept.19 were 1800 m, on Sept.20 at 12Z, 2930 m, and 2000 m at 12Z on Sept.21. Obviously all of the precipitation fell in the form of rain (Figure 2.6).

The only radar images available for this event are shown in Figures 2.7 and 2.8. These were taken around 16-17Z on Sept.21, four to five hours after the end of the simulation, when the radar finally became operational. They do, however, indicate the continued SE flow and moderate reflectivities over the southern and eastern mountains of the Kenai Peninsula. It should be noted that due to the mountains there is some serious beam blockage of the 0.5° slice to the southeast and east.

Figure 2.9 shows observed rain for Sept.19-21. Several points are evident:
1) With south/southeast flow, the windward slopes to the south and east received heavy rain; 2) the rainfall gradients are indicative of the strong influence that topography has on rain distribution; and 3) the rain along the western coast of the peninsula is probably due to

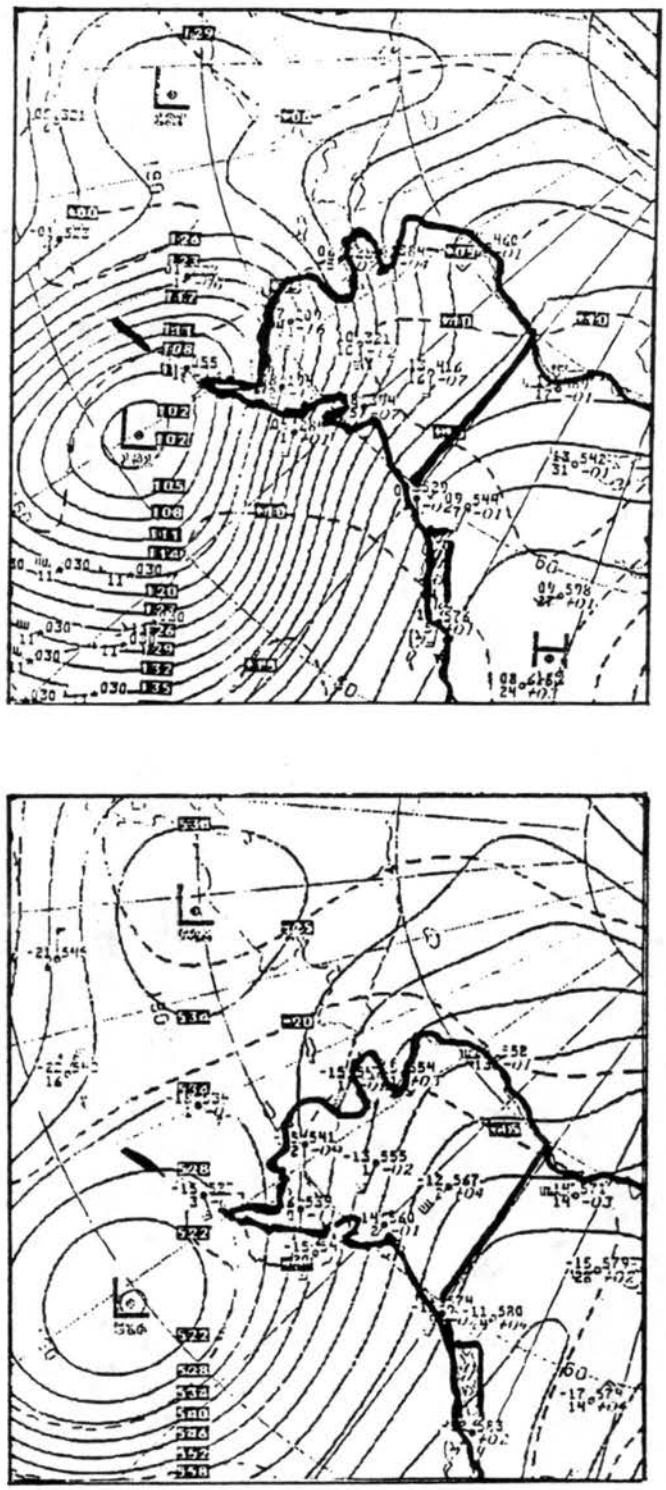

Figure 2.3: Valid at 12Z Sept 20 (top) 850 mb heights, contour interval 30 m and (btm) 500 mb heights, contour interval 60 m

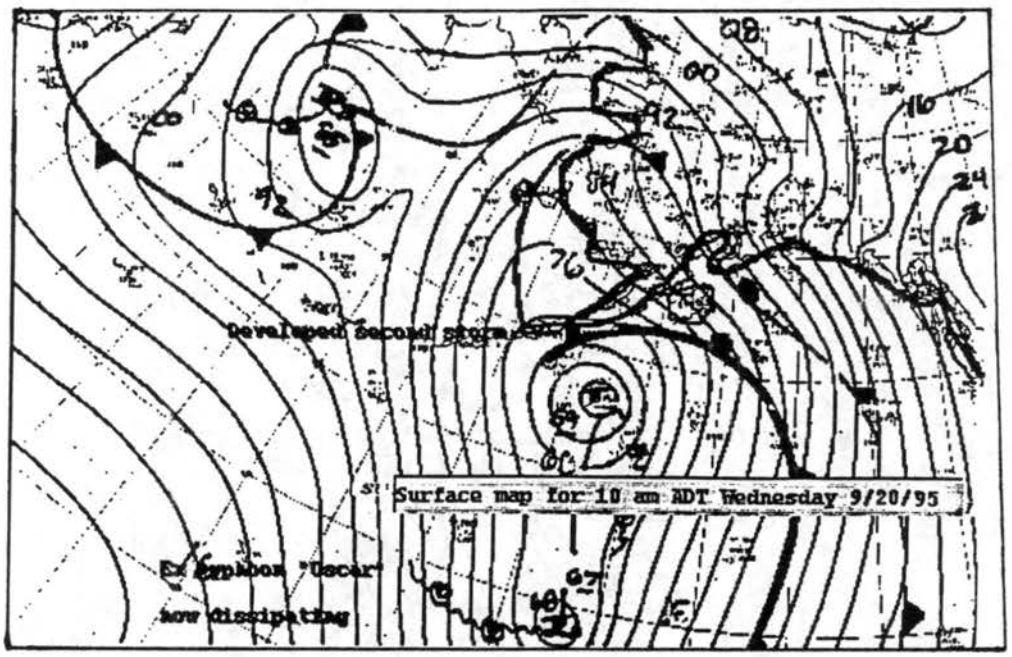

Figure 2.4: surface map valid at 18Z Sept.20, contour interval variable.

Figure 2.5: NOAA-12 infrared mosaic valid at 5Z Sept.20

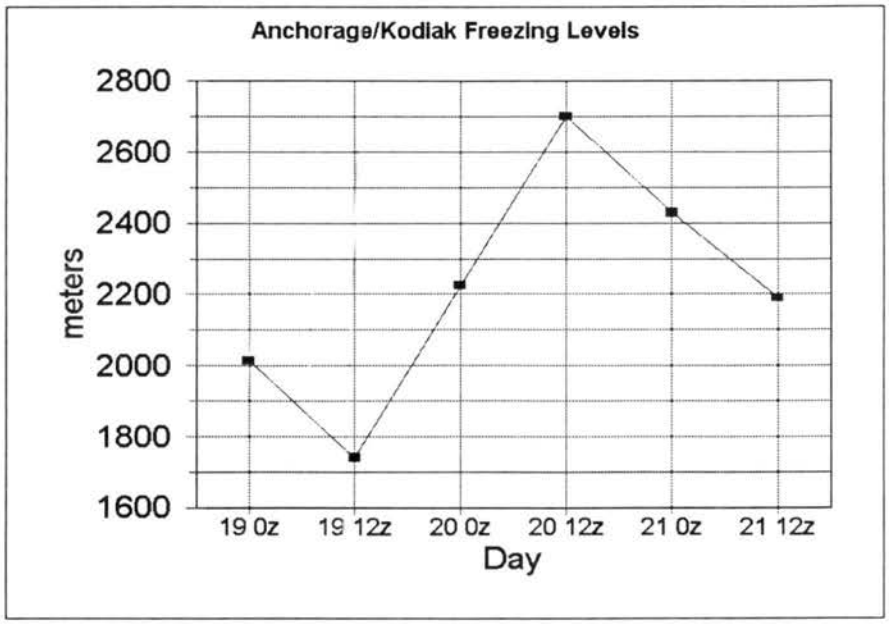

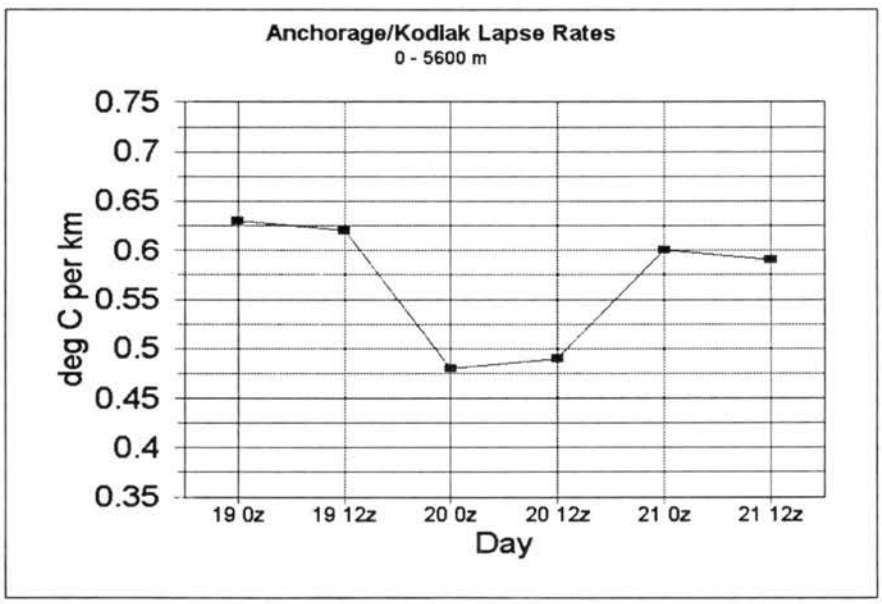

Figure 2.6: (top) averaged freezing levels (m) for Anchorage and Kodiak. (btm) averaged lapse rates from surface to 5600 m for Anchorage and Kodiak. Both plots valid from 0Z Sept.19 through 12Z Sept.21

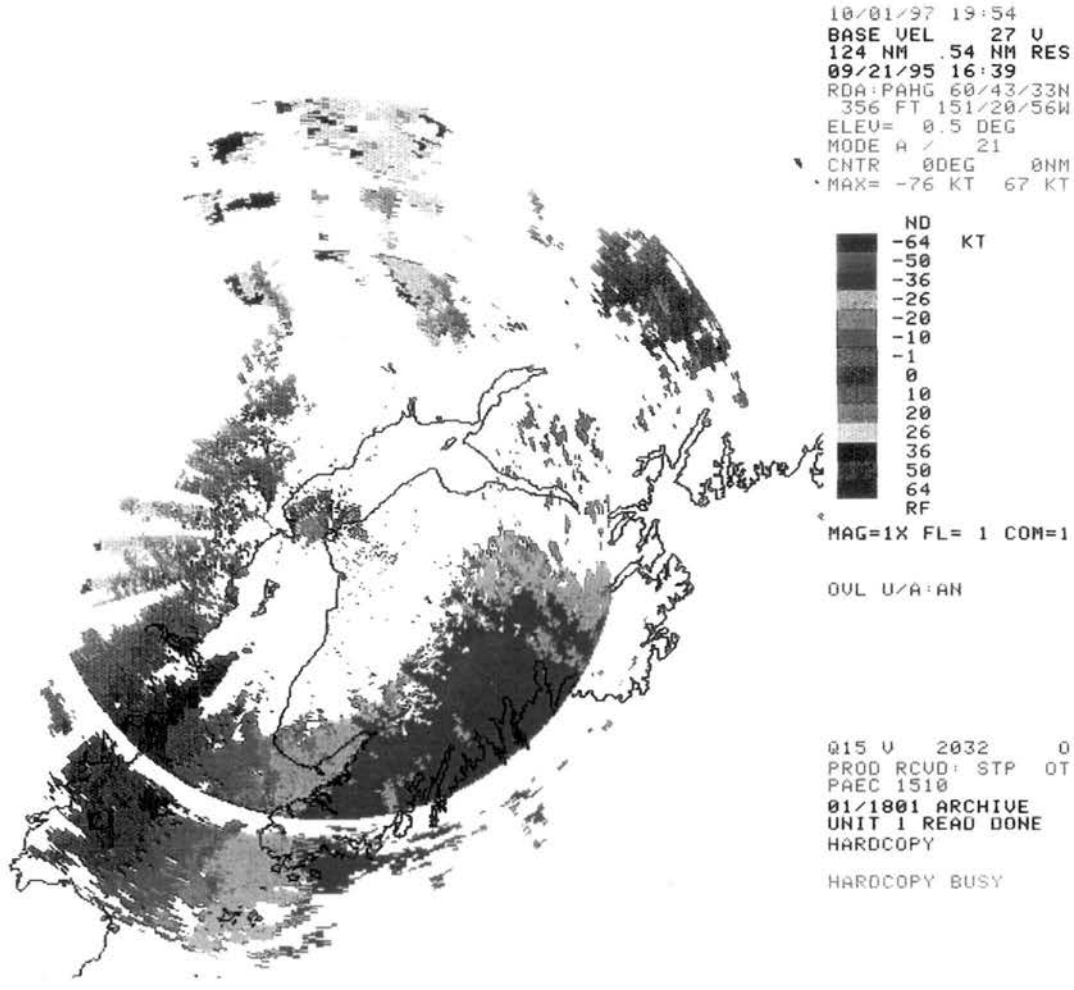

Figure 2.7: Radar scan of base velocity (knots) valid at 16:39Z, Sept.21, 1995

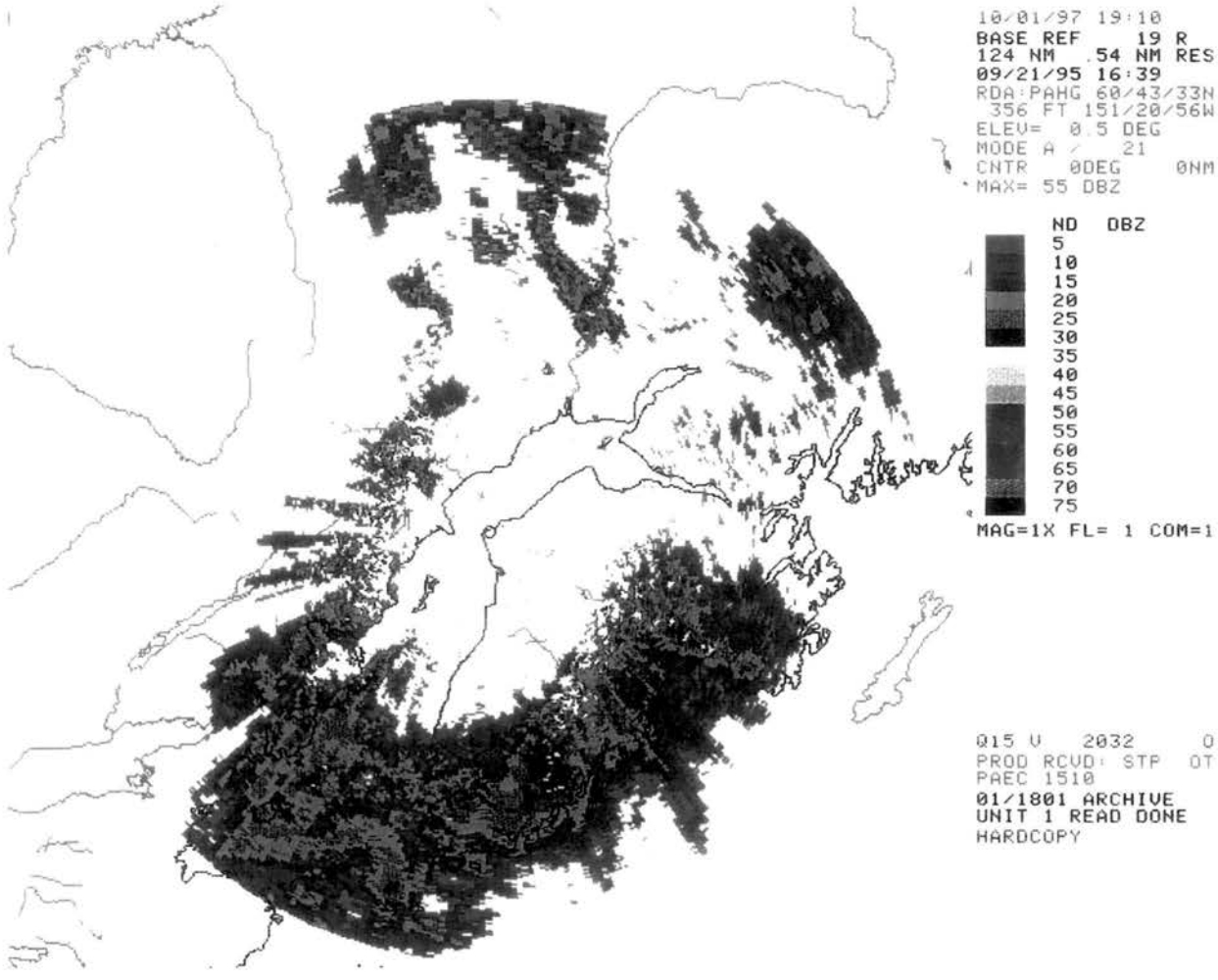

Figure 2.8: Radar scan of base reflectivity (dBZ) valid at 16:39Z, Sept.21, 1995

mesoscale features such as some type of convergence zone or embedded convection that moved across the area from the mountains.

Flooding began on Seward area streams and rivers by the morning of the Sept.20. Due to a lack of river gages and unknown amounts of storage by glaciers, basin runoff cannot be used to reconstruct rainfall amounts in the mountains surrounding Seward. Based on totals from Seward and Whittier which both are sited at the base of 1000+ m mountains, rainfall on the windward mountain slopes was probably in excess of 25 cm.

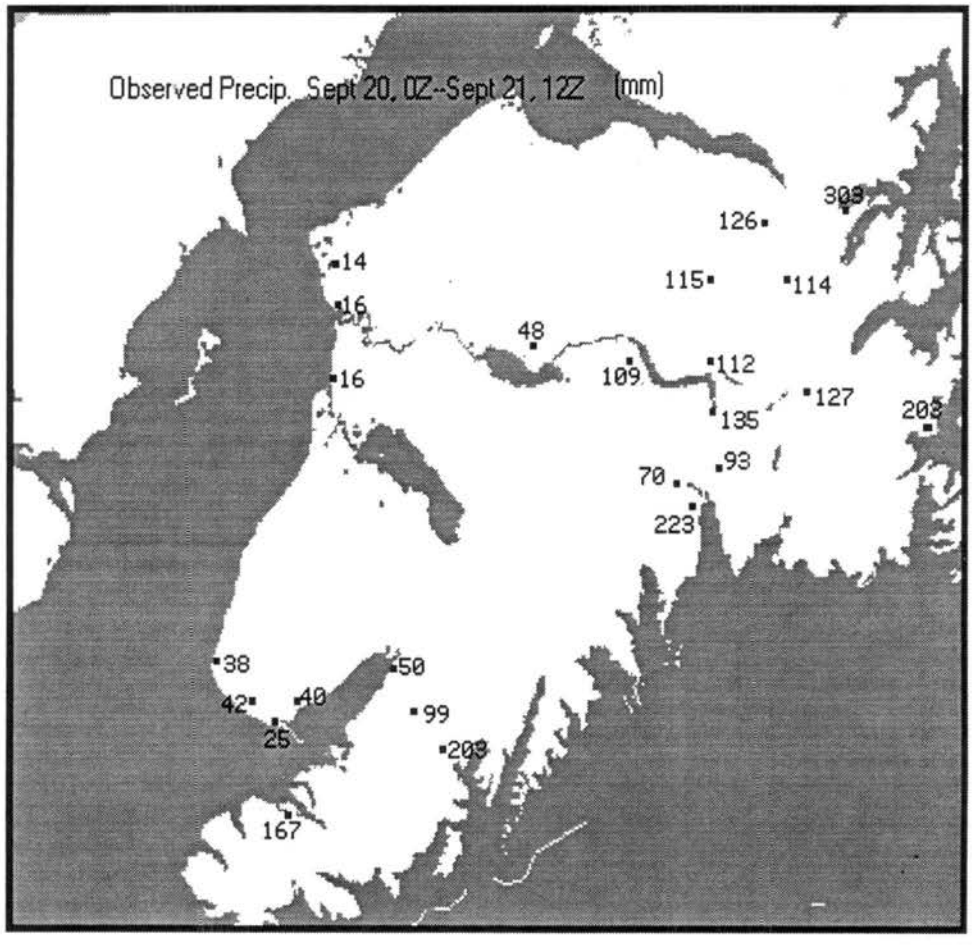

Figure 2.9: Observed precipitation (mm) from 0Z Sept 20.-12Z Sept 21

2.6-Model Set-up and Initialization

Figure 2.10 shows the model topography which was generated from a 30 arcsec USGS data set, with a horizontal grid spacing of 5 km. In preliminary simulations, this topographic data set was used but was smoothed considerably. Silhouette smoothing highly generalizes the topography, filling in valleys and combining individual mountains, resulting in topographic resolution much poorer than 5 km. For this case study, silhouette smoothing was not used, however some manual smoothing was performed on the extreme NE corner of the domain, where very steep terrain was causing numerical instabilities. Since the area of interest is at the center of the domain and wind directions are from the south, this smoothing should not adversely affect the results.

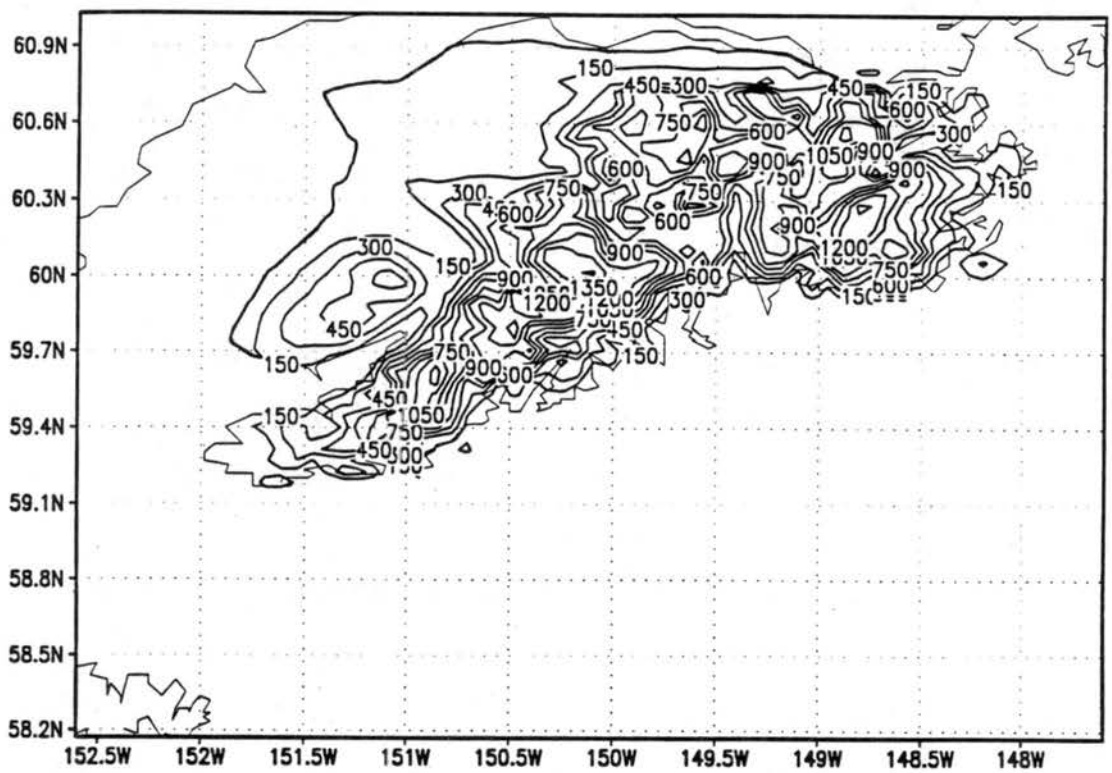

Figure 2.10: model topography (contour interval 150 m) of the Kenai Peninsula with Δx, Δy = 5 km

The domain is 330 km by 325 km with a horizontal grid interval of 5 km. There are 33 model layers in the vertical, with a layer interval of 200 m at the bottom boundary, stretching to 1000 m in the upper layers. The top of the domain is at 14.6 km and the upper most five layers contain a Rayleigh Friction scheme which absorbs upward propagating gravity waves, reducing the chances of artificial reflection of waves back to lower layers. The model ran with the full microphysics package activated, where the mean rain droplet diameter is specified from a default value in the code, and the number concentration is diagnosed from the mean diameter and prognosed mixing ratio (Walko *et al* 1995). The vegetation parameterization was set to emulate a coniferous forest (Tremback and Kessler 1985). The justification for this choice is that coniferous forest is the single most common ground cover on the Kenai Peninsula, despite the fact that glaciers cover the coastal mountains and the northern mountains are bare above 500 m. This choice should have little impact on this simulation since the atmospheric forcing overwhelms the surface fluxes. Since there was no soil moisture data available, these values were set to represent moderately wet conditions. Based on observed data, the sea surface temperature was set to 283^0 K. In order to maintain mass continuity over the model domain, the winds were spun-up over the first 15 minutes of the simulation.

The radiation scheme is based on the work of Mahrer and Pielke (1976), which includes both short-wave and long-wave parameterizations. Turbulence is based on the original work by Smagorinsky (1963) but modified by Tremback (1990), where the horizontal and vertical diffusion coefficients are calculated separately. The Coriolis parameterization was also activated for all the simulations discussed in this study.

RAMS was initialized using the Isentropic Analysis package (ISAN), which generates a single initialization file and then a series of time-dependent lateral boundary files. These files are constructed from three data sources: 1) NCEP gridded pressure data (2.5°X 2.5°), 2) upper air soundings and, 3) surface observations. The user is able to select what data are to be used and how to weight it in relation to the other two data sets (Cram 1993). The original ISAN grid covers a much larger area than the actual 330 km X 325 km topographic grid used in the actual model runs, so it contains sounding data for example from both Kodiak and

Anchorage, even though those two sites are outside of the final model domain. Once the simulation has begun, the model's lateral boundaries and upper five layers are nudged toward the respective ISAN file every 12 hours using the Davies (1976) nudging. This is routinely done with variable initialization in order to make sure that the model fields receive input from weather systems that propagate into the domain from the sides and top of the model.

For the simulations documented in this chapter, the Kodiak soundings were weighted more heavily than the Anchorage soundings, since the latter is in an area of strong downslope winds. In an area like the Kenai Peninsula where only a few surface observations are routinely available, the initialization file is constructed primarily by the coarse resolution pressure grid data. This data in turn is interpolated down to the much finer 5 X 5 km model grid. The end result is an initialization file that lacks mesoscale features. Fortunately the September 19-21 event was a powerful synoptic scale storm that is handled moderately well by the ISAN routine. However, the lack of mesoscale features does have some influence on the formation of precipitation on the SW tip of the Kenai Peninsula, and will be addressed in the following sections.

The uncertainty in the initial fields results in an unknown amount of uncertainty in the model results in areas where there is little or no data. This suggests the implementation of an ensemble approach to precipitation estimation, for both historical cases and in a forecast mode. For this case study, two additional variable initialization, 36 hour simulations were conducted. The purpose of these additional simulations is to measure the change in a given field (in this case precipitation), due to a small perturbation in one of the atmospheric variables from its control run value. The amount that a variable is perturbed is an expression of the amount of uncertainty in the initial fields. The results of these simulations are presented in section 2.8.

2.7- Model Results: Kenai 5

Potential temperature (θ) at 6 hrs (6 hours into the simulation), is shown in Figure 2.11. The primary feature is the lee side warming of 2°-4° C, due to the downslope winds. This temperature pattern remains nearly constant throughout the duration of the

simulation for the lowest model levels. Aloft, however, temperatures cool as the simulation progresses, the surface to 5600 m lapse rate increasing from 5.3° C km^{-1} during the first half of the simulation to 6.2° C km^{-1} during the second half (compare to Figure 2.6). The winds at this same time are from the SE at most model levels, in good agreement with the observations.

Figure 2.12 is a plot of the mean sea-level pressure (**MSLP**), which compares favorably with the surface map (Figure 2.4) at the corresponding time. Since most of the Kenai Peninsula is mountainous, the calculation of the (**MSLP**) is only an approximation. This approximation becomes less and less accurate as the height of the mountains increase (Wallace and Hobbs 1977 p.60). Analysis of the wind fields throughout the simulation indicate that modest blocking is occurring as SE flow traverses the Gulf of Alaska and impacts the southern and eastern mountains of the peninsula. The Froude Number in the Gulf of Alaska ranged from 0.9 at the start of the simulation to 1.2 at the end, suggesting that lower atmosphere stability decreased as the storm progressed.

Figure 2.12 also shows higher pressure in the eastern half of the domain, which appears to be a result of the blocking of low-level flow by the steep terrain. This pattern is similar to a number of cases that Chien and Mass (1997) have observed over western Washington, which they refer to as *coastal ridging*. Schwerdtfeger (1975) and Parish (1982) describe the establishment of a barrier jet due to the cooling of air as it attempts to flow over a mountain barrier under stable atmospheric conditions. Pierrehumbert and Wyman (1985) suggest that the establishment of a week barrier jet occurs when the length scale of the barrier is larger than the Rossby radius of deformation (R=Nh/f). For this particular case the length scale of the Kenai Mountains is roughly 200 km and the radius of deformation is about 120 km. Hence it appears that the **MSLP** pattern shown in figure 2.12 is a result of this process.

Figure 2.13 is a plot of vertical wind component (**W**) at the lowest model level, (positive values for ascent). Superimposing this field over the terrain (not shown), indicates that the updrafts are co-located over the steepest slopes on the windward side of the mountains, with the strongest downdrafts to the lee of the mountains.

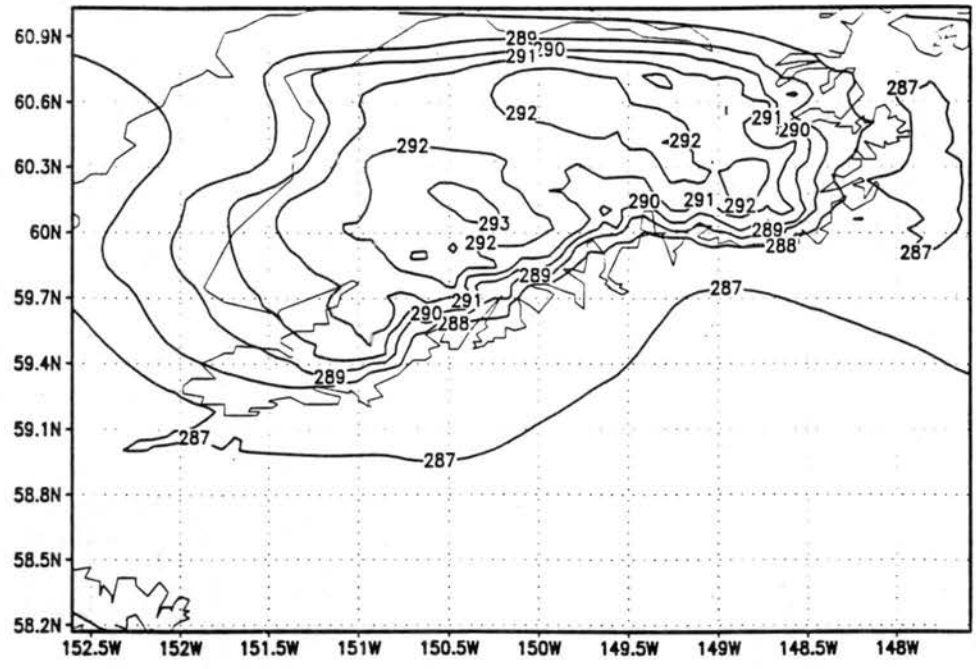

Figure 2.11: Valid at 6z Sept 20. Theta at surface, contour interval one degree Kelvin.

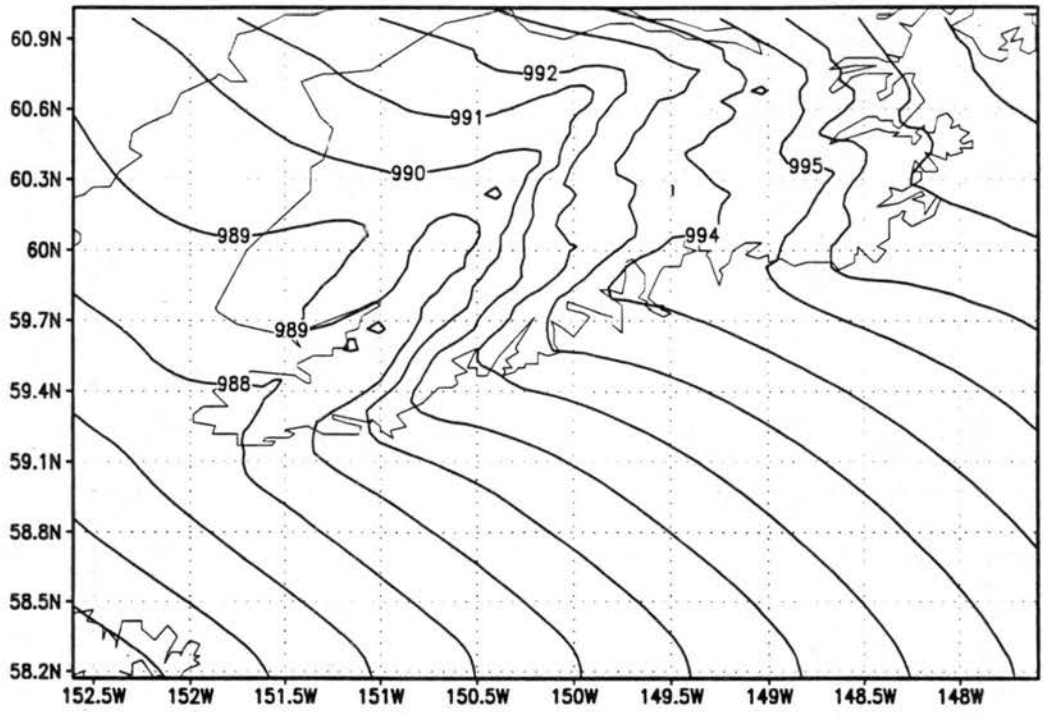

Figure 2.12: mean sea-level pressure (mb) for 12z Sept 20.

A south to north transect across the domain (Figure 2.14) shows that the **W**-component is actually more complicated than Figure 2.13 may first indicate. Once the flow passes over the first barrier, the **W** field *near the surface* is a combination of upstream effects (e.g.-down sloping), and interaction with the local topography. Aloft, however, the flow is dominated by gravity waves that are generated as the flow interacts with the upstream topography.

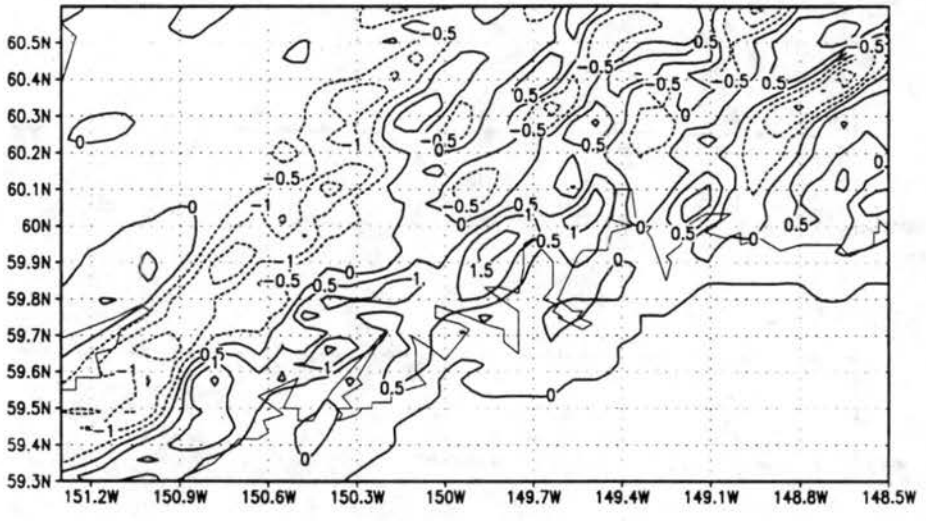

Figure 2.13: Zoom of vertical velocities (contour interval 0.5 m s^{-1}) for 12z Sept 20.

Comparing Figure 2.14a to 2.14b shows that the strongest updrafts are over the steepest slopes (59.6°-59.8°). It is interesting to see that the updraft at 59.75° has the same magnitude near the surface as the one upstream but it does not extend to the same height. The reason for this appears to be that the downdraft of the gravity wave generated as the flow moved up the 1000 m high windward slope, is putting a cap on how high this second terrain updraft can extend. These two figures also show the strong downdraft at 59.9° occurs over terrain that is still 1500 m high, but is 30-45 km downstream of the windward slope. This is important

because atmospheric stability is negating any small upslope flow at 59.9°; in a less stable atmosphere it is hypothesized that the downdraft would be weaker or give way to a weak updraft. This should also mean that precipitation over a plateau or wide mountain is basically generated near the upstream edge, and its subsequent distribution to the lee is primarily a function of horizontal advection.

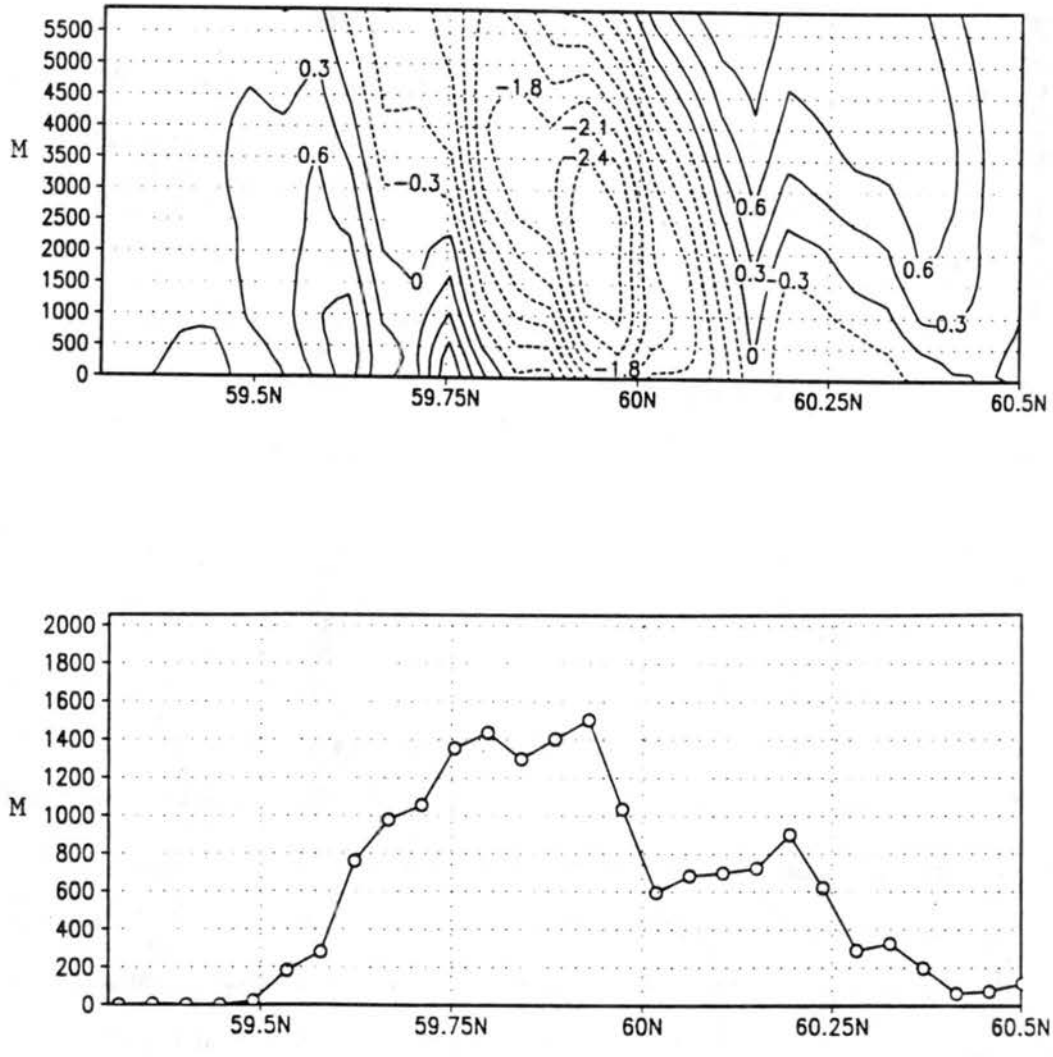

Figure 2.14: North-South cross section through longitude 150.5°W, valid at 12z Sept 20 (top) vertical velocities (contour interval 0.3 m s^{-1}, ordinate height in m above the surface), (btm) topography (m)

Figure 2.15 shows **W**, condensation mixing ratios (**RCOND**), and cloud water mixing ratio (**RCLOUD**). Comparing **W** to **RCOND** shows that the areas of maximum condensation occur at or near the tops of the strongest updrafts. It is also evident that the gravity waves generated to the lee of the barrier induce significant downdrafts where the condensation rate is low (12 and 24 hrs). But as the strength of the downdrafts decrease (36 hrs), condensation increases, and pristine ice formation occurs above 2000 m. Bruintjes *et al* (1994) found that mid-level gravity waves played an important role in the distribution of precipitation across the storm they studied. In that storm the majority of condensation and hydrometeor generation took place in gravity wave updrafts that were 2-5 km AGL, because the low-levels were dry. **Kenai5** in contrast produces the bulk of its precipitation at levels between 500-1200 m AGL, an indicator that condensation is the *product* of forced vertical ascent and moisture availability. The role gravity waves play in this simulation is that the strong descending motion probably keeps the settling hydrometeors from advecting further downwind than they would if the downdrafts were absent.

Precipitation:

Total precipitation (in this case rain) for the 36 hour simulation is presented in Figure 2.16. A maximum rainfall total of 550 mm occurs over the steepest slope (with respect to SE flow). From this plot it is evident that the rain is anchored to the terrain. Just off of the southern coastline , rain totals range from 10 to 50 mm, an indicator that upstream effects are important. A qualitative comparison of Figure 2.16 to Figure 2.9 reveals a number of differences.

The model produces only light (>10 mm) rain over the western coastal plain, which is clearly an underestimate of the observed values. This result is not unexpected since model rain is dominated by the strong SE flow and of course the western coastal plain lies to the lee of the mountains. What mechanism is responsible for the rain that was observed in this region is unknown, but it is possibly linked to the mesoscale features and/or boundary layer flows that the model does not resolve.

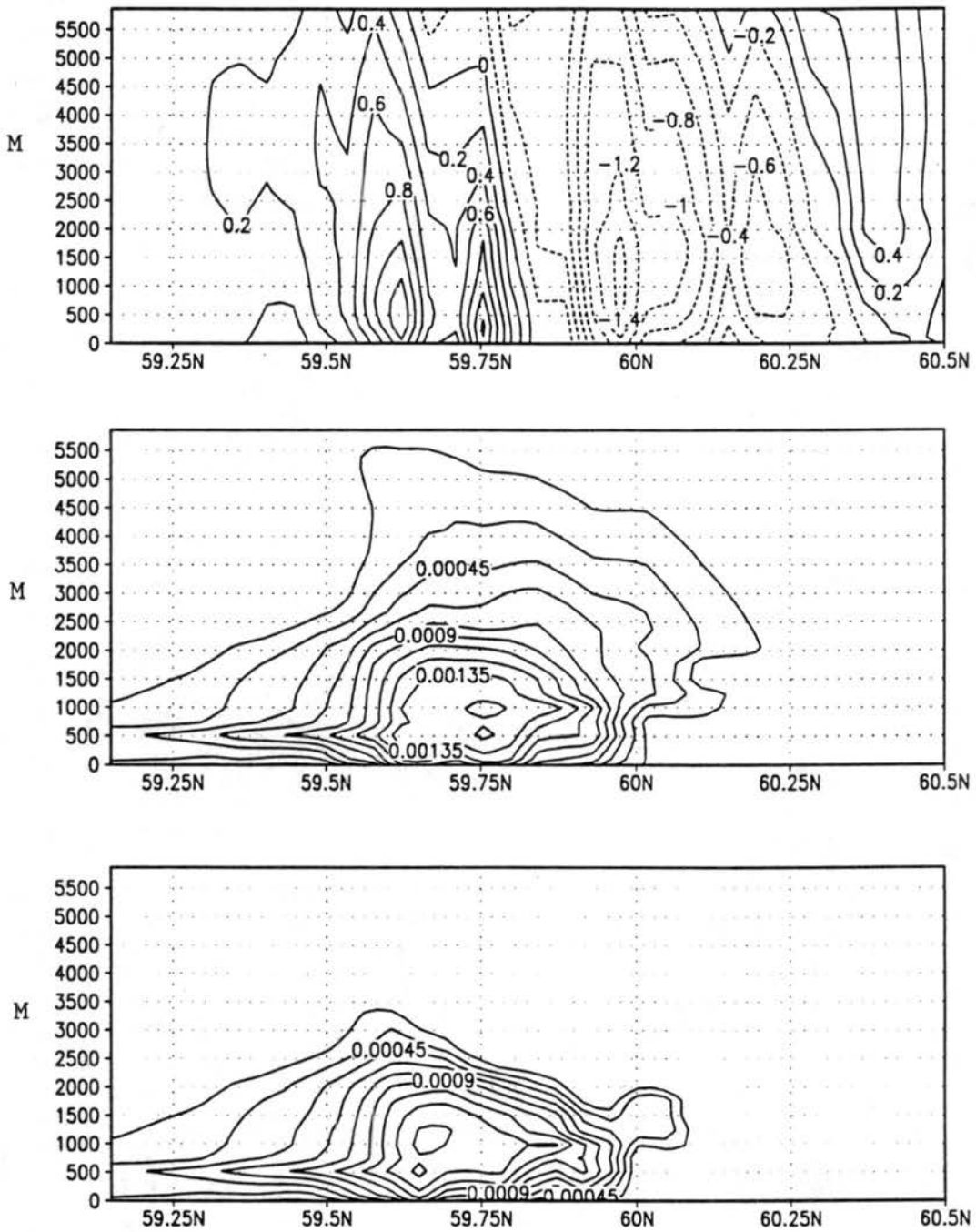

Figure 2.15: North-South cross sections through 150.5°W, valid at 0z Sept 21. (top): Vertical velocity, contour 0.2 m s^{-1} (mid): **rcond**, contour interval 0.00015 kg kg^{-1} (btm): **rcloud**, contour interval 0.00015 kg kg^{-1}

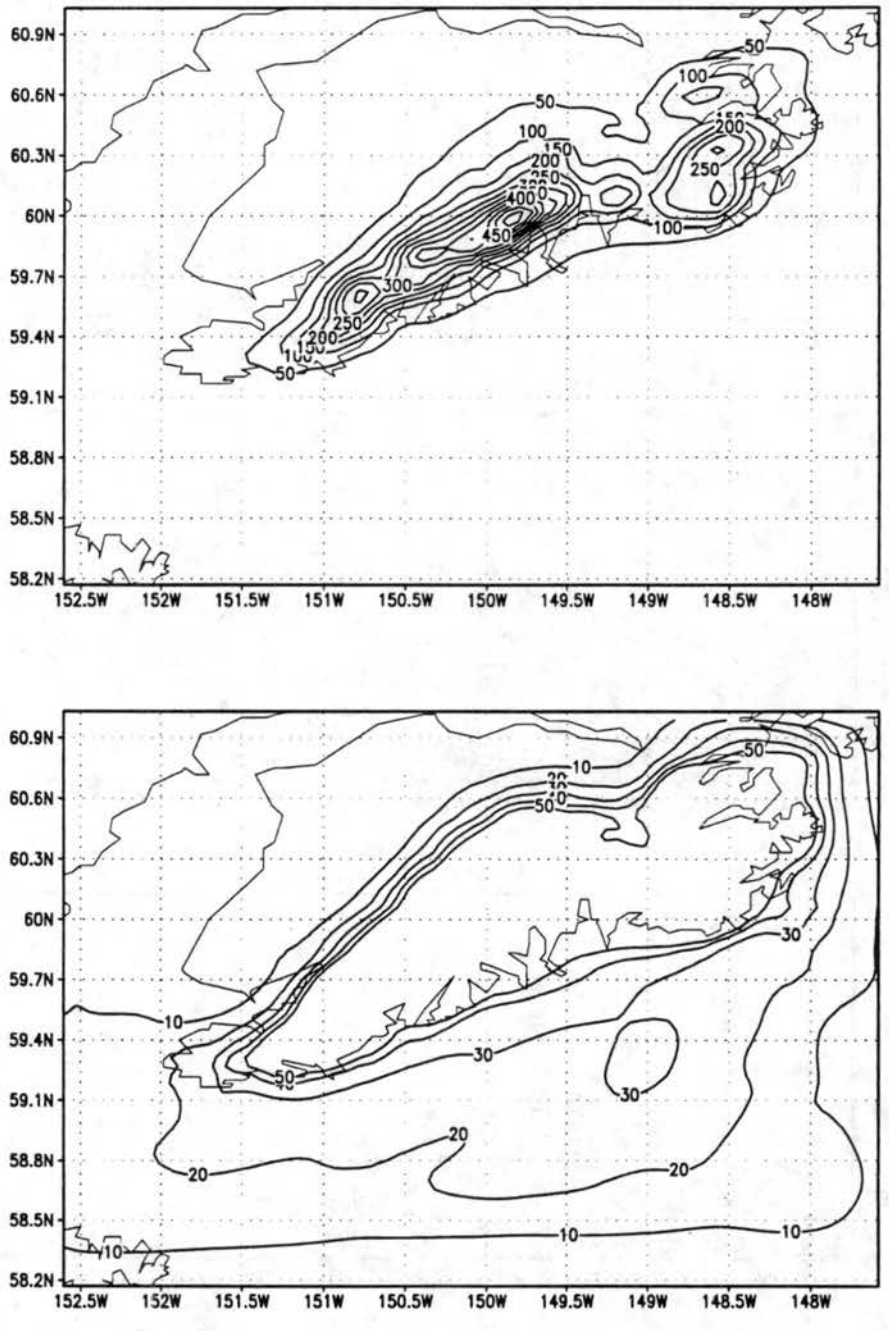

Figure 2.16: 36 hour total accumulated precipitation (mm) valid at 12z Sept 21. (top): precipitation greater than 50 mm, contour interval 50 mm (btm): precipitation less than 50 mm, contour interval 10 mm.

Another region the model underproduces rain for is the extreme NE; this is to be expected since there was some smoothing of the terrain in this area and the steep terrain of Prince William Sound is not included in the model domain. The model does seem to perform an adequate estimation of rain over the remaining areas.

An analysis of the temporal distribution of precipitation shows that along and upstream of the southern coast that rainfall rate decreases after 12 hrs. In the eastern mountains, however rain intensifies between 24 and 36 hrs, as low-level blocking is reduced and the easterly low-level winds intensify. Over the central interior, the accumulation rate is largest from 0 to 12 hours, which is consistent with the timing at the hourly gages.

The analysis of any model variable in itself is not trivial, even over flat terrain, because the model grid points are usually not co-located where observations are taken, as noted by Thompson (1993) and Snook (1993). This problem is compounded in complex terrain because the model topography is only an approximation of the real topography, and a one-to-one comparison of the two can result in serious discrepancies, in large part due to a deficiency in the model terrain. Young and Pielke (1983) discuss the issue of terrain resolution in mesoscale models. For the relatively flat ground of NE Colorado, Snook (1993) used an overlapping quadratics scheme to interpolate model data to the observed values. Katzfey (1995a,b) used an areal approach which will conceptually be adopted in this study.

Instead of attempting to make a point-to-point comparison for the 21 precipitation gages used in this study, an areal mean was computed for seven areas, after which the observations were compared to the model. The justification for this approach is that as a number of authors have noted (Spreen 1947, Hjermstad 1970), in mountainous terrain, precipitation has only a moderate correlation with the elevation of the site, but it is highly correlated with the slope, aspect, and surrounding terrain configuration, in addition to the site elevation. Hence, since the model terrain is only a crude representation of the real terrain, an areal approach seems viable; as long as one recognizes that in the process a certain amount of data smoothing will occur.

The criteria for the selection of the seven areas is based on the clustering of the gages and the homogeneity of the terrain. For the observational data set the mean precipitation was derived for the cluster of gages in that area. In the model, a mean was constructed by using the gridded data that occupied a given predefined area. These areas are the same ones used to construct mean precipitation values in the two sensitivity simulations which are described later in this chapter.

Thompson (1993) reviewed a number of statistical methods used to analyze meteorological data sets. For this study where the observational data set is small, a bias difference method is used, and is defined as:

$$BIAS = 1/n \quad \sum | (P_{obs} - P_{model}) |$$

where **n** is the number of comparisons, $\mathbf{P_{obs}}$ is the observed precipitation, and $\mathbf{P_{model}}$ is the modeled precipitation (after 36 hours). A bias score of 39 mm was found for this simulation. Figure 2.17 shows a graphical representation of the observed versus modeled precipitation, the linear correlation coefficient $r^2 = 0.83$.

In general the model underpredicted precipitation that was observed at the lower elevations. At higher elevations along the southern coastline where values range from 300-500 mm, one can only speculate that these values are reasonable since no comparison data is available. Unfortunately hydrologic analysis is not possible due to a lack of rating curves for the rivers that drain these mountains, and in addition, the presence of large glaciers and icefields means that there is an unknown amount of storage in the hydrologic system.

In the previous section, reference was made to upstream condensation plumes (Figure 2.15). It is suggested here that these plumes are an important part of the enhancement of the precipitation upstream of the coastline but play a smaller role over the barrier. A number of lifting mechanisms are possible: frontal, cold air damming and upstream propagating disturbances (chapter 1). Since the model was initialized without mesoscale features and none of the initial plots suggest any synoptic fronts, these lifting mechanisms can be eliminated.

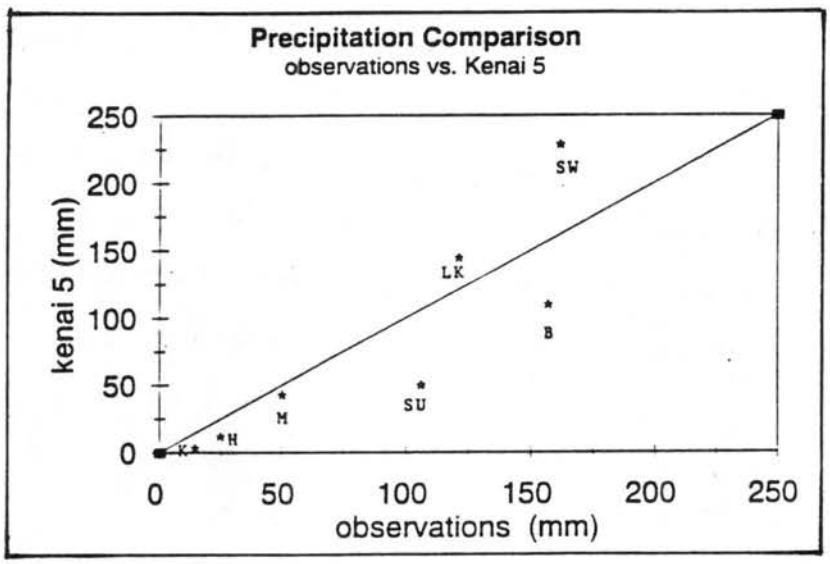

Figure 2.17: precipitation comparison, observations versus control run (mm) B=Bradley Lake, H=Homer, K=Kenai, LK=Kenai Lake, M=Mystery Creek, SU= Summit/Turnagain, SW=Seward

Despite the strong surface winds, it appears from analysis of θ at 12 and 24 hrs, that there is some pooling of cooler air just off the southern coastline. This seems consistent with the fact that the condensation plumes at 12 and 24 hrs are centered around 1000 m AGL, when the pooling of cooler air is significant. At 36 hrs, the cooler air is absent and the plume is closer to the ground. This is by no means conclusive but it is at least suggestive that even in cases when the Froude Number is approximately one, upstream lifting can be important. The detection of upstream propagating disturbances is beyond the scope of this study but is an area that needs further investigation.

Figure 2.18 indicates that much of the upstream condensation can be attributed to areas where the equivalent potential temperature (θ_e), decreases or is constant with height. Since these same areas have ascent rates ranging from 0 to 0.3 m/s, it is suggestive that either upstream blocking or some unspecified mechanism is creating lift in the onshore flow to trigger

the release of potential instability. The condensation mixing ratios are not large (< 0.007 kg kg^{-1}), however they are certainly responsible for precipitation generated over the Gulf of Alaska. These figures seem to indicate that this process enhances precipitation over the coastal zone, but plays only a minor role in the generation of heavy precipitation over the barrier.

Bradley (1985) suggested that potential instability is considerably less efficient in the production of condensate than a more stable nearly saturated atmosphere; this topic will be investigated in section 3.4 of this study. However, it is suggested here that potential instability may still play some role in the formation of orographic precipitation in a stable atmosphere. With θ_e given as:

$$\theta_e = \theta \exp(L W_{sat} / T C_p)$$

where **L** is the latent heat, $\mathbf{W_{sat}}$ is the saturated mixing ratio, **T** is the isentropic condensation temperature, and $\mathbf{C_p}$ the specific heat at constant pressure. In a weak stable layer potential instability could be released if the ratio of $\mathbf{W_{sat}}$ to **T** *decreases* with height faster than θ *increases* with height (drying or cooling aloft). It should be noted that since θ_e is a function of temperature and moisture, a wide range of vertical temperature and moisture profiles can lead to the same θ_e profile.

Overall, regions of terrain ascent are the primary regions for condensation and precipitation formation, however, the upstream release of potential instability pre-conditions the onshore flow. The release of potential instability upstream could also enhance the moisture content at mid-levels (seeder cloud in a conceptual orographic model), in turn increasing the coalescence or aggregation rates in the terrain forced feeder clouds. Browning *et al* (1974) found evidence of potential instability being released as much as 100 km upwind of the hills of south Wales, during the passage of the warm sector of an extratropical cyclone. They also found that it was released at both low and mid-levels, and acted as an important source of seeding material.

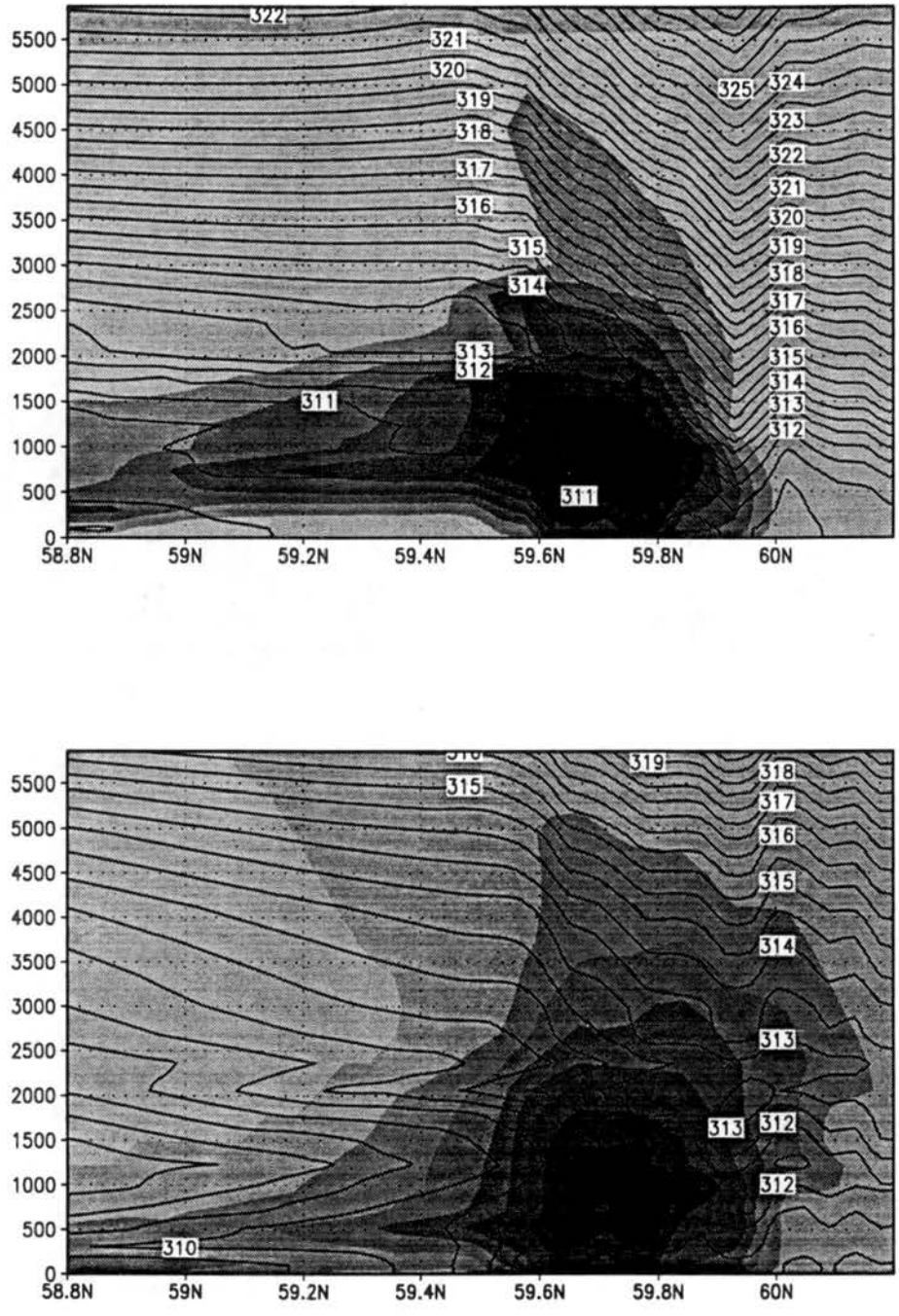

Figure 2.18: Condensation mixing ratios (shading with contour interval 0.002 kg kg^{-1}) and potential temperature (contour interval 0.5° K), for north-south cross section at 150.5° W.
(top) valid at 12z Sept 20 (btm) 0z Sept 21

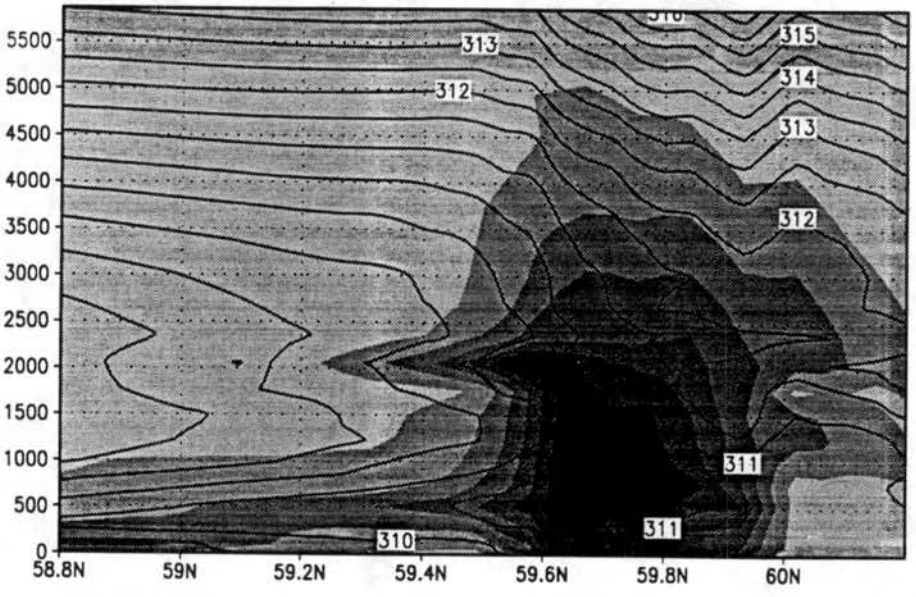

Figure 2.18 continued. Valid at 12z Sept 21

2.8 -Kenai 6 and 7, two variations of kenai 5

In addition to the control run **kenai 5**, two more simulations were conducted in order to evaluate the model sensitivity to various perturbations in initial fields or model parameters. The set-up for **kenai 6** was identical to **kenai 5,** however, wind speeds from 0 m to 2100 m, were increased by 4 m s^{-1}. The concept of ensemble forecasting will be addressed in chapter 4, however, for the present discussion it should be noted that there is in general significant uncertainty in the initial state of the atmosphere (more over the oceanic regions), which of course leads to uncertainty in initial model conditions. In the context of numerical modeling, in addition to uncertainty in the actual measurements of the atmosphere, a given amount of uncertainty is added by the interpolation of observations/analysis to a models' grid structure.

Kenai 7 differs from **kenai 5** in that the model set-up was altered in that the vegetation parameterization was made more realistic by allowing the vegetation types to be declared as a function of terrain height, which is a better representation of the ground cover on the Kenai Peninsula. Specifically, from sea-level to 500 m coniferous forest was declared, from 500-900 m tundra, and above 900 m glacier ice. In the model these vegetation types will alter the surface fluxes of heat and moisture via thermal conductivity, diffusivity, longwave emissivity, and surface albedo. In addition the horizontally homogeneous sea surface temperature (**SST**) in **kenai 7** was reduced from 283° K to 278° K. Figure 2.19 shows observed **SST**'s on Sept 20, 1995. In the western regions of the Gulf of Alaska, temperatures were uniform, however it can be seen to the south of the Aleutian Islands, that large temperature gradients can exist. What effect these **SST** gradients have on Autumn storms that have a long southerly fetch is unknown. What is of interest is to see if changes made to **kenai 7** have any significant impact on the production of precipitation, during a powerfully forced synoptic system such as occurred on Sept 19-21, 1995.

Kenai 6:

Since **kenai 6** was initialized and nudged with wind speeds increased by 4 m s^{-1}, a similar speed difference should be evident in the simulation. Figure 2.20 displays the wind speed difference (**kenai 5- kenai 6**), at 4 hrs, for two model levels.

In Figure 2.20a the horizontal slice is taken through the lowest model level (99 m); what is apparent is that the differences are much smaller as the flow approaches the coastline. In Figure 2.20b, which is at a height of 1493 m, the pattern is still evident but shows an increase in the differences. Closer examination reveals that over the Gulf of Alaska the low-level winds in **kenai 6** are close to the values in **kenai 5**. This indicates that despite higher wind speeds in **kenai 6**, low-level blocking is still an important process. Figure 2.21 is a zoom plot of the **W**-field showing the difference at 99 m valid at 0z Sept 21. The only significant differences occur over the steep windward slopes and average to an increase in **kenai 6** of about 0.1 m s^{-1}. This topic is resumed in section 3.5.

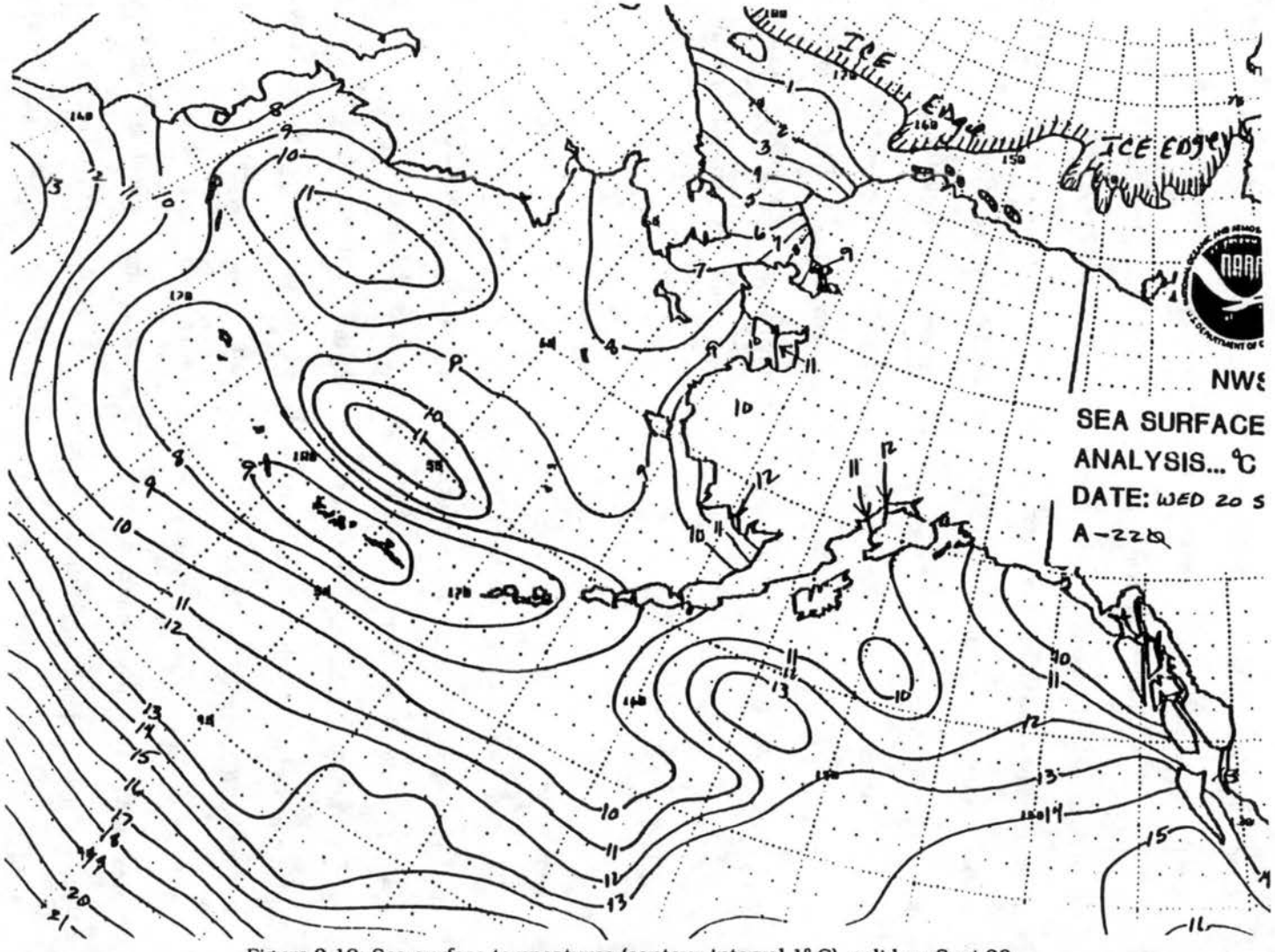

Figure 2.19: Sea surface tempeatures (contour interval 1° C), valid on Sept.20

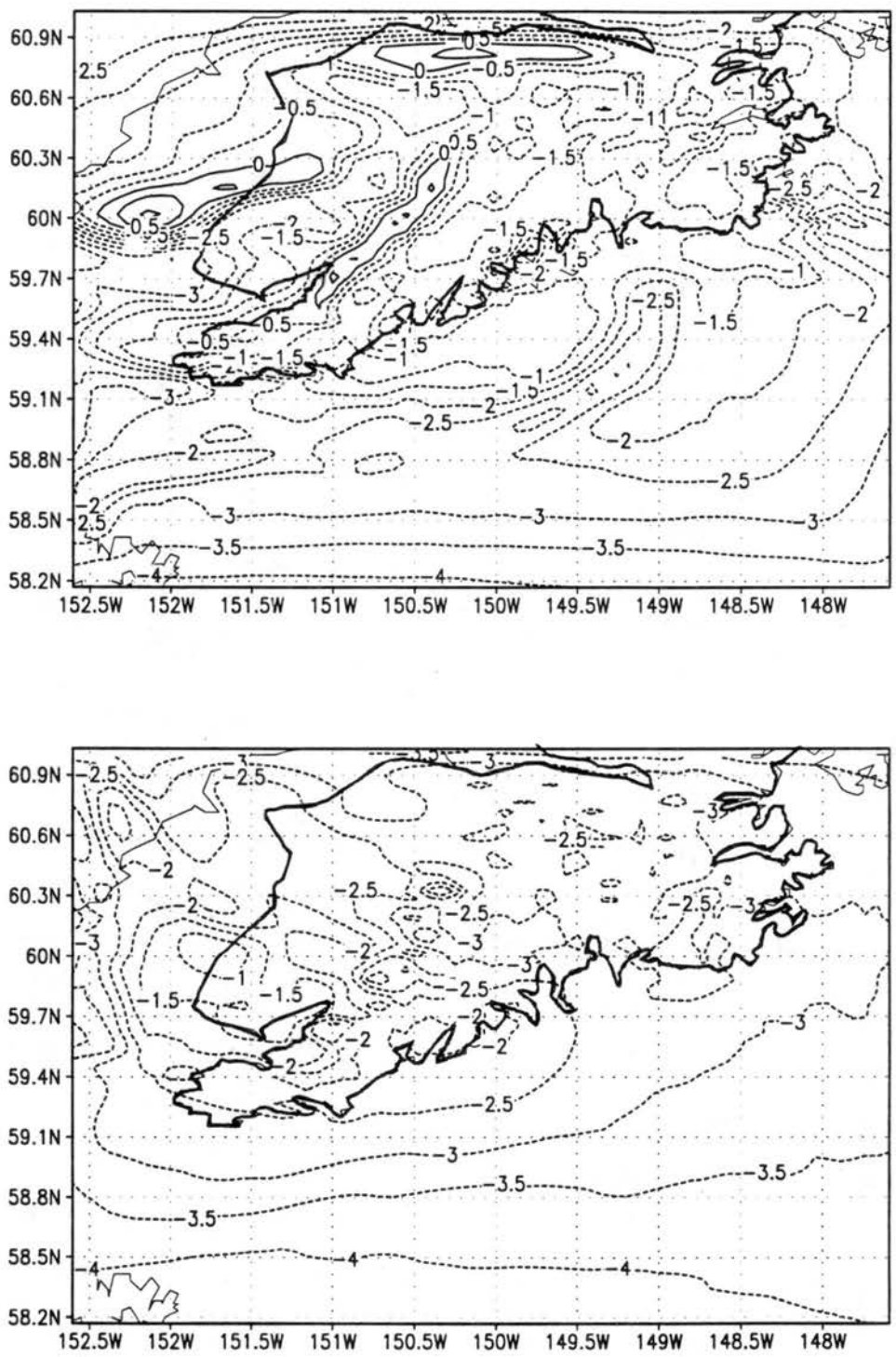

Figure 2.20: Horizontal wind speed differences (**kenai 5- kenai 6**) valid at 4z Sept 20, contours in 0.5 m s^{-1}. (top) at 99 m (btm) at 1492 m

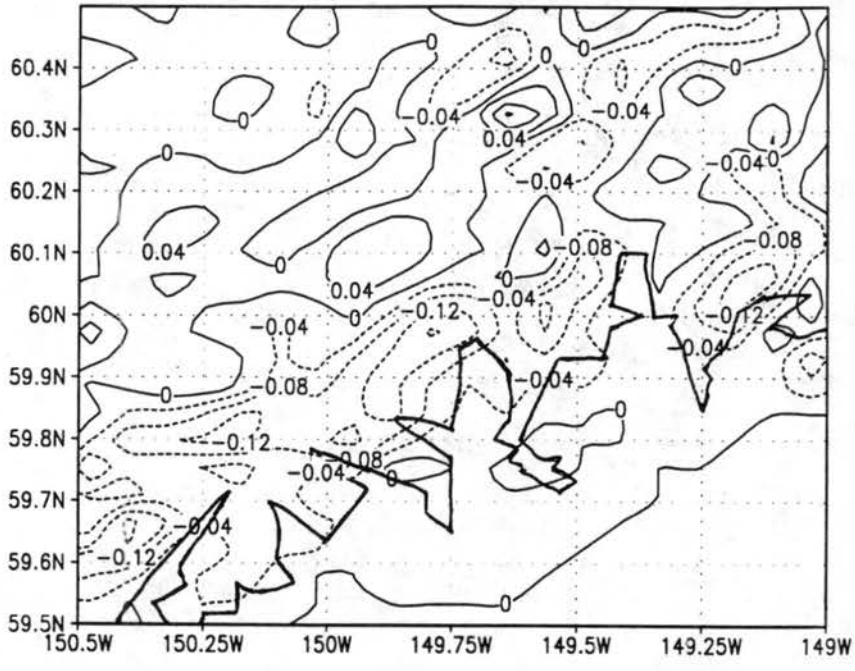

Figure 2.21: Zoom of vertical velocities (contour interval 0.04 m s^{-1}) for **kenai 5-kenai 6** valid at 0z Sept 21. Solid lines upward motion, dashed lines downward.

Figure 2.22 shows the difference in total 36 hr precipitation (**kenai 6-kenai 5**). Upstream of the coastline the increase precipitation is generally less than 15 mm. Over the steep slopes however, precipitation increases by 60-90 mm. To the lee of the barrier, precipitation is also increased significantly as the higher horizontal wind speeds advects it downwind from its generation over the barrier.

This plot is important because it shows a much greater difference in precipitation than the statistics based on the seven sampling areas do. The bias score for **kenai 6** is 41 mm with r^2= 0.84, very similar to those of **kenai 5**. What these numbers suggest is the limitation of statistics that are in turn based on a small sampling size, which in turn occur in areas of sparse data coverage. Figure 2.22 also indicates that the most significant differences occur at higher

elevations, and since the gages are biased toward low elevations (as they are in most mountainous locations), the statistics are not able to reflect these large differences.

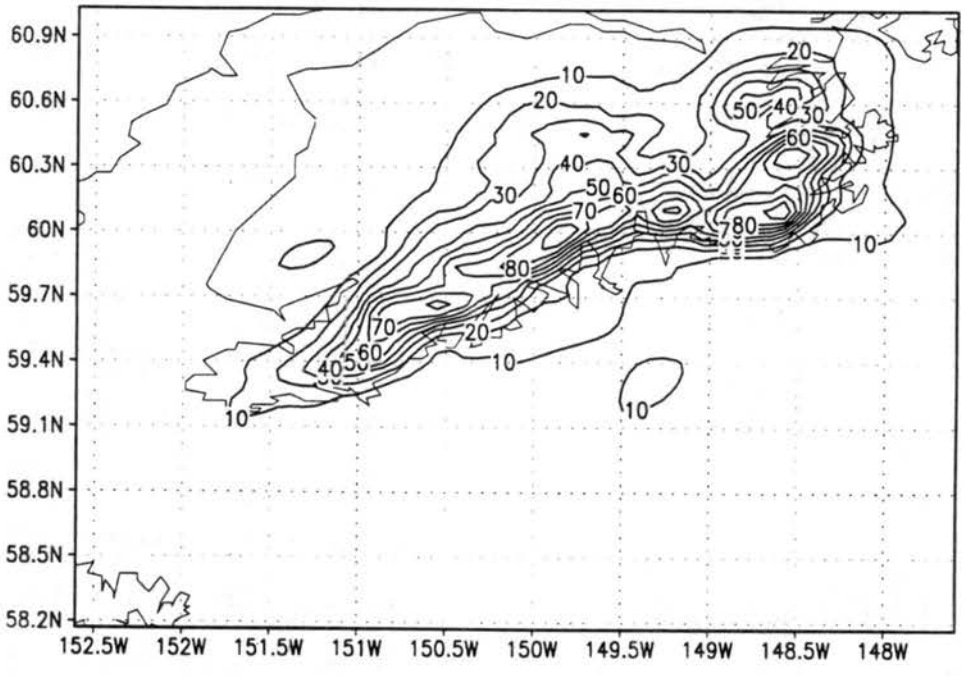

Figure 2.22: **kenai 6-kenai 5** total 36 hour accumulated precipitation (contour interval 10 mm)

Wind speeds affect the generation of precipitation in two ways: an increase in **U** should increase the magnitude of updrafts over steep terrain; and secondly, it will advect more water vapor through a given cross section per unit time. Higher wind speeds also affect the distribution of precipitation by advecting it further to the lee of the barrier. Hence uncertainties in initial wind speed conditions can lead to substantial differences in the amount of model accumulated precipitation.. It is hypothesized here that these wind speed affects will also be a function of the atmospheres stability. This and a number of other issues will be addressed in chapter 3 where a series of related sensitivity simulations are discussed.

Kenai 7:

Figure 2.23 shows the difference between **kenai 5** and **kenai 7** for total 36 hour precipitation. It is evident that there is virtually no difference over the Gulf of Alaska despite the 5° C decrease in **SST's**. Over the mountains, precipitation in **kenai 7** was reduced by 3-5%. The bias score for **kenai 7** was 43 mm. As with **kenai 6** it is interesting to compare Figures 2.22 and 2.23, keeping in mind that the bias score for **kenai 6** was 41 mm. This further illustrates the need to construct graphical difference plots in areas of sparse data, one should place less reliance on statistics since they could easily lead to erroneous conclusions.

Overall the cooler **SST's** and more realistic vegetation/land surface classification had minimal impact on the resulting precipitation. This does not mean that proper classification of the land surface is not important for many other types of simulations. However, in this particular case and in cases with strong synoptic forcing, the impact that the surface parameterizations have on the heat and moisture fluxes is small. The same remarks can be made about uncertainties in **SST's**, however, it is important to remember that as Autumn storms move northward from the southern and central Pacific Ocean, modification of these storms occurs as a result of interaction with the sea surface. The magnitude of this impact is yet to be determined, but in the simulations presented in this study, the limited size of the domain precludes the inclusion of a large upstream area over the North Pacific Ocean. If **SST's** had been increased instead of decreased, it is doubtfull if it would have made much difference in the results of **kenai 7**, since the model moisture is for the most part derived from the initial sounding.

2.9- Discussion

The initialization of the Sept. 19-21 storm seems to be in relatively good agreement with the NCEP analyzed fields, although due to a lack of surface and rawinsonde stations within the domain, there is, no doubt, a significant amount of uncertainty in those fields. Despite model and initialization deficiencies, RAMS is able to simulate a heavy precipitation event, and

it is apparent that for this case at least, that orography played the primary role in the generation and distribution of the precipitation. It is also quite probable that RAMS will perform better for this geographic location in cases with large-scale well defined synoptic scale forcing than in cases when the synoptic forcing is less well-defined. The reason for this is that the model is primarily initialized by synoptic scale data, hence a weaker less organized storm will have less chance of being initialized properly.

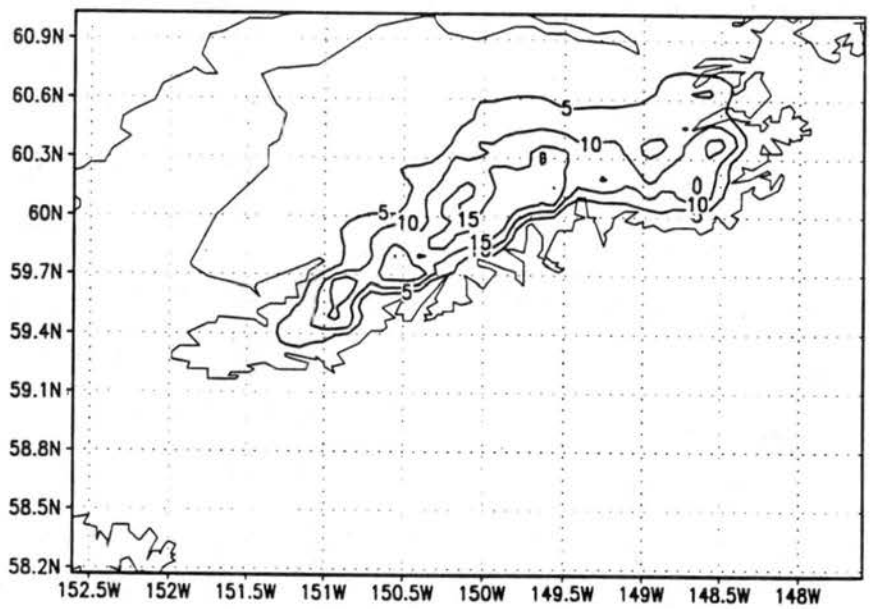

Figure 2.23: Precipitation difference for kenai5 minus kenai 7, valid for 12z Sept 20 (contour interval 5 mm)

It was apparent that the perturbation in wind speeds of 4 m s^{-1} was much more significant than perturbations in **SST's** and land surface classification, which leads to the conclusion that uncertainty in initial conditions *of state variables, such as temperature, wind*

speed, wind direction, and moisture will lead to much larger uncertainty in precipitation than initial uncertainty in **SST's** and land surface classification. In addition, the strict use of statistics in data sparse regions has to be cautioned; graphical representations should be a key component in interpretation of the results.

As eluded to in Chapter 1, there are limited examples in the literature of heavy precipitation events being simulated by a 3D primitive equation model. Bruintjes *et al* (1994) found that gravity waves were important in determining the distribution of precipitation across northern Arizona. In that case, however, the boundary layer was very dry, so terrain forced updrafts were a source for gravity wave generation, but did not play as large a role in cloud and precipitation formation as might be expected. This illustrates the significant difference between continental versus maritime storms; low-level flow in maritime environments tends to be at or near saturation during a storm. This means that a large percentage of the precipitation is generated from low-level moisture that condenses in the terrain forced updrafts; the net result is more precipitation on and over windward slopes when compared to the amount of moisture advected downwind by mid-level gravity waves. The implications are that precipitation gradients are much larger in maritime mountains than in continental regions, since precipitation tends to be distributed over a larger area via gravity waves in the latter case. The extreme maritime climate of the Southern Alps has many similarities to Alaska's Kenai Peninsula, hence the modeling work of Katzfey (1995a,b) is closely related to this study. In three cases modeled by Katzfey, the model he used was able to simulate roughly 50% of the peak and area-averaged precipitation. For **kenai 5-7**, RAMS tended at least for the Sept.19-21 storm, to underestimate precipitation at the lower elevations. At higher elevations it can only be speculated that the model performed within reason. Comparing high to low elevation precipitation (Seward compared to 1300 m on the windward slope) in **kenai 5**, gives a ratio in the 2:1-3:1 range, which is certainly reasonable. In the next chapter this will be discussed further, and it will be shown that the vertical increase of precipitation is a function not only of moisture and terrain configuration, but the atmospheric stability as well.

Results from **kenai 5-7** suggest that a number of processes are at work in a maritime mountainous environment, and are schematically presented in Figure 2.24.

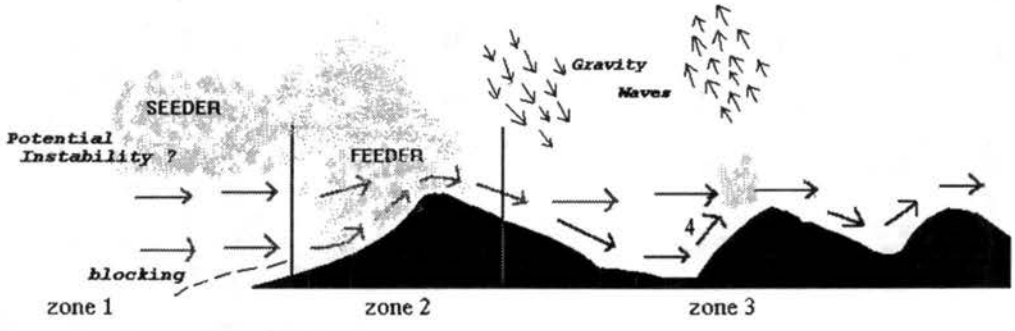

Figure 2.24: Schematic of an maritime mountainous environment

In **zone 1**, blocking with Fr~1.0 creates enough lift to trigger **potential instability,** this in turn preconditions the flow upstream of the first barrier. It also generates more precipitation over the ocean and coastline than would be seen if no blocking had occurred. In the real atmosphere additional influences such as frontal lifting, passing shortwaves and other instabilities could also produce upstream preconditioning. **Zone 2** shows a terrain-forced updraft, which is the source for gravity waves, and if there is enough moisture available, clouds and precipitation. **Zone 3** is a region that is one to seven kilometers above the surface where gravity waves dominate. These waves can carry various amounts of moisture depending on what is available upstream. In general, if gravity waves contain any hydrometeors, they will

be in the ice phase. This means they can be advected further downwind than cloud or rain droplets, and it also means they are subject to mass loss due to sublimation (Meyers and Cotton 1992). Gravity waves are also responsible for downslope warming. In **area 4,** low-level flow still follows the terrain, but the updrafts have significatly less condensation compared to their counterparts over the windward slopes, due to the the reduction in water vapor.

This schematic does not imply that potential instability is released upwind of the barrier in every event. If potential instability is present then other upstream lifting mechanisms could also be responsible for its release. In some cases gravity waves may or may not play an important role in the distribution of precipitation. In general, a spectrum of processes are involved in what is generally termed "orographic precipitation"; certainly much more than smooth forced ascent.

The next step is to attempt to answer some of the questions raised in this chapter. The utilization of RAMS horizontally homogenous option will be exercised in the following chapters because it allows the user to initialize and track the models output in a more controlled environment. The following issues will be addressed: 1) What role does stability have in controlling terrain forced updrafts, gravity waves, and precipitation? 2) How sensitive is the model to perturbations in wind speed and direction? 3) the value of the ensemble forecasting in the generation of QPF's; 4) The issue of terrain resolution. As the terrain resolution increases one would expect that the steeper slopes in the model will produce stronger updrafts and subsequently more precipitation, and finally; 5) what role does the horizontal grid interval play in the generation of model precipitation?

Chapter 3

MODEL SENSITIVITY EXPERIMENTS

3.1-Introduction

A wide range of numerical modeling studies that deal with atmospheric processes and are reported in the literature, fall into a category of simulations frequently referred to as horizontally homogeneous initial conditions (HHIC). These types of simulations as the name implies, are initialized with fields that may vary in the vertical but are homogenous in any given horizontal slice. Variable initialization as described in chapter one, is a more general technique that can under certain circumstances, generate a more realistic initialization than HHIC. Both techniques have their own benefits and limitations.

The decision on which technique to implement should be based on a number of factors: 1) The scale of the phenomena to be investigated. This dictates the size of the model domain. The larger the domain, the less likely that initial fields are going to be horizontally homogeneous; 2) The type of phenomena; 3) Quantity and quality of observed data. In data void regions HHIC may be warranted; and 4) The purpose of the simulation.

The strength of variable initialization is that it allows for spatial inhomogeneities to be initialized. Its major limitations are that it is computer intensive and the modeler has less control over the domain-wide initial conditions, being dependent upon objective analysis techniques. The biggest limitation of homogeneous initialization is that it does not allow for horizontal inhomogeneities at the start-up, such as fronts or convergence zones, although they are free to develop as the simulation progresses. Two significant benefits to this approach, however, are 1) it is much less time consuming, allowing for a considerably larger number of simulations for the same computer resources, and 2) since the model is initialized by a single

sounding the initial conditions are well understood. What this means is that HHIC is more conducive to what are generally called sensitivity studies. In these types of studies a control run is performed based on the best set of initial conditions. The subsequent runs are set up so usually only one variable is perturbed from its control run value, and the model is re-run to determine the significance of that perturbation on the model fields. Once a suite of these runs have been constructed, then model analysis can take the form of *factor separation* (Stein & Alpert 1993. section 3.6), or ensemble forecast (section 4.2).

The set-up of the model used in this chapter is similar to that used in chapter two except for the initialization process. A large number of simulations are presented in this chapter; each simulation was run for a total time of 6 hours. It takes the model from 2 to 3 hours to reach a quasi-equilibrium state with respect to wind speed, temperatures, precipitation rates, etc. There is no magical value in simulations with a duration of six hours, however it was judged that due to the number of simulations that were attempted, and due to the volume of data generated, that there was little benefit to extending the run time for these cases. In general, a doubling of the six hour total precipitation is a good estimate of the precipitation generated over a full 12 hour simulation.

One of the primary benefits of the HHIC technique is that it allows the modeler to focus attention on specific model physics and how it may or may-not relate to the real atmosphere. In light of this discussion, section 3.2 considers the role that wind direction plays in the enhancement of orographic precipitation; section 3.3 focuses on moisture ; 3.4 stability; 3.5 focuses on the sensitivity to wind speed; and section 3.6 considers factor separation.

3.2-Wind Direction

The direction in which the mean flow approaches an elevated barrier is important because as Douglas and Glasspoole (1947) noted, updrafts reach their maximum values when the flow is orthogonal to the barrier axis. This can be seen from: $W \approx \mathbf{U} \cdot \nabla Z$ where Z is the terrain height. Since **U** is a vector, both its magnitude and direction are important. The gradient is calculated along the direction of the inflow which in most circumstances may not

correspond to the steepest part of the slope.

Inflow changes direction because either a storm is moving across the domain or some dynamic process such as blocking is occurring. In a low to moderate blocking scenario, only the winds in the boundary-layer are deflected from the original direction. In cases of extreme blocking, a barrier jet may form (Wesley 1991, Meyers and Cotton 1992), creating a localized wind maximum parallel to the barrier.

In this section three simulations (**k6, k16, k17**) were conducted in order to investigate the difference in model-generated precipitation for three different wind directions. Using **k6** as the control run (wind speed= 20 m s^{-1}, lapse rate= -5° C km^{-1}, surface temperature= 12°C, wind direction= 180°), **k16** was set-up identically except the winds were initialized out of 150°, and in **k17** from 210°.

Figure 3.1 displays the total precipitation for these runs. In **k17** the flow is parallel too much of the southwest-northeast axis of the barrier, hence the precipitation is minimal except around 149° W where a series of slopes with southwest aspect generate moderate precipitation. The difference between **k6** and **k16** is not as dramatic. On the eastern third of the peninsula precipitation is reduced in **k16** because the southeast facing slopes are less steep than their southerly or southwest counterparts. Over the central and western regions of the barrier, many of the steepest slopes have a southeast orientation, boosting the precipitation maxima by some 15-30%.

3.3-Perturbed Moisture Fields

Moisture availability is obviously critical to the formation of precipitation, however it is a difficult field to measure. Rawinsonde data provides the bulk of the moisture data, and it is well known that at high relative humidity, the sensors have a low bias (Schwartz and Doswell 1991). As a first guess it is possible that during heavy precipitation events (especially rain events), rawinsonde data underestimates atmospheric moisture by 3-6%.

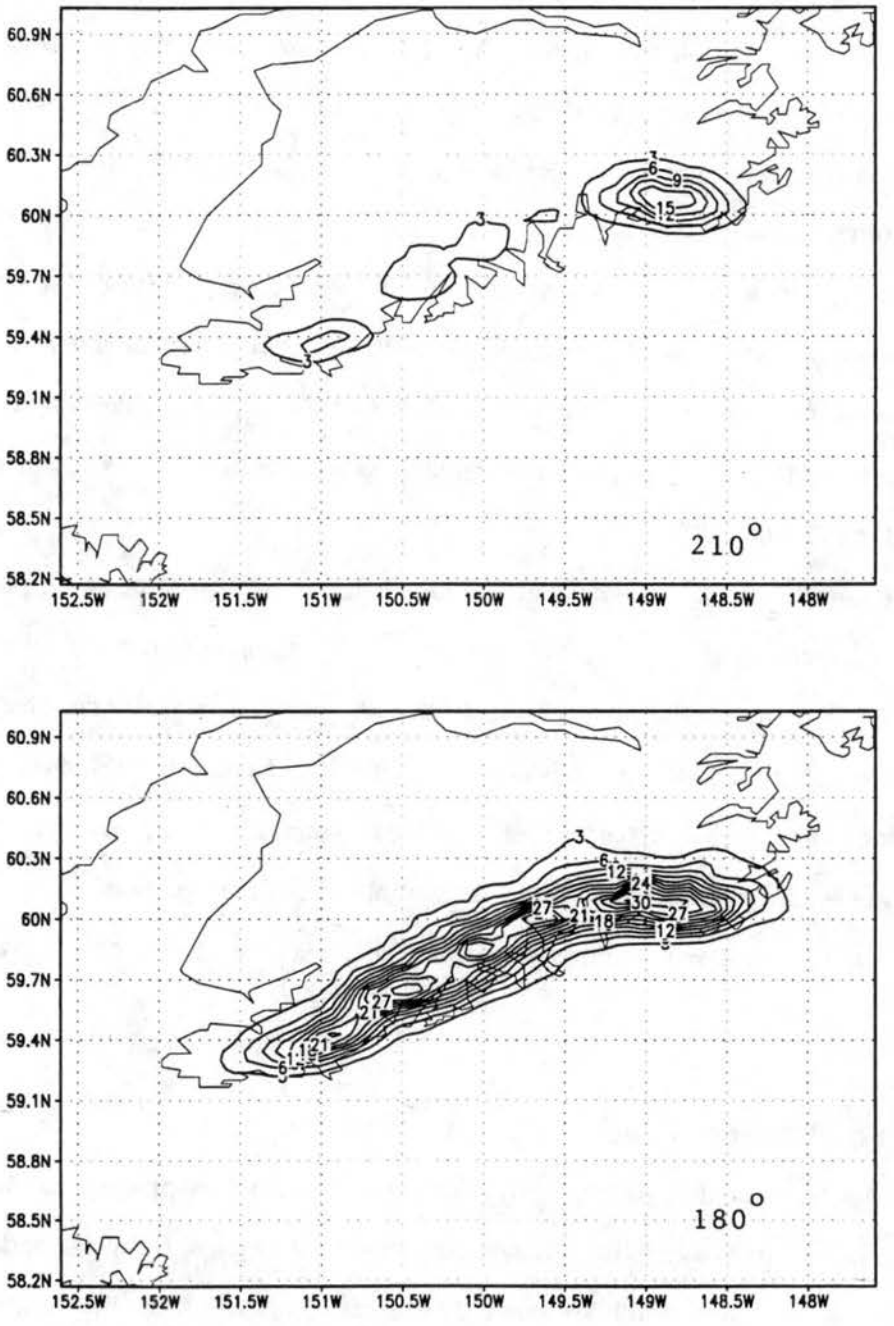

Figure 3.1: Total precipitation as a function of wind direction (contour interval 3 mm). (top) **k17**, wind 210° (btm) **k6**, wind 180°

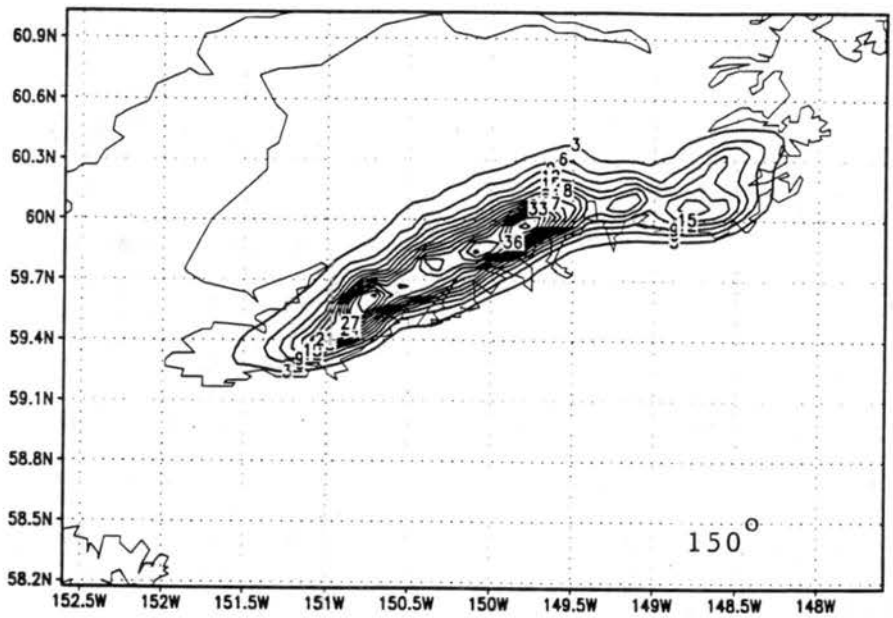

Figure 3.1 continued: **k16**, wind 150°

In order to investigate the sensitivity of RAMS to perturbations in the initial moisture field, three simulations were conducted using three different initial moisture values. In the set-up of these runs, the moisture was specified by using dew point temperatures. The difference between the air temperature and dew point temperature is the dew point depression. Using **k6** as a control run, dew point depressions were then perturbed by ±1° C (Table 3.1).

Table 3.1: Moisture Simulations			
run	dew point depression	moisture difference	averaged precip.
k13	-2° C	-0.44 gm kg^{-1}	77 mm
k6	-1° C	0	198 mm
k14	0° C	+0.65 gm kg^{-1}	271 mm

Table 3.1: Comparison of simulations that were initialized with three different dew point depressions. Averaged precipitation based on 10 N-S cross sections.

Examination of the **W**-component for these three runs reveals a roughly 10% increase in the magnitude of the terrain-induced updraft as moisture is increased. Downstream of the barrier crest gravity wave downdrafts are 5-10% weaker in **k14** when compared to **k6**. In an area some 50-20 km upstream of the coastline, ascent rates are only in the 0.05-0.1 m s^{-1} range, but they are notably stronger in **k13** than in **k14**. Within 20 km of the coast however, ascent rates in **k14** are larger.

These perturbations in the **W**-component appear related to the release of latent heat over the barrier as described by Meyers and Cotton (1992) and Katzfey (1995b). In the latter study Katzfey noted that the release of latent heat increased the ascent rates over the barrier in addition to decreasing the vertical stability. The net result was increased low-level convergence over the mountains, and weaker gravity waves to the lee. In terms of precipitation, peak rain over the mountains increased as a result of latent heating effects, while it decreased in the surrounding regions.

Increased moisture may result in a slight reduction in upstream blocking, but appears to be partially compensated for by triggering of potential instability. Table 3.1 indicates the non-linear nature of the production of precipitation with respect to the availability of moisture, while Figure 3.2 displays total precipitation for one N-S cross section. The volume of precipitation produced between **k13** and **k6** is much greater in terms of percentage than from **k6** to **k14**. It seems probable that in the case of a saturated (**k14**) or nearly saturated atmosphere, that a large percentage of moisture condenses and forms precipitation well upstream of the barrier (tens of kilometers), so that by the time the flow reaches the barrier it is drier than the initial sounding would suggest.

3.4-Stability

The role which atmospheric stability plays in orographic precipitation generation or enhancement has been neglected in most studies, with the exception of Bradley (1985), who suggested that a stable, slightly sub-saturated atmosphere is a more efficient producer of precipitation than a potentially unstable atmosphere.

In this section a series of five runs all with the same surface temperature of 12° C but with lapse rates ranging from -4° C km^{-1} to -8° C km^{-1} , were generated in order to evaluate the role of atmospheric stability on the distribution of precipitation (table 3.2).

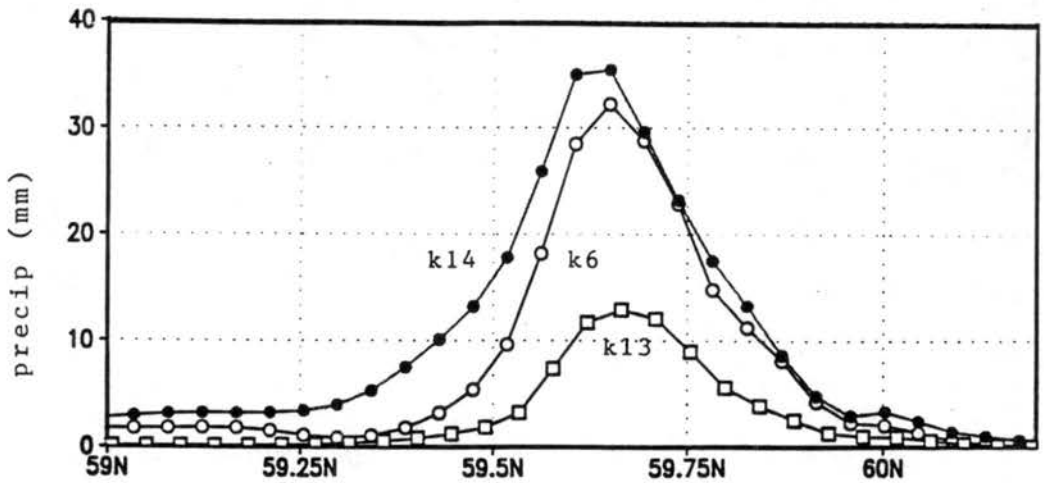

Figure 3.2: Total precipitation (mm) for N-S cross section through 150.5° W. Solid circles **k14**, open circles **k6**, and open squares **k13.**

Table 3.2: Stability Simulations			
run	lapse rate (° C km^{-1})	Froude Number	ave. precip (mm)
k11	-8	1.60	77
k9	-7	1.33	146
k1	-6	1.21	187
k6	-5	1.06	198
k12	-4	0.96	92

Table 3.2: Pertinent model data for five stability simulations. The Froude Number is calculated upstream of the barrier at the end of the 6 hour simulation. Winds were from the south at 20 m s^{-1} with a surface temperature of 12° C

Moisture for each run was initialized using a dew point depression of -1° C. This results in runs that have varying amounts of initial moisture, hence, in general, one would expect *a priori* that precipitation will decrease with increasing lapse rates. Comparison of total precipitation from one run to the next, therefore, has to be handled with caution. What is of primary interest are changes in vertical velocities and the areal distribution of precipitation.

In order to establish a typical lapse rate for heavy precipitation events that occur over the Kenai Peninsula, 15 events were analyzed for 1000mb-700mb and 1000mb-500mb lapse rates. These events consisted of days with a minimum of 6 cm of rain recorded at Seward, and occurred during the months of August, September, or October. This includes the 24 hour precipitation record for the state of Alaska, which occurred on October 10, 1986, resulting in 38.3 cm of rain at Seward. The results are:

1000-700mb: mean lapse rate= -5.2° C km^{-1} Std. Dev.= -0.7° C km^{-1}

1000-500mb: mean lapse rate= -5.5° C km^{-1} Std. Dev.= -0.5° C km^{-1}

This sampling indicates that heavy rain events occur within a moderately stable atmosphere.

Figure 3.3 shows that as lapse rates increase, vertical velocities experience a complex evolution. For all five runs the following scenario holds true: As the lapse rates increase, the terrain induced updrafts increase in height, and the magnitude of the strongest updrafts increase from 0.6 m s^{-1} in **k12** to 1.2 m s^{-1} in **k11**. The reason that updrafts increase in this last example is because the inflow to the barrier in **k11** is roughly 4 m s^{-1} stronger than in **k12**, due to the stronger upstream blocking occurring in the latter.

From 500 m to 3000 m AGL, the 0.2 m s^{-1} contour for example extends approximately 10 km further upstream in the runs with lower lapse rates when compared to the higher lapse rate cases, due to blocking. To the lee of the crest (59.8° N for figure 3.6), the gravity wave downdrafts are more extensive but not necessarily of a larger magnitude, in cases when the lapse rates are lower. These examples point to the importance of the interaction between stability, blocking, and vertical motion. There is a trade off between the velocity of the air

approaching a barrier and the stability via blocking, once a terrain updraft has generated gravity waves, the stability downstream of the barrier determines the extent and magnitude of the resulting waves.

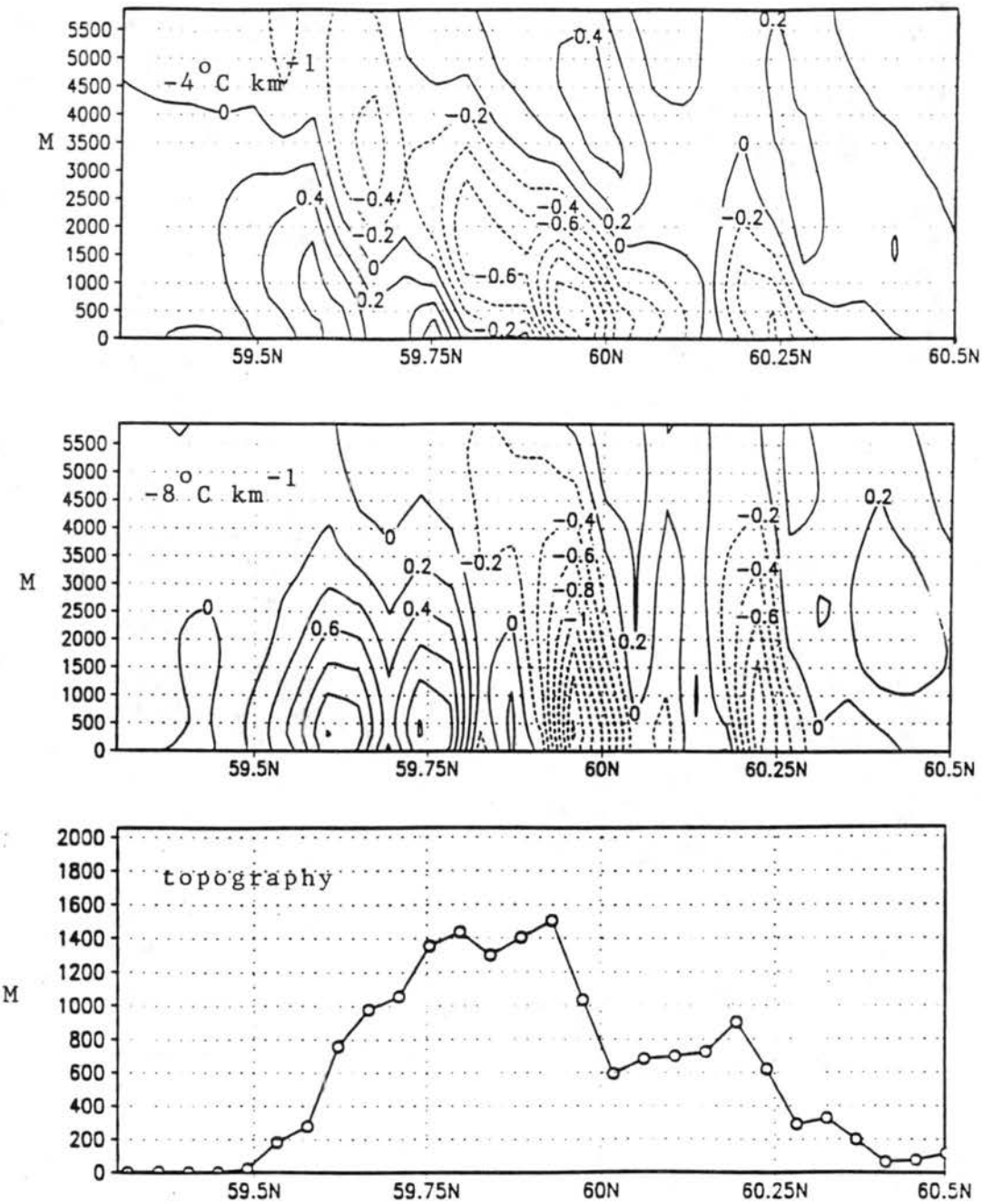

Figure 3.3: Vertical velocities (contours 0.2 m s^{-1}) for N-S cross section through 150.5°W.
(top) **k12,** lapse rate =-4° C km^{-1} (mid) **k11,** lapse rate =-8° C km^{-1} (btm) topography (m)

As seen in figure 3.4, as lapse rates increase the general trend is for more precipitation to fall out to the lee of the barrier. This occurs at the expense of the accumulated precipitation over the windward slopes, in other words, the ratio of precipitation on the lee to the windward slopes decreases as the stability increases. Figure 3.5 shows the precipitation ratio P_{lee}/P_{wind} as a function of the Froude Number. One would be tempted to conclude from this plot that at a Froude Number around 1.0, the highest potential for large precipitation and flooding would occur. However, the volume of precipitation must be taken into account, and it will be shown in the next section that wind speeds play an important role in that process.

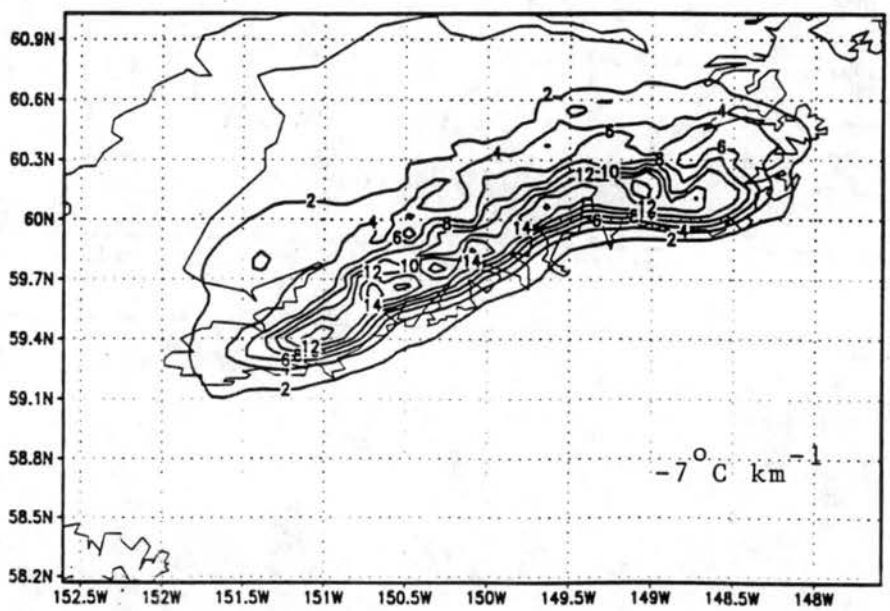

Figure 3.4: Total precipitation for **k9** (lapse rate =-7° C km^{-1}, contour interval 2 mm)

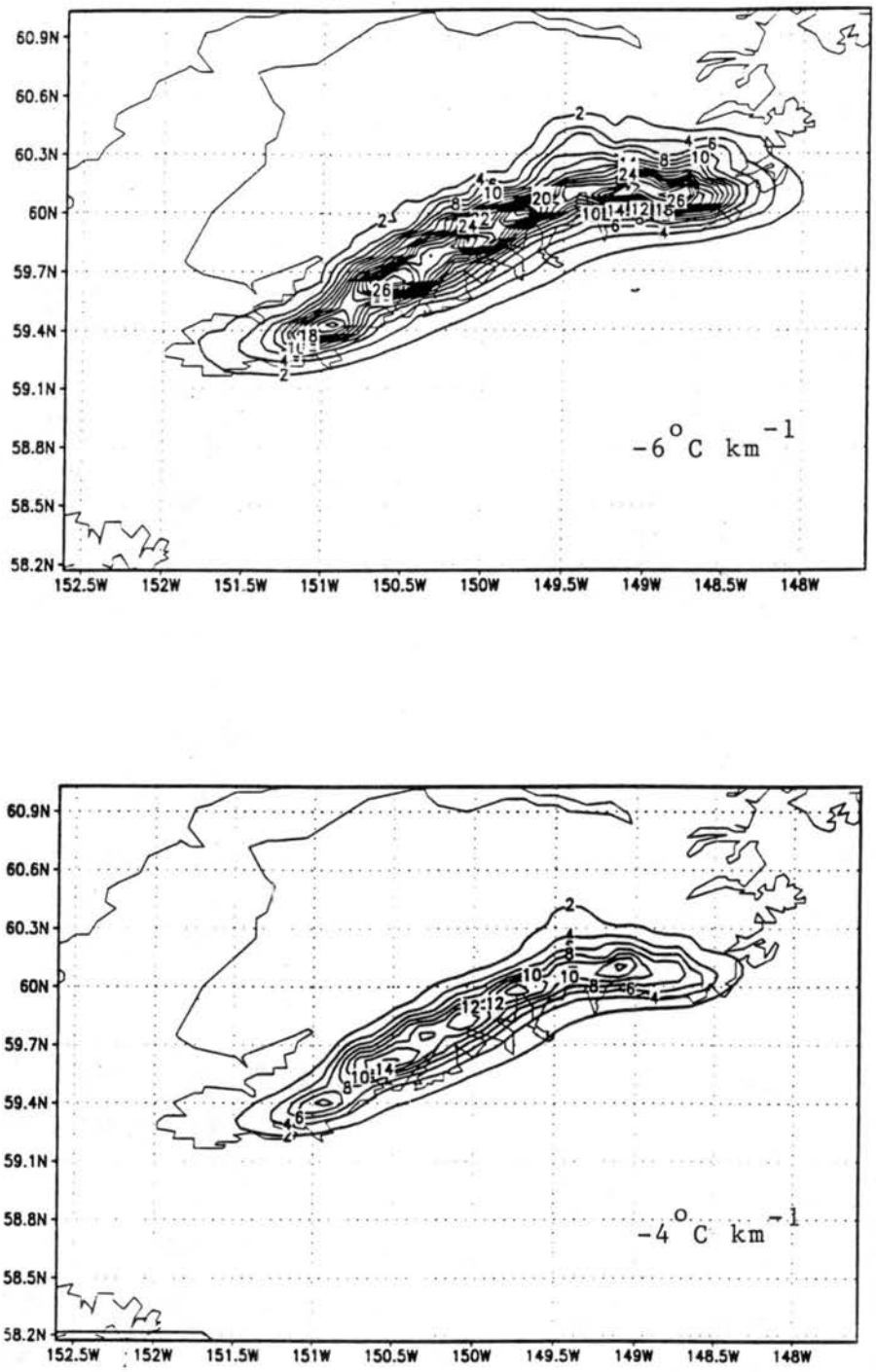

Figure 3.4 continued: (top) **k1**, lapse rate =-6° C km^{-1} (btm) **k12**, lapse rate =-4° C km^{-1}

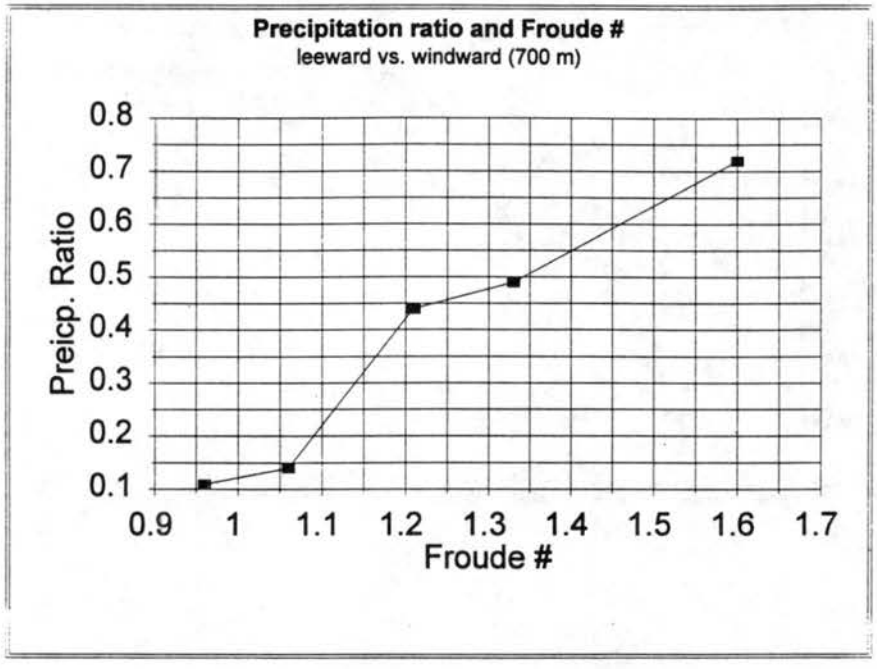

Figure 3.5: Precipitation ratio of leeward versus windward slope (along 700 m contour) as a function of the Froude Number.

Comparing individual runs provides deeper insight into the production of precipitation. Comparing **k12** to **k6** (table 3.2) shows that a larger volume of precipitation was generated (215%) in the case of the latter, *despite a lower initial total mixing ratio.* Examination of the condensation mixing ratio shows that condensation is increased at an elevation of 2 km, both upstream and directly over the barrier in **k6**. For comparison, in **k9** and **k11** mid-level gravity wave downdrafts are either significantly reduced or have been replaced by updrafts, allowing hydrometeors to form further downstream in these cases. It should also be noted that in **k11** the resulting precipitation is less anchored to the terrain than in the more stable cases. This is especially true to the lee of the windward barrier. The important implication is that in a weakly

stable atmosphere, precipitation begins to become detached from the terrain (i.e. the probability that heavy precipitation could occur in a valley or at low elevations starts to become equal to the probability at higher elevations).

In order to evaluate the role of potential instability in this suite of runs, plots of condensation mixing ratio and θ_e for **k11** and **k6** are shown in figure 3.6. In **k11** the highest condensation mixing ratio occurs directly over the steep windward slope and has a value of 7 gm kg^{-1} , while in **k6** it reaches 12 gm kg^{-1}.

It is evident that more condensation is occurring upstream of the coast (59.5° N) in **k6**, but **k11** generates a larger area of condensation downstream of the barrier. Are the upstream condensation plumes in **k6** related to potential instability ? Even though these plots are far from definitive, Figure 3.6b suggests that these plumes are forming in regions that are weakly stable with respect to θ_e. If all five runs that make up this suite are considered, then it appears that potential instability may enhance condensation upstream of any terrain in an atmosphere that is moderately stable (-6 to -7° C km^{-1}). However, this may not enhance precipitation. In a very stable atmosphere (**k12**), potential instability is not expected to be realized because of the overwhelming influence of the vertical profile of θ. In addition, extreme blocking and flow diversion limits areas of updrafts. For near neutral (**k11**) or unstable cases, there is little upstream lifting of the approaching flow, hence potential instability is initiated over the barrier itself and may not be distinguishable from strong updraft cores. In cases of moderate stability the combination of upstream lifting due to modest blocking and a favorable θ profile seems to allow for the release of potential instability.

In order to further investigate the hypothesis that potential instability may increase condensation and precipitation upstream, an additional run (**k15**) was designed to enhance low-level instability. This run had an identical set-up as **k1** except the dew point depression was set to 0° at the surface and increased linearly with height to a value of -2° at 2 km, and from 2-6 km it remained constant at -2°. This set-up represents an increase in convective instability over **k1** due to the drying with height. This profile preserves the -6° C km^{-1} lapse rate while maintaining the same amount (within 1.5%), of the moisture in the lowest 2 km as in **k1**.

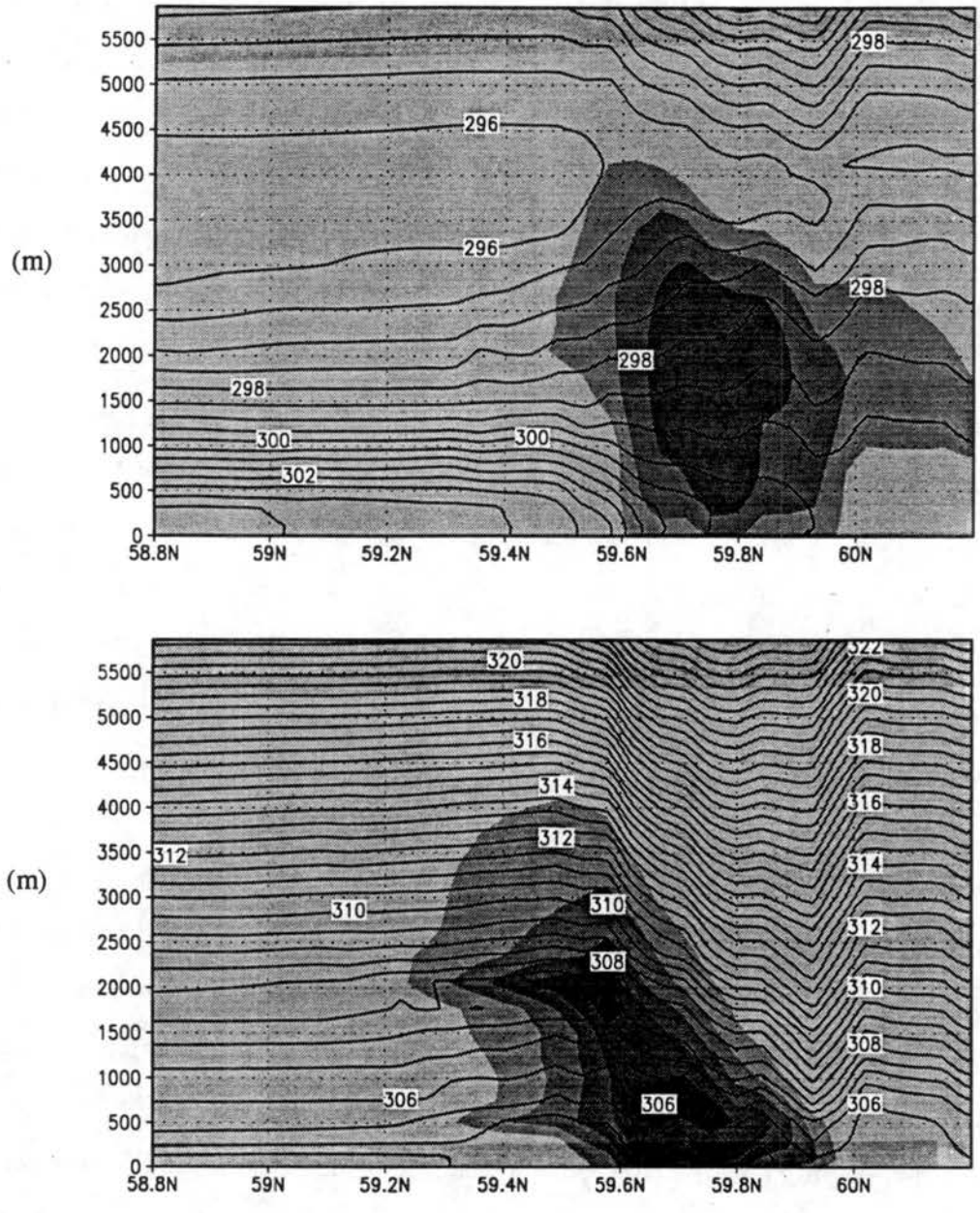

Figure 3.6: Condensation mixing ratio (shading with contour interval of 0.002 kg kg^{-1}) and equivalent potential temperature (contour interval 0.5° K), for N-S cross section through 150.5° W. (top) **k11,** lapse rate =-8° C km^{-1} (btm) **k6**, lapse rate =-5° C km^{-1}

Inspection of the **w**-component in **k15** (not shown) indicates a slight reduction in vertical velocities, however condensation was enhanced upstream of the coastline. In the lowest 3 km, θ_e indicates that **k15** is more unstable than **k1**. Using the aforementioned 10 N-S cross sections, precipitation in **k15** is reduced by 15%. This reduction in precipitation is uniformly distributed across the barrier. The implication is that when potential instability is triggered it does not appear to be as efficient at producing precipitation as does smooth forced ascent in a stable atmosphere; a confirmation of Bradley's (1985) suggestion. What this *does not mean* is that convective instabilities are not important in the orographic precipitation process. If these results are representative of the atmosphere, then it means that the most efficient means of producing heavy precipitation is when the atmosphere is stable enough to generate upstream blocking but not stable enough to prevent modest amounts of embedded cumulus convection.

It also has to be kept in mind that an instability may be released upstream of the barrier that is completely independent of the terrain (i.e. baroclinc or symmetrical instabilities), which will be an added complication to the idealistic results presented in this study. These are certainly only preliminary results that need further investigation and validation. A set of aircraft observations through the upstream region of a maritime mountainous region such as the Southern Alps, during a heavy precipitation event would certainly help clarify this issue.

3.5-Perturbed Horizontal Wind Speeds

In order to obtain a comprehensive understanding of the sensitivity of precipitation and vertical motion to perturbations in the horizontal wind speed, a suite of four runs is presented. This suite (**k10**, **k6**, **k8**, **k7**) was initialized with southerly flow that was uniform with height, with speeds of 15, 20, 25, 30 m s^{-1}, respectively. The lapse rate for each run was -5° C km^{-1}, which was noted in section 3.4 as a typical value for heavy Autumn precipitation events along the Southern Kenai Peninsula and North Gulf Coast. Moisture was specified using a dew point depression temperature of -1° C from the surface to 3 km.

Figure 3.7 shows vertical velocities for a N-S cross section. As expected, dramatic

increases in terrain induced updrafts and gravity wave downdrafts/updrafts are evident for the higher wind speed cases. Not only are the magnitudes increased but the size of the updrafts/downdrafts are expanded as well. Larger gravity wave velocities are to be expected since the perturbation vertical velocities are a function of the mean horizontal wind speed (Durran 1990). As the horizontal wind speed is increased it is evident that the ascent rates upstream of the barrier (at 59.5° N), are also increased significantly.

Analysis of the perturbation pressure for **k6** (not shown) indicates a +1.5 mb value at 6 hrs, while in **k7** it is +5.0 mb. These values are maxima located at the base of the windward barrier, and decrease with height. The implication is that there is a larger decrease in the horizontal wind speeds from 0 hr to 6 hr in **k7** versus **k6**, because of greater dynamic mountain blocking in the former. Due to mass continuity, the winds in the east-west or vertical dimensions will increase accordingly (Meyers and Cotton 1992).

It should also be noted that at 6 hrs the winds are no longer pure southerly; instead the dynamic mountain blocking has caused the flow in the first 500 m of the model atmosphere to become more S-SE as it approaches the coastline. The effect is larger at lower wind speeds.

Inspection of the total water vapor mixing ratio (**rtotal**), shows lines of constant **rtotal** tilt upward toward the barrier well in advance of the coastline. As the horizontal wind speeds increase the tilt moves further and further upstream. In addition, plots of θ for **k7** and **k10** show that the isentropes in **k10** begin to slope upward, relatively close to the coastline and only below 2 km. In the higher wind speed case (**k7**), tilting begins further upstream and extends to a height of about 3 km.

Condensation mixing ratios increase with increasing horizontal wind speed, primarily in the terrain induced updrafts directly over the steepest slopes. There is an additional increase in condensation in a zone extending roughly 30 km upstream of the barrier. Cloud droplets form at altitudes below 3 km AGL, while from 3 to 4.5 km pristine ice. For the higher wind speed simulations presented in this section, increases in condensation mixing ratios were minimal for areas downwind of the coastal barrier.

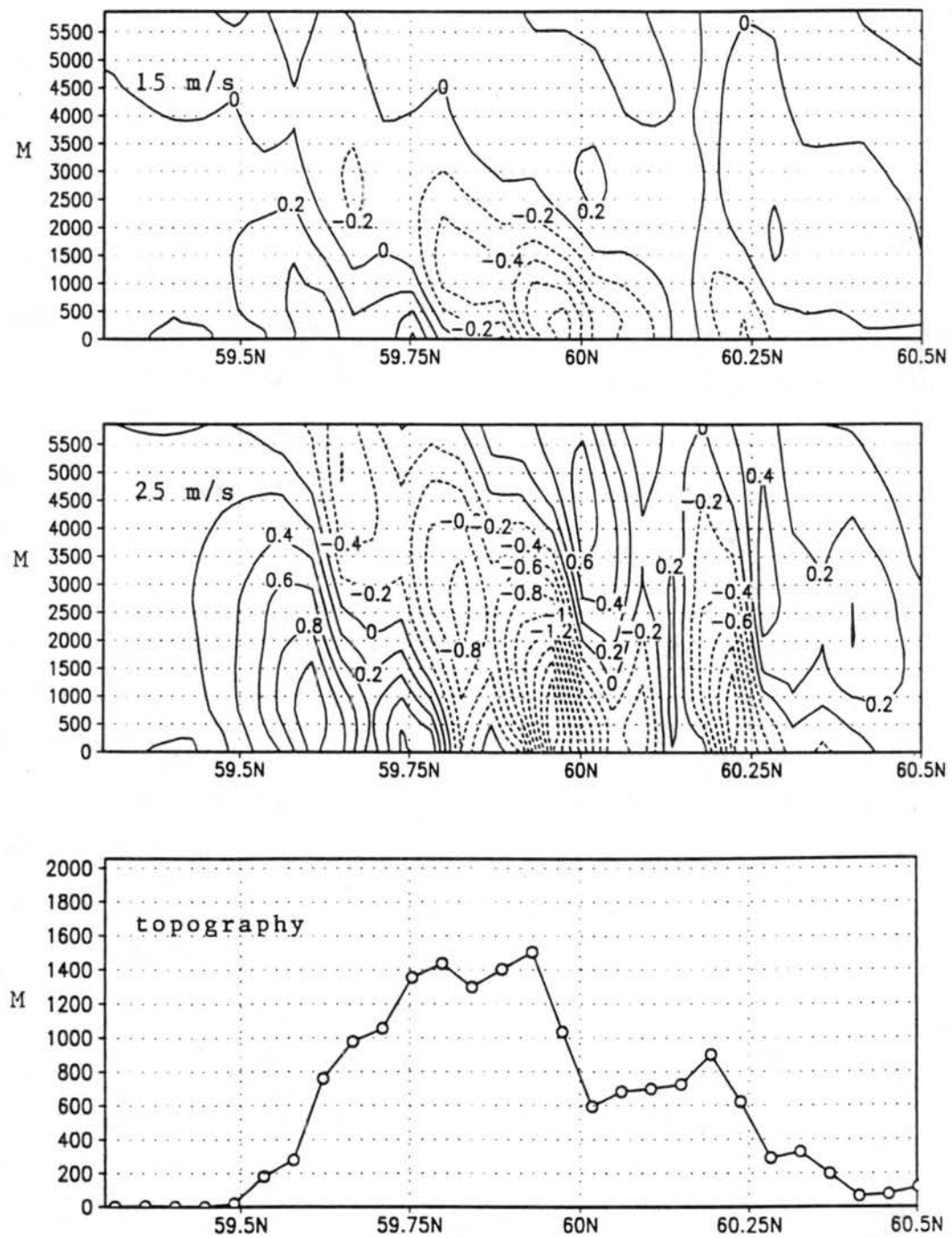

Figure 3.7: Vertical velocities (contour interval of 0.2 m s^{-1}) for N-S cross section through 150.5°W. (top) **k10**, wind speed =15 m s^{-1} (mid) **k8**, wind speed =25 m s^{-1} (btm) topography (m) for comparison.

Precipitation:

Figure 3.8 shows the total precipitation after 6 hours for the 15, 20, 25, 30 m s^{-1} horizontal wind speed cases. It is apparent that both the volume and areal distribution of precipitation is sensitive to the range of perturbations introduced in this suite of runs. There is little enhancement upstream of the coastline (generally 2-5 mm increase over the Gulf of Alaska for the 20-30 m s^{-1} cases), despite the enhanced condensation described earlier in this section. There is however significant increases over the windward barrier and to the lee of the barrier. There is also some evidence that with this type of predominately southerly flow, that significant moisture is advected up the Resurrection Valley (lon: 149.4°W), well into the interior. Overlaying plots of precipitation on topography show that the precipitation maxima occur slightly to the lee of the steepest slopes and not necessarily over the highest ridges or summits.

A number of investigators (Carruthers and Choularton 1983, Bradley 1985) have suggested that as wind speeds increase, the region of maximum precipitation moves downwind in response to the advection of hydrometeors. Bradley (1985) found that precipitation maximum moved some 50 km downwind in one stable case. This was attributed to the fact that low-level condensation rates (feeder cloud) exceeded the amount of moisture that hydrometeors originating from higher level clouds (seeder clouds) could washout. This was due to the fact that in these early models the seeder cloud rates were fixed (no dynamic forcing involved). Those results are directly opposed to the results found in this study. The results presented here show that precipitation does increase to the lee of the barrier as wind speeds are increased, but in general the precipitation maxima do not shift downstream. This does not necessarily hold true in an atmosphere that is either neutral or unstable. Figure 3.9 shows the average precipitation for 10 N-S cross sections as a function of the initial horizontal wind speed. This indicates a very linear response for the volume of precipitation but this plot does not of course say anything on how precipitation is distributed across the model domain.

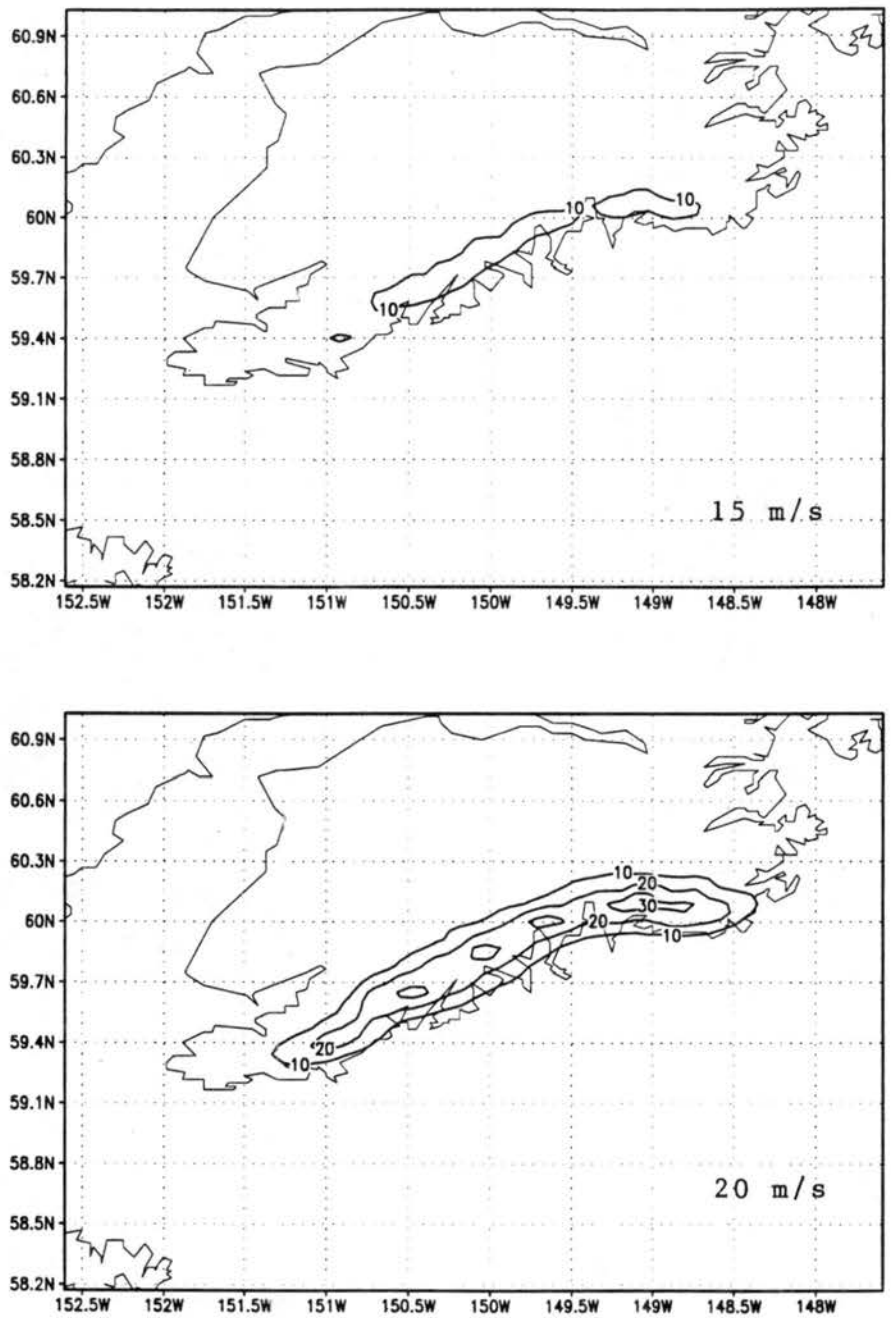

Figure 3.8: Total precipitation (contour interval 10 mm). (top) **k10**, wind speed =15 m s^{-1} (btm) **k6**, wind speed =20 m s^{-1}

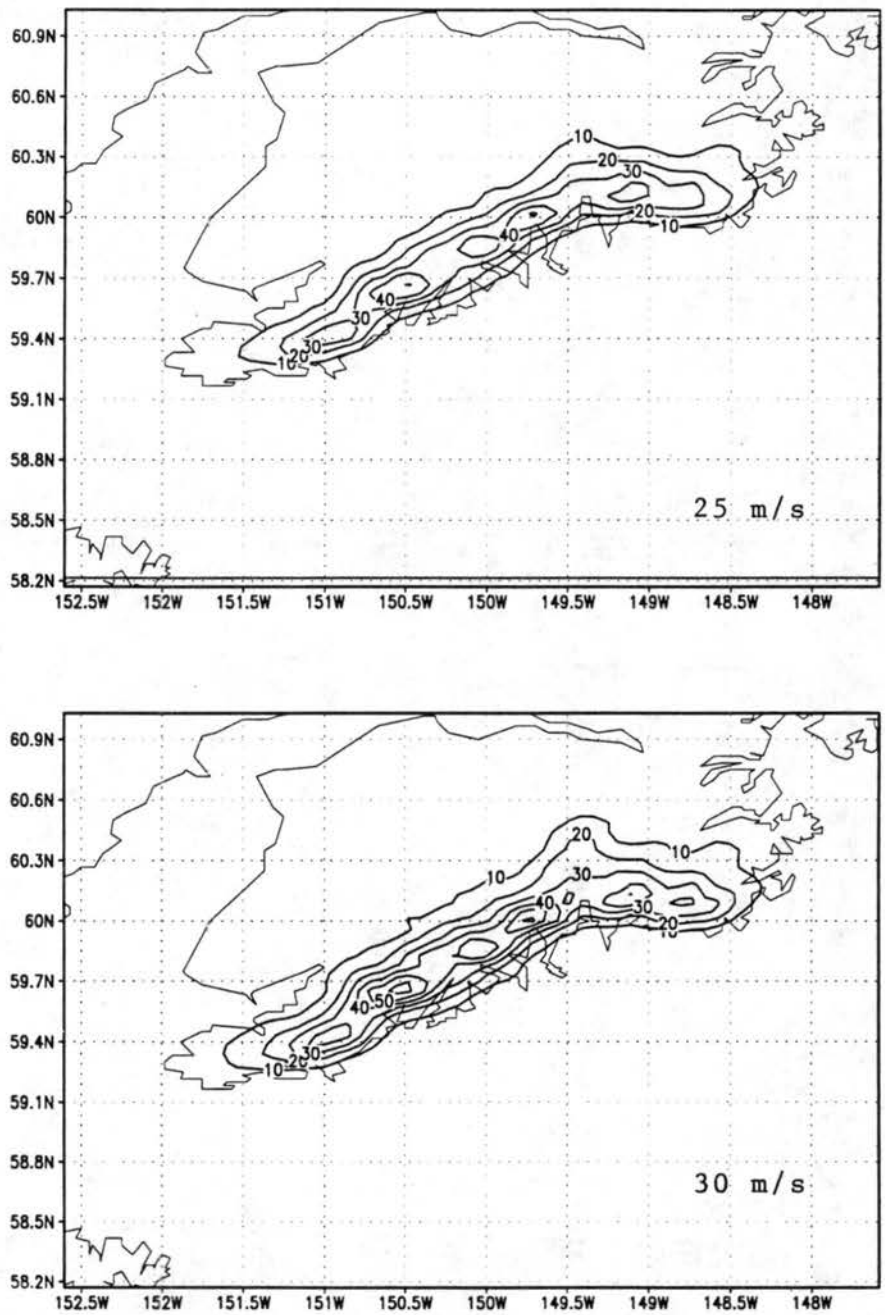

Figure 3.8 continued: (top) **k8**, wind speed =25 m s^{-1} (btm) **k7**, wind speed = 30 m s^{-1}

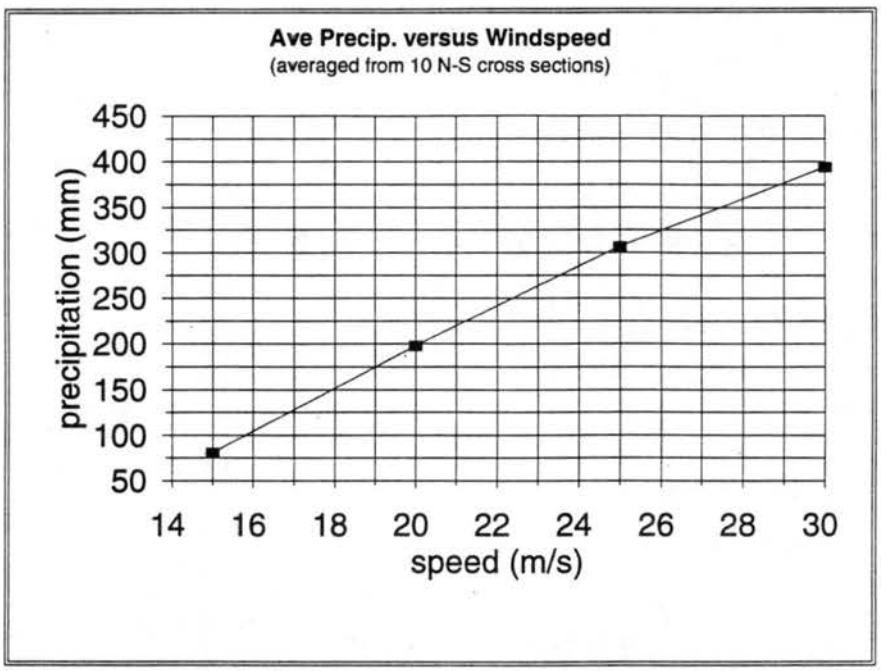

Figure 3.9: Precipitation (mm) averaged for 10 N-S cross sections as a function of wind speed (m s^{-1})

It is also of some value to repeat this wind speed experiment for additional lapse rates. Figure 3.10 displays averaged precipitation for lapse rates of -4, -5, -6 and -7° C km^{-1}. Since the dew point temperatures were held constant at -1° C, the amount of moisture decreases as the lapse rates increase. As a result the lines in Figure 3.10 are not expected to be coincident, but a comparison of their slopes is noteworthy.

Considering the case with a lapse rate of -4° C km^{-1}, its plot shows the effects of blocking at wind speeds at or below 20 m s^{-1}. Its value is significantly less than the other three despite having considerably more moisture. At the higher wind speeds, it leaves the blocking regime and precipitation increases accordingly, however, it is still below the -5° C km^{-1} case. In this stable of an atmosphere, vertical velocities over the barrier are suppressed when

compared to the later cases. At a speed of 15 m s^{-1}, the next three cases are identical. As speeds increase however, the *rate* at which the -6° and -7° C km^{-1} cases increase is reduced. Inspection of the condensation and cloud mixing ratios (not shown), reveals a better developed cloud in the -5° C km^{-1} case that extends from the highest parts of the windward barrier and extends roughly 20 km upstream. It is suggested here that not only is the volume of cloud liquid volume important in determining precipitation rates or amounts, but in addition, the distribution of liquid water within a cloud is important because the areas of highest cloud liquid water act as *feeder* clouds. For example, as the wind speeds are incrementally increased, the wettest portions of the cloud continues to grow horizontally and extend further upstream in the -5° C km^{-1} case. In the -6 and -7° km^{-1} cases as winds increase, the wettest portion of the cloud develops directly over the upper region of the barrier and grows vertically. This last scenario seems less efficient in producing widespread precipitation than a horizontal cloud.

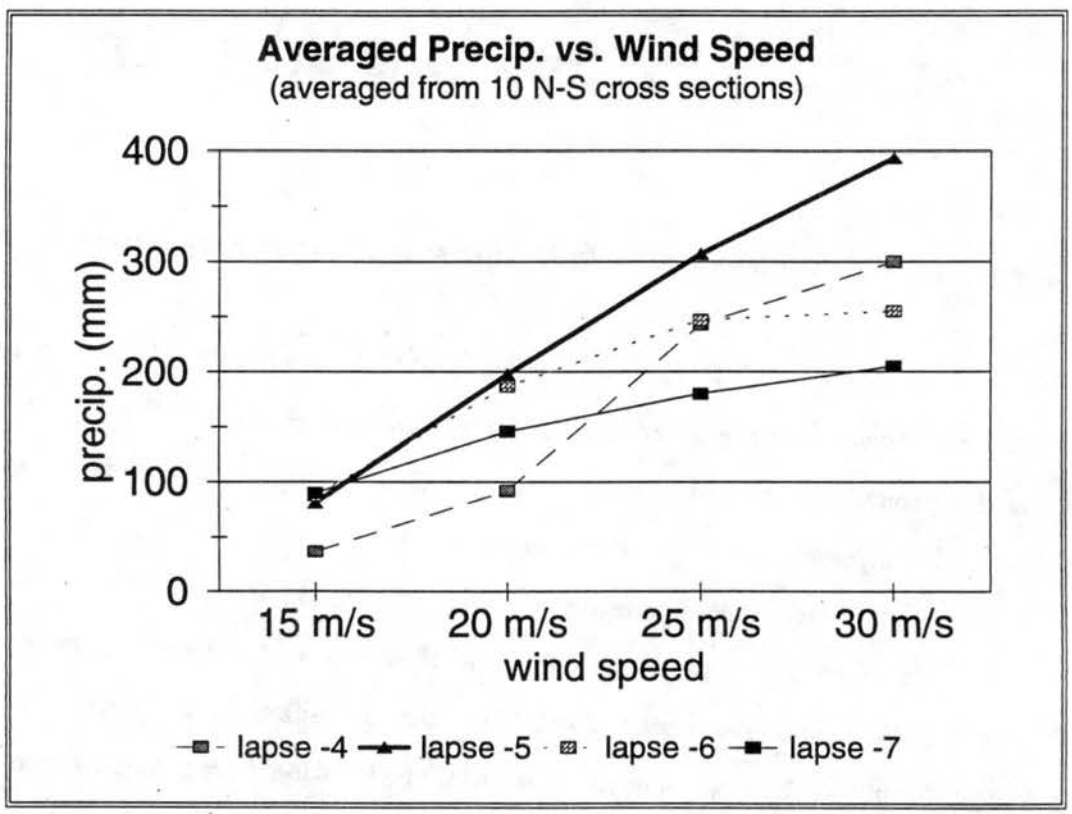

Figure 3.10: Precipitation (mm) averaged for 10 N-S cross sections as a function of wind speed (m s^{-1}), for four different lapse rates (° C km^{-1})

In summary, as wind speeds increase in a stable atmosphere, both updraft speeds and condensation rates in general, are enhanced upstream and over the barrier, the exception being the vary stable case. The stronger horizontal winds advect precipitation so that a large percentage accumulates over the highest part of the barrier, with the remainder being carried to its lee. However, since the slopes of the lines in Figure 3.10 decrease as the lapse rates increase, it is suggestive that for this terrain configuration, that the most efficient dynamic-microphysical interaction occurs with a lapse rate near -5° C km^{-1}.

3.6-Factor Separation

Experiment 1- Wind Speed and Lapse Rate:

Using factor separation, Stein & Alpert (1993) have demonstrated the ability to isolate the contributions that various factors have on a particular model solution. In this technique a *factor* can be any parameterization such as microphysics or cumulus convection, boundary or initial conditions, as well as such a fundamental property as orography; model elements that can be either switched *on* or *off* (Alpert *et al* 1996, Poulos 1996, Romualdo *et al* 1997). However this technique has not been widely used for the perturbation of state variables, such as temperature, wind speed, and moisture to name a few. It will work for state variables (Alpert; personal communication), although the interpretation of the interaction term is not self evident. One also has to be careful of the nomenclature, for example, with on-off switches the factor is either on or off, but state variables are always on; it just has a different or perturbed value. Hence in this section, *perturbation* will be substituted for *factor* when appropriate.

Following the development of Stein & Alpert (1993), if two factors are under consideration, then a total of four simulations are needed for the analysis. In this section the two factors are wind speed and lapse rate. The following four runs are:

k6	control run:	V= 20 m s^{-1}	Lapse rate= -5° km^{-1}
k7		V= 30 m s^{-1}	Lapse rate= -5° km^{-1}
k1		V= 20 m s^{-1}	Lapse rate= -6° km^{-1}
k2		V= 30 m s^{-1}	Lapse rate= -6° km^{-1}

The analysis consist of three difference calculations:

k7-k6: This is the effect of a 10 m s^{-1} wind speed increase.

k1-k6: This is the effect of a increase in lapse rate of -1° km^{-1} (as noted earlier since dew point depression is used to initialize moisture, the moisture decreases as the lapse rate increases.)

k2+k6-(k7+k1): This represents the *interaction* between the perturbed wind speed and lapse rate.

The interaction requires some interpretation, much more so when the factors are perturbed variables and not on-off switches. If this term is zero then it suggest that there is no interaction among the two perturbations, in other words the precipitation generated in **k2** would be strictly due to the increase in wind speed and lapse rate, but with no interaction. If this term is positive it means that the two perturbations interacted in a positive manor, generating more precipitation than they could have individually (i.e. analogous to constructive wave interference). If the interaction term is negative, the two perturbations had a negative affect on each other and the total precipitation is less than the sum of the individual contributions.

Values for these four runs are based on the accumulated precipitation from 10 N-S cross sections:

k6:	1980 mm
k7-k6:	1958 mm
k1-k6:	-105 mm
k2+k6-(k7+k1):	-1277 mm

We have already noted from section 3.5 that a wind speed perturbation of +10 m s^{-1} generated about twice (198%) as much precipitation. An increase in lapse rate only decreased precipitation by about 6% despite **k1** being initialized with less moisture, (at least for those two

lapse rates, section 3.4 indicated that there is significant differences at other lapse rates). The interaction term is of course negative and relatively large, it indicates that *a given wind speed perturbation does not create the same response for two different lapse rates.* This also can be seen from **k2-k1**: +681 mm, about a third of the value given for **k7-k6**.

Experiment 2- Wind Speed and Moisture:

In order to make this discussion complete, it is interesting to consider a case when the two factors are wind speed and moisture (dew point depression), and the two perturbations represent an increase in wind speed and moisture. Individually these perturbations will increase the production of precipitation. If the interaction term is zero, then as described above, there is no interaction. If the term is positive, the interaction reinforces each perturbation. The interesting scenario is if the value is negative, it then suggests that there are limiting constraints on the production of precipitation.

In this second experiment wind speed and moisture levels were perturbed, and the following four runs were considered:

k6	control run:	V= 20 m s^{-1}	Dew point depression= -1° C
k7		V= 30 m s^{-1}	Dew point depression= -1° C
k14		V= 20 m s^{-1}	Dew point depression= 0° C
k18		V= 30 m s^{-1}	Dew point depression= 0° C

following with the same type of analysis as used in *Experiment 1*;

k18 + k6 - (k7+k14) = - 174 mm, which suggest that the interaction of a wind speed increase of 10 m s^{-1} and a moisture increase of 0.65 gm kg^{-1} (by lowering the dew point depression), is slightly less than each perturbation contributing individually. Detailed analysis of the combined runs is not practical, but we speculate that the increased condensation in **k18** resulted in an increase in localized heating over the barrier from latent heating, which in turn alters the stability in such a way that vertical velocities are perturbed. In fact inspection of the

W-component field for **k18** and **k7** show identical updraft velocities over the barrier, however from the barrier crest and extending downstream, the gravity wave downdrafts are slightly weaker in **k18**. The net result is a slight decrease in precipitation. At this point it is difficult to explain all interactions taking place in this simulations, however what it does illustrate is the non-linear interactions of state variables.

3.7-Summary

From the simulations presented in this chapter, a number of conclusions may be reached:

1. The model is sensitive to perturbations in initial conditions that lie within the realm of what would be considered observational uncertainty. This means that model output will show a considerable amount of dispersion for a restrictive set of initial conditions. This will be discussed further in the next chapter.
2. Although not conclusive, the release of potential instability is possible in an atmosphere that is moderately stable with respect to θ. This is supported by the observations of Wratt *et al* (1996) where they observed "convective processes triggered by the release conditional instability through uplift." However, this may not enhance precipitation over the barrier if **PI** is released too far upstream of the barrier.
3. Due to the non-linear nature of the atmosphere, the application of one set of results from one specific set of initial parameters to a run with a different set of initial parameters needs to be preformed with caution. For example, one is tempted to suggest that a wind speed perturbation of ±3-4 m s^{-1} is equivalent to a ± 0.5 gm kg^{-1} perturbation in moisture. However, these types of perturbations are also a function of stability and the temperature profile, so generalizations have to be used with some discretion.

Chapter 4

ENSEMBLE SIMULATIONS

4.1-Introduction

All models suffer from errors to a certain degree. Errors in forecast fields (i.e. any output), are caused by two sources; the first are model errors such as imperfect parameterizations, poor terrain representation, and truncated governing equations to name a few. The second source is due to inaccuracies in the observed or analyzed fields, which are in turn used as initial and boundary model data. The net result is that there is an unknown amount of uncertainty in the initial fields, and due to the non-linear nature of the governing equations, the error growth increases in time, as indicated in Figure 4.1.

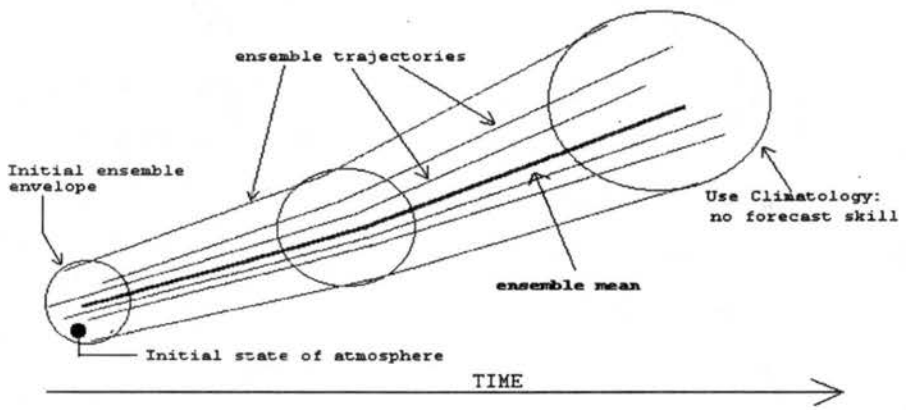

Figure 4.1: Phase space trajectories for ensemble members, conceptually taken from Brooks *et al* (1995).

In the 1960's, Lorentz (1965) and Epstein (1969) were working with systems of dynamic equations and observed that small perturbations in initial conditions often lead to a multiplicity of diverging solutions. The application to numerical weather forecasting was evident, and pointed to the necessity of the ensemble approach. Due in large part to a lack of computer resources, ensemble numerical weather forecasting at the national level was not initiated until the early 1990's.

The ensemble method consist of a control simulation, whose initial conditions are based on the most probable analysis. There are two sources of uncertainty in the analysis; first there is always an unknown amount of measurement error due to the finite number of observations of the atmosphere; secondly, errors are a result of the analysis models' first guess, which tends to be large in data sparse regions. Since it is understood that these initial fields contain an unknown amount of uncertainty that can grow quite rapidly in the forecast model, perturbations are introduced to the initial field in order to allow the model atmosphere to reach a number of probable solutions.

In an operational framework the European Center for Medium-Range Weather Forecasting (ECMWF) uses four-dimensional data assimilation (4DDA) to generate analyzed fields, while NCEP uses a 3D variational technique. A number of techniques have been developed to generate perturbations that are used in the hemispheric medium range (6 to 10 days) forecast models. All of these techniques require some *a priori* knowledge of the magnitude of the perturbations (i.e.- the amount of error in the analysis). Following the outline of Toth *et al* (1993), there are four widely accepted techniques used to generate perturbations:

1. Monte Carlo perturbations are generated using random numbers that are in turn added or subtracted to the value of a state variable at each grid point. The advantage of this technique is its simplicity and objectivity, the disadvantage as noted by Mureau *et al* (1993), is that randomly selected perturbations may not represent that aspect of the solution which has the most significant influence on the synoptic-scale flow.
2. Lagged Average Forecasting includes previous (older) forecast as members in a suite of ensemble members. Perturbations are generated by taking difference fields between a forecast and the most current analysis. These differences, after being weighted in proportion to its age (i.e.-how old it is with respect to the most current simulation), are added to the current analysis which are in turn used as the new set of initial conditions (Toth and Kalnay 1993).

3. Singular Vectors is the preferred technique for the generation of perturbations at ECMWF. It has been demonstrated that for a linear model, the fastest growing perturbations (errors) can be obtained by taking the eigenmodes of the product of the linear model propagator and its adjoint (Mureau *et al* 1993).

4. For its medium range ensemble forecast, NCEP uses the Breeding of Growing Modes technique (Toth *et al* 1997). In this method a small balanced perturbation (both negative and positive) is added to a given field, which is in turn run for 24 hours in the forecast model. The output is then compared to the most current analysis valid at the same time. The difference between the model output and the analysis is computed, then rescaled (using kinetic energy as the rescaling variable). This new value is then in turn added and subtracted to the latest analysis, which is used as the new initial condition.

These last three techniques use what has been referred to as "dynamic conditioned errors" (Toth *et al* 1997). The principle is that perturbed fields should represent the fastest growing errors that were introduced during the analysis cycle. A number of variations to these four techniques have been developed over the years. Mullen and Baumhefner (1989) for example using a global spectral model, generated perturbations whose magnitude and phase were a function of the scale of motion. In these types of simulations, spurious inertial-gravitational modes are filtered out before being applied to the model.

In the last few years there has been interest in using ensemble forecasting techniques for short range forecast (Brooks *et al* 1995, Mullen & Baumhefner 1989, 1994) as well as for mesoscale models (Du *et al* 1997). Many of the techniques and methodologies used for medium and long range models (Kalnay and Tracton 1993), will be applicable to these newer modeling efforts. A sampling of some of these studies is given below.

Stensrud and Fritsch (1994) used the Pennsylvania State University-National Center for Atmospheric Research (NCAR) Mesoscale Model Version 4 (MM4), to study mesoscale convection over the northeast USA. Due to a lack of data at the scale of tens of kilometers to a few kilometers, the authors created synthetic soundings and surface observations that were merged with the initial analysis, in order to simulate convection at the smaller scales. They created an ensemble forecast based on members that used either the original analysis or the modified analysis containing the synthetic data. They argue that ensemble forecasting is a necessity for these type of events because a single high resolution forecast will probably miss

important mesoscale features that are not contained in a single high resolution analysis.

Houtekamer and Lefaivre (1997) created an ensemble based on two types of perturbations; the first were perturbations in initial conditions; the second consisted of the selection of various model parameterization schemes, what may be termed model perturbations. They selected seven different types of perturbations, for example, the time scale for horizontal diffusion, Kuo versus Manabe convection schemes, and the inclusion of supplemental observations to the analysis package, to name a few. By the selective grouping of simulations they were able to form an eight member ensemble, which represents a significant reduction in the number of possible (49) combinations of perturbations.

The basis of this technique is that the forecast is assumed to be a linear combination of the ensemble mean and any errors introduced by the influence of model perturbations:

$$F = F_{ens} + \sum_{j=1}^{k} C_j X_j(t)$$

where C_j is the error coefficient and X_j is the difference field for perturbation option j, and F_{ens} is the ensemble mean. A merit function and then a general least squares routine are used to solve for the C_j's. When each C_j=0, the ensemble mean is considered the best possible forecast for that particular set of model parameters. The key is that the merit function needs a set of detailed observations in order for it to work, hence this method is not practical except in data rich areas.

Du *et al* (1997) explored a case of cyclogenesis over the eastern USA, using a 25 member ensemble forecast from MM4. The model was set up with a Δx, Δy of 80 km, with lateral boundary conditions supplied from the NCAR Community Climate Model (CCM1). Their conclusions can be summarized as the following:

1. Ensemble averaging always improved the total precipitation root mean square error. However, since the averaging of the ensemble members is a smoothing operation, regions of light (heavy) precipitation became wetter (drier) with an expanded (smaller) area when compared to the control run.
2. 90% of the improvement in a 25 member ensemble forecast could be obtained by ensembles with as few as 8-10 members.
3. The model was quite sensitive to initial conditions.

Using a set-up with a Δx, Δy= 40 km, the authors found that ensemble QPF's from the 80 km grid was more accurate than a single forecast from the 40 km grid. However, it should be noted that the decrease in model horizontal grid interval from 80 km to 40 km over the central and eastern USA, is not enough to resolve the Appalachians and associated mountains with any kind of realism.

Assumptions and Limitations:

It is important to note that all numerical models have limitations since they are constructed using truncated (including linearized) equations and contain parameterizations that have various levels of sophistication. The following is a list of several assumptions that are applicable to the ensemble section of this chapter. First, it is assumed that RAMS is a "perfect model". This means that simulation error is due to uncertainty in initial conditions and is not due to any deficiencies in model parameterizations or resolution. Of course RAMS is not a perfect model, but in order to determine whether any modification to model physics or parameterizations is a real improvement, the model must be tested on many cases before that can be determined (Houtekamer and Lefaivre 1997). So it is assumed as a working hypotheses that RAMS is a perfect model, allowing us to test the utility of the ensemble approach. For the simulations used in this chapter, only state variables are perturbed, hence identical model parameterizations were selected for each simulation.

Secondly, the preceding discussion on ensemble forecasting has focused on techniques used for medium range spectral models. What is envisioned for the near future is the use of mesoscale models at the regional and local office level at the NWS. It is within this context that the following discussion and the remainder of this chapter is presented. These models would use variable initialization with data originating from global analyses (Kalnay and Tracton 1993), or another model such as the meso-eta (Hamill and Colucci 1997). However, since the results presented in this chapter are generated from horizontally homogeneous initialization it is assumed that an ensemble methodology used from horizontally homogeneous initialization will apply to those of variable initialization and also will be easier to understand.

Thirdly, one of the fundamental issues in ensemble forecasting is the task of generating perturbed initial conditions. Somewhere in the process judicious selection of the perturbations as well as the amplitude of those perturbations has to be undertaken. This requires *a priori*

knowledge of possible errors in either the analysis or as illustrated in this chapter, for a single sounding.

For example, the results of section 3. 5 indicated what wind speed perturbations of ± 5 m s^{-1} and ± 10 m s^{-1} do to the distribution of orographic precipitation. In the case of the Kenai Peninsula, it is probable that the uncertainty in rawinsonde data from Kodiak Island varies by less than ± 10 m s^{-1}; a better estimate would be ± 5 m s^{-1}. Hence ensemble members should be constructed using this value as the upper limit to the uncertainty of the observations. In addition to simulations initialized with single perturbations, there is nothing to suggest that uncertainty in initial conditions cannot extend to multiple state variables, for example wind speed and relative humidity. The number of ensemble members can grow rapidly when considering a number of perturbations and their possible interactions. In this study it is assumed that an ensemble forecast consists of a finite number of members, and that are all equally likely states of the atmosphere at the time of initialization. It is also possible that one of the ensemble members is closer to the true state of the atmosphere than the ensemble mean. However, there is no *a priori* knowledge as to which member this is true for, so we are forced to assume that the ensemble mean is the best possible forecast (Brooks *et al* 1995).

4.2-Ensemble One

Figure 4.2 is a spaghetti diagram of the total 6 hour precipitation for the north-south vertical cross section through longitudes 150.5° and 149.5°. This ensemble consist of 15 members and is based on the control run **k6.** Each line in Figure 4.2 represents the total accumulated precipitation for a north-south cross section. Table 4.1 lists the members and their associated perturbations. Six of the 15 members combine two or more perturbations while, four of those six contain three perturbations.

It can be seen from Figure 4.2a that upstream of 59.3° N (the coastline), and downstream of 60°N, the magnitude of precipitation is small and the solutions in that region are quite insensitive to the different perturbations. Over the windward slopes however, precipitation ranges from as low as 6 mm to a high of 49 mm for a single grid point. The member which generated the least amount of precipitation was **k24**; which had strong stability and low wind speeds, leading to significant blocking of the incoming flow. The member with the highest precipitation was **k8**.

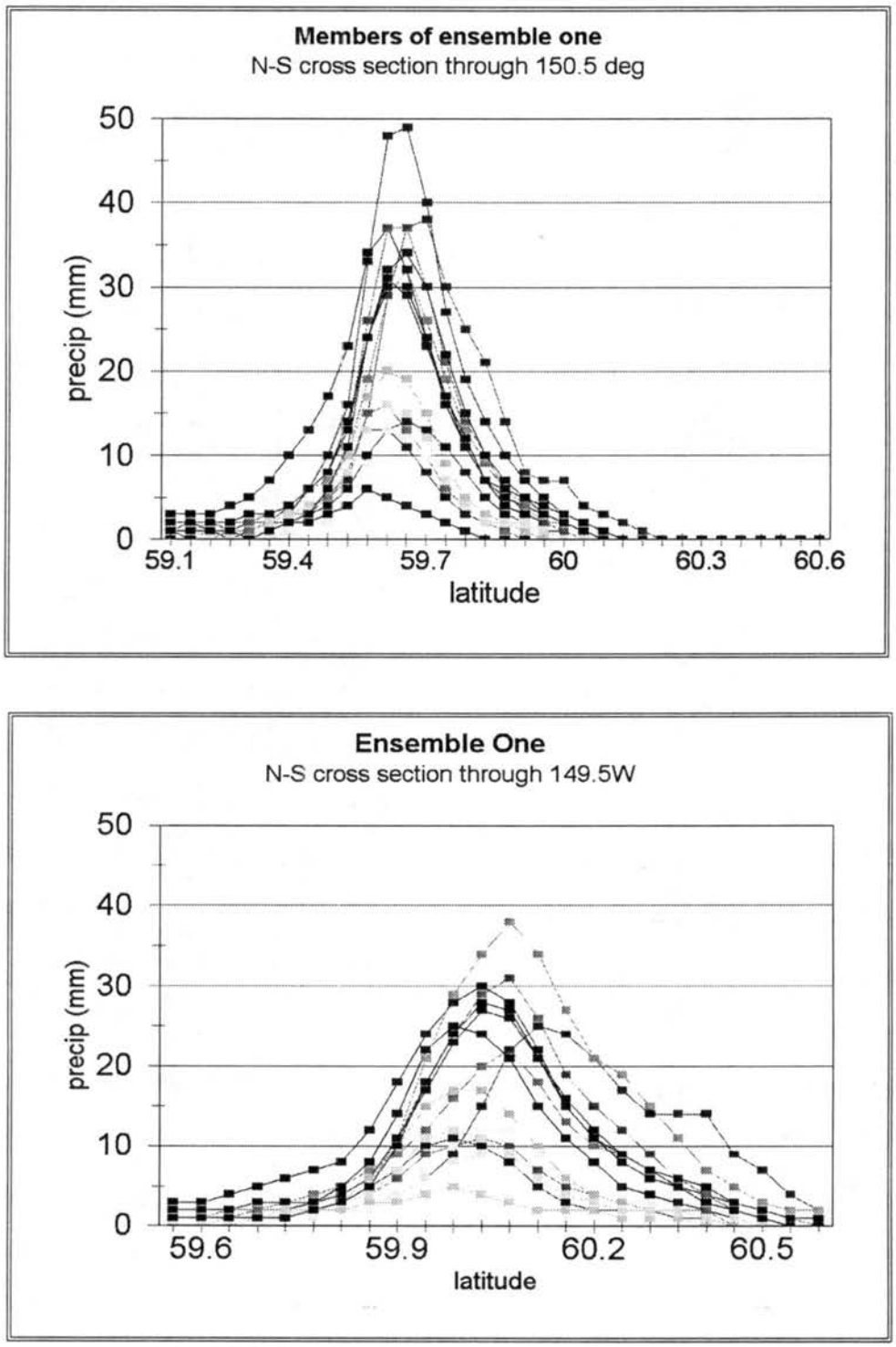

Figure 4.2: North-South cross sections of six hour precipitation (mm) from **ensemble one**. (top) through 150.5° W , and (btm) 149.5°W

Table 4.1 Ensemble One Members					
run	lapse rate (deg km^{-1})	dew point depression (deg)	wind speed (m s^{-1})	wind direction (deg)	comment/ perturbation
k1	**-6**	-1	20	180	
k3	**-6**	-1	**25**	180	
k4	**-6**	-1	**15**	180	
k6	-5	-1	20	180	control
k8	-5	-1	**25**	180	
k10	-5	-1	**15**	180	
k12	**-4**	-1	20	180	
k13	-5	**-2**	20	180	
k14	-5	**0**	20	180	
k23	**-4**	-1	**25**	180	
k24	**-4**	-1	**15**	180	
k26	-5	-1	**22.5**	180	
k27	-5	-1	**17.5**	180	
k28	-5	-1	20	**195**	
k29	-5	-1	20	**165**	

Table 4.1. Members of **ensemble one**. Bold highlights are the perturbations with respect to the control run (**k6**)

The large spread of ensemble members can mean either one of two things: first, the initial perturbations were too large, or secondly, due to the highly non-linear nature of the processes involved in the generation and distribution of orographic precipitation, reasonable uncertainty in initial conditions leads to a wide spread in values.

Figure 4.3 displays two examples of the *ensemble mean* precipitation plotted with the topography for north-south cross sections through 150.5° W and 149.5° W. In Figure 4.3a

precipitation is highest over the windward slopes but falls off rapidly over the crest and to the lee. In a region where the topography has more of a 'stair-step" nature (figure 4.3b), the peak precipitation still occurs well upwind of the barrier crest.

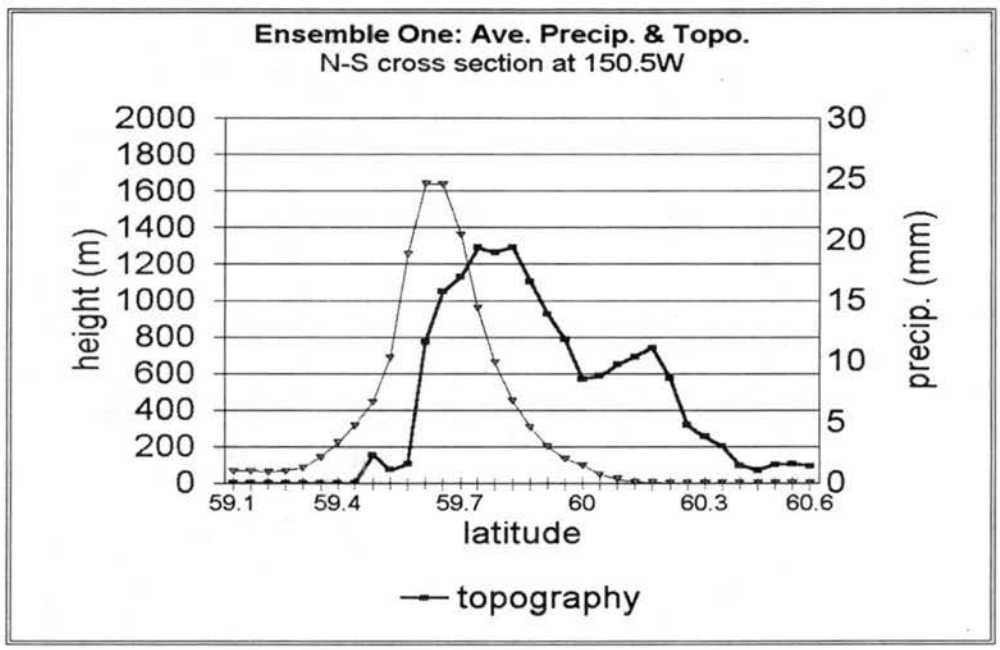

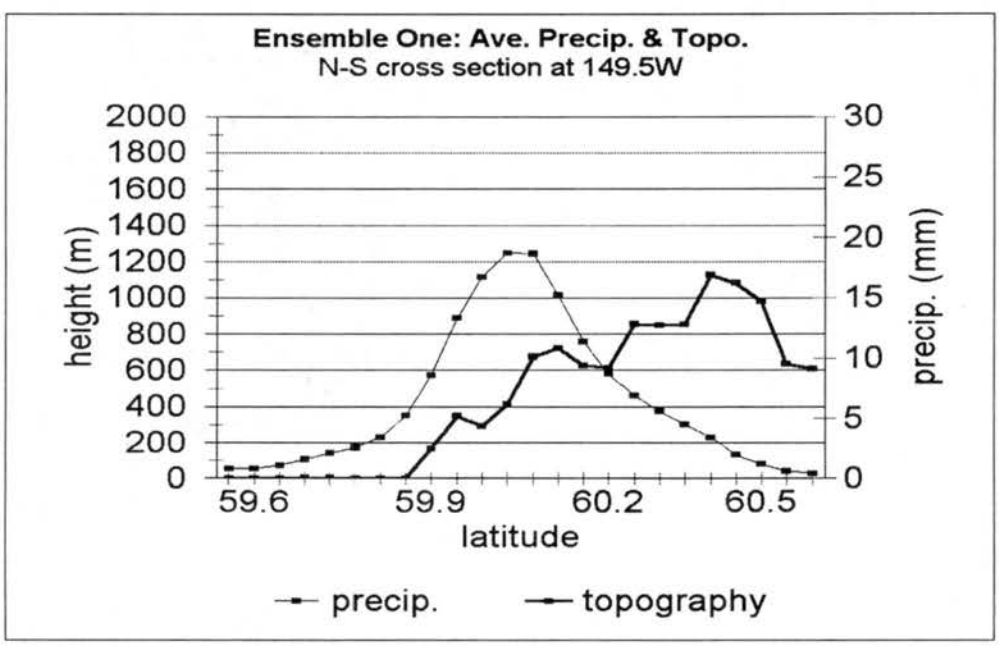

Figure 4.3: North-South cross sections of ensemble mean precipitation (mm) and topography (m) for; (top) 150.5°W; (btm) 149.5°W

Figure 4.4 displays plots of the ensemble mean superimposed with the standard deviations for both 150.5° W and 149.5° W. As one would expect, upstream and downstream of the coastal barrier, the spread in precipitation is low.

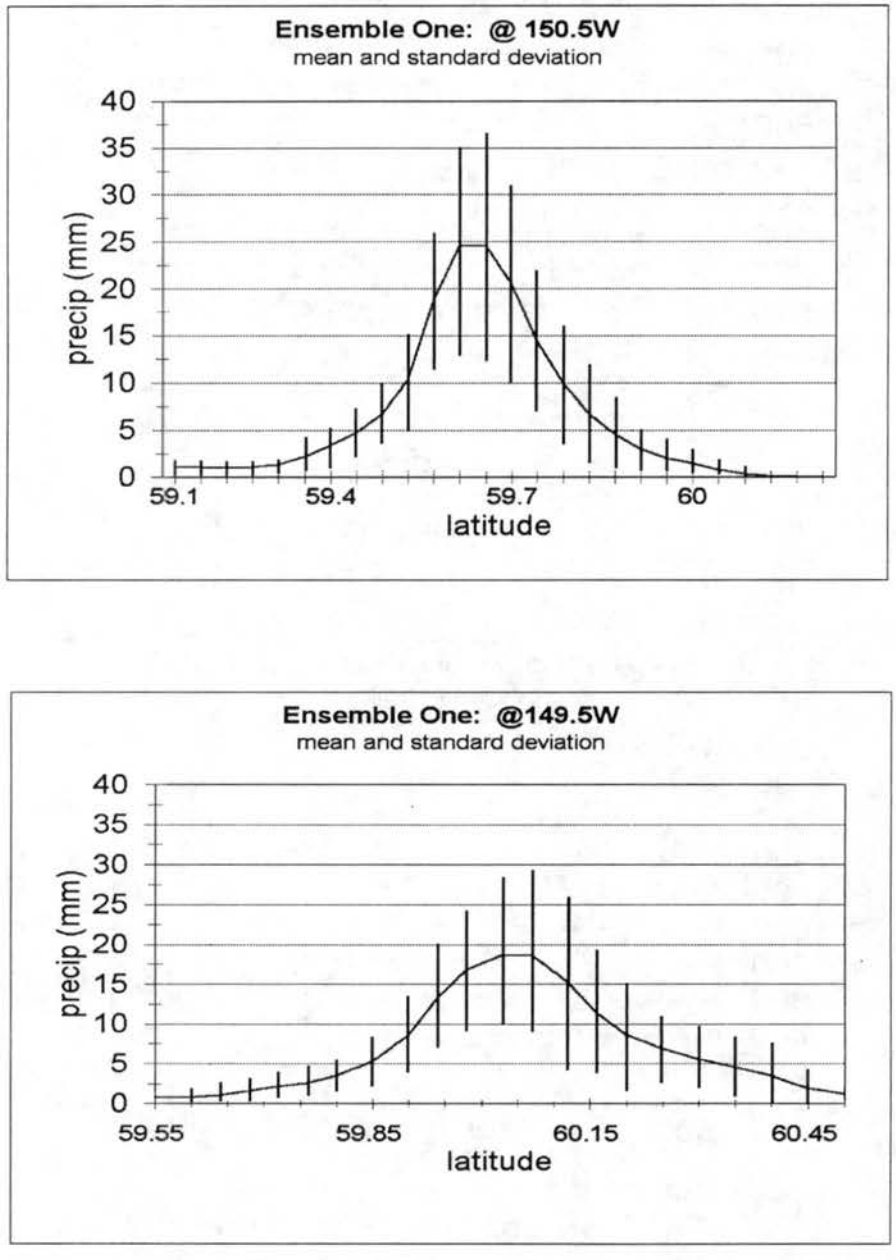

Figure 4.4: Ensemble mean precipitation (mm) and standard deviations for; (top) 150.5°W; (btm) 149.5°W

However, for a given amount of precipitation there is a noticeable increase in the standard deviation for leeward slopes when compared to the windward slopes. This is probably due to the fact that by the time the flow is to the lee of the barrier crest, the dynamic-thermodynamic-microphysical interactions result in a much larger family of solutions. Over the upper half of the barrier it is all too evident that standard deviations and hence the spread is very large. This indicates that the ensemble mean should provide the best possible solution (forecast). This wide spread also suggests that the confidence in the "forecast" is lower than in areas of the model domain where the spread is significantly smaller (Toth *et al* 1997).

Inspection of Figure 4.2a reveals the clustering of the ensemble members into two groups (referred to as low cluster and high cluster), in addition to two extreme outliers. If the outliers are discarded and the means for each of the clusters are computed and compared to the ensemble mean, it provides a range of values that could be used to bracket the ensemble mean. (Figure 4.5). Comparison of clustering means to the standard deviations (not shown), indicates a slight tightening of the range for the former method.

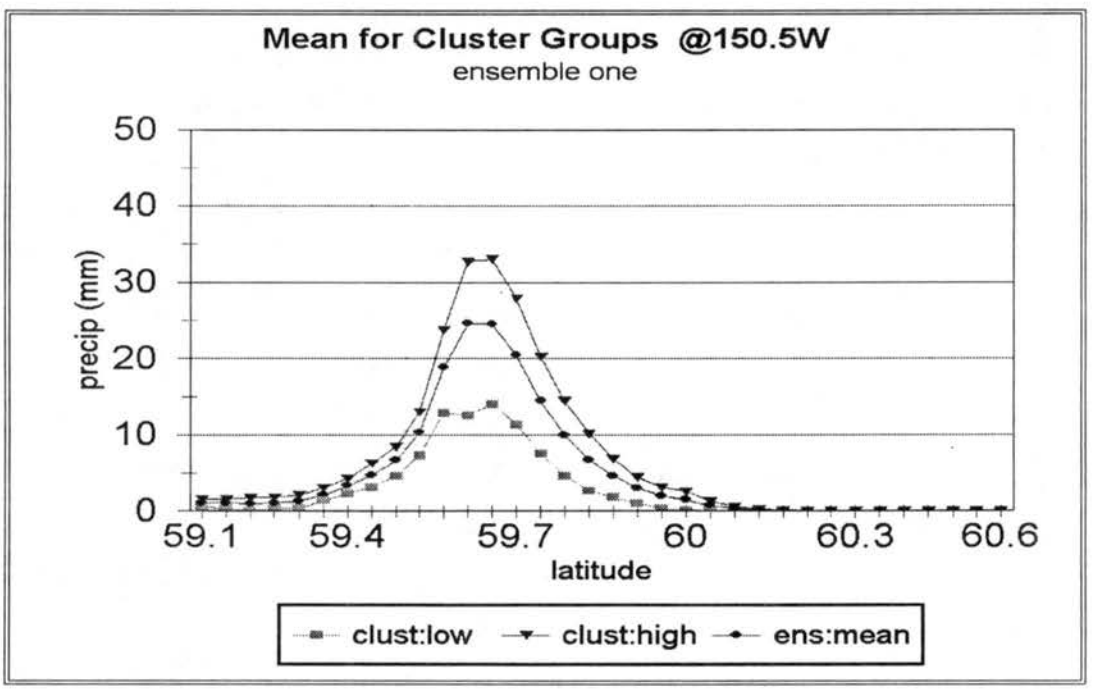

Figure 4.5: Cluster groups and ensemble mean precipitation (mm) through 150.5°W

Figure 4.2b on the other hand does not indicate any significant clustering. It appears that this is due to the fact that flow up the 30 km long Resurrection Valley is influenced by the "surrounding" terrain in a more dramatic fashion than occurs at coastal locations (at 150.5°W for example).

The low cluster contains six members while the high cluster has seven members. It is constructive to ascertain why the ensemble members form two clusters. Wind speeds near 20 m s^{-1} seem to be a dividing line between the two clusters, although simulations which were initialized with wind speeds of 20 m s^{-1} can be in either cluster. It does not appear that atmospheric stability, at least for the range of values used in **ensemble one**, are a significant factor in the creation of the two clusters. For example, simulations using a lapse rate of either -4 or -6°C km^{-1} can be in the low or high cluster, and is primarily a function of the wind speeds. This can best be understood by recalling from sections 3.3-3.5, that vertical velocities are a function of the horizontal wind speed in addition to atmospheric stability. So to a certain extent the reduction in initial moisture (function of lapse rates), is off-set by the increased updraft speeds, so that the moisture flux can be similar for the two simulations that are initialized with different lapse rates.

Since there were only two simulations in **ensemble one** that perturbed the dew point depression without any changes in the lapse rates, it is not possible to comment on the role which it plays in clustering, except that the moisture flux is a function of wind speeds. Wind direction on the other hand is highly non-linear in terms of the generation of precipitation. In the real atmosphere both storm movement and low-level blocking alter the angle which the flow impacts a given barrier. Due to this process, simulations with perturbed wind directions will in most cases have a large spread in model generated precipitation.

Comparison of the ensemble mean with the control run (**k6**), indicates that the mean is approximately equal to **k6** for light amounts of precipitation, but is 17% lower in areas of heavy precipitation, not unlike the results of Du *et al* (1997). Since the perturbations were balanced (±) to start with, the interaction of perturbations tends to limit the production of precipitation at the higher thresholds (see section 3.6).

By reviewing the four types of perturbations listed in Table 4.1, it is possible to refine the perturbation first guesses. The initial moisture (via dew point depression) is probably the variable with the most uncertainty. From section 3.3 it was demonstrated that the model is quite sensitive to dew point depression perturbations of ±1.0° C, hence it is quite

possible that these perturbations should be lowered to ±0.5° C, a more realistic representation of the uncertainty. Much of the same could be said for other variables such as wind speed perturbations; it is possible that they should be adjusted from ±5 m s^{-1} to ±3 m s^{-1}. These are the types of difficult questions the modeler has to wrestle with during the early stages of model set-up.

If the soundings that are used in model initialization were located closer to or in the area of interest, then a detailed analysis of these soundings could be performed, in view of trying to determine the magnitude of the perturbations. For example, if the soundings show that heavy precipitation only occurs when the wind speeds at 850 mb are stronger than 23 m s^{-1} and if they rarely exceed 30 m s^{-1}, then a perturbation of 3 m s^{-1} to 4 m s^{-1} would be warranted. In the case of the Kenai Peninsula, where the most relevant soundings are taken from Kodiak Island, several hundred kilometers to the south, this procedure would be more difficult because of the distances involved and the influence that local topography has on those soundings.

At this juncture it is important to evaluate the utility of ensemble forecasting using balanced perturbations in runs that are initialized horizontally homogeneous. Since the ensemble mean is a smoothing operation, it is susceptible to one or two "outlying" simulations, for example, **k24** where blocking greatly reduced the generation of precipitation, causing the ensemble mean to be inordinately lowered. This would suggest that either the original perturbations were unrealistic (not all equal likely states), or that there is simply a large amount of uncertainty in that parameter. The real question here is: is the generation of an ensemble mean cost effective for horizontally homogeneous simulations ? Only if the ensemble mean differs from the control in a significant amount. What may be more cost effective is to conduct three simulations, a control run and then a maximum using the largest positive perturbations and then a minimum based on negative perturbations. This gives a possible range of QPF's without all of the intermediary runs. Much of the same argument could be said for variable initialization using balanced perturbations, the ensemble mean may not be cost effective relative to the control run unless the perturbations are unbalanced (e.g.-wind speed perturbations across the domain are not necessarily equal, but are a function of proximity to rawinsonde stations, terrain, initial wind speed). In this case it would probably be best to use NCEP's perturbed analysis, where the analysis errors have been dynamically enhanced.

In summary, due to the highly non-linear nature of the generation and or enhancement of precipitation over mountainous terrain, ensemble QPF forecasting appears to be the only way

to create a legitimate precipitation product. *However,* the selection of the perturbations, the number of ensemble members to be used, and the display and analysis of ensemble runs is far from being obvious, and will require serious consideration.

4.3-Resurrection River Basin

The Resurrection River basin, located northwest of Seward, is the most flood prone basin in the State, hence it is of great interest to apply the ensemble forecast technique to this basin. With the orientation of the basin along a northwest-southeast axis, the largest precipitation (rain) events are associated with southeasterly flow up Resurrection Bay. Since the model topography does not perfectly match the actual terrain, a compromise is required when drawing basin boundaries. In this example, if the area is preserved then much of the steep terrain in the western extremes of the basin would be excluded. On the other hand, if the height and overall best representation of the terrain is preserved, the basin area is considerably larger than the actual area.

The basin boundaries drawn for the following analysis were done so in order to preserve the actual range of elevations found in the basin, trying to keep the area as close to the actual area as possible. The resulting model basin contains 32 grid points that have an elevation range of 41 m to 1274 m, with a mean of 652 m. The model basin area is 750 km^2 compared to an approximate "actual" basin area of 454 km^2. This is approximate because the western boundary is poorly defined due to the fact that it crosses the northern portions of the Harding Icefield, whose drainage characteristics remain unknown.

If we take each ensemble member and calculate a basin average and standard deviation for precipitation, it gives some indication of the amounts of precipitation that could fall in the basin over a 6 hour period. The lowest average was 3 mm from **k24**, and the highest was 28 mm from **k8**. The basin ensemble mean is 15 mm compared to the control run mean of 18 mm. The ensemble means' standard deviation is 6 mm, so there is a high probability that the observed precipitation would fall within the 10 mm to 20 mm range. The range is large and can only be refined if the initial perturbations are narrowed or if the range is weighted by some climatological statistic. The ensemble members that produced the highest precipitation were associated with wind speed increases. For example, with the same lapse rate, the run that increased wind speeds by 5 m s^{-1} (**k8**), produced about 20% more precipitation than the run that increased moisture by 0.65 gm kg^{-1} (**k14**). The lowest production of precipitation was

associated with lower wind speeds and blocking (**k24** and **k10**).

Figure 4.6 displays two plots that represent the probability of 6 hour accumulated precipitation exceeding either 10 mm or 20 mm. These plots were generated from the 15 member **ensemble one** suite. Prior to the analysis, four thresholds were selected (5 mm, 10 mm, 15 mm, 20 mm), that are representative of the accumulated precipitation. A probability of exceedence at each grid point is constructed for the four categories based on the 15 ensemble members (Du *et al* 1997). For example, at a given grid point, if 10 of the 15 ensemble members indicate that precipitation for the period exceeds the threshold value, then the probability of exceedence is 67%. From Figure 4.6 it is clear that the area of heaviest precipitation occurs over the slopes that are nearly orthogonal to the incoming flow. Precipitation drops off significantly in the northwest corner of the basin in large part due to its interior position. The advantage of displaying data in this fashion is that it clearly shows the areal distribution of precipitation, the disadvantage being that it takes multiple plots to display all of the data.

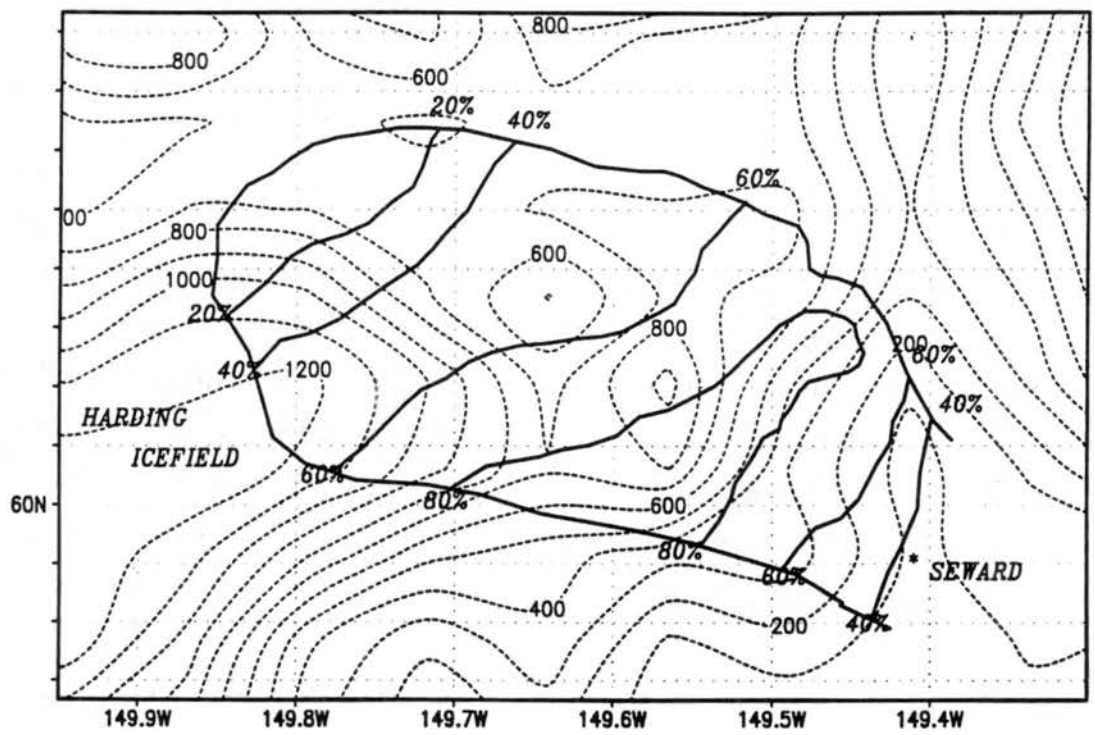

Figure 4.6: Solid lines are the probability of exceeding the 10 mm threshold, for 6 hour accumulated precipitation. Dashed lines are elevation (contour interval 100 m).

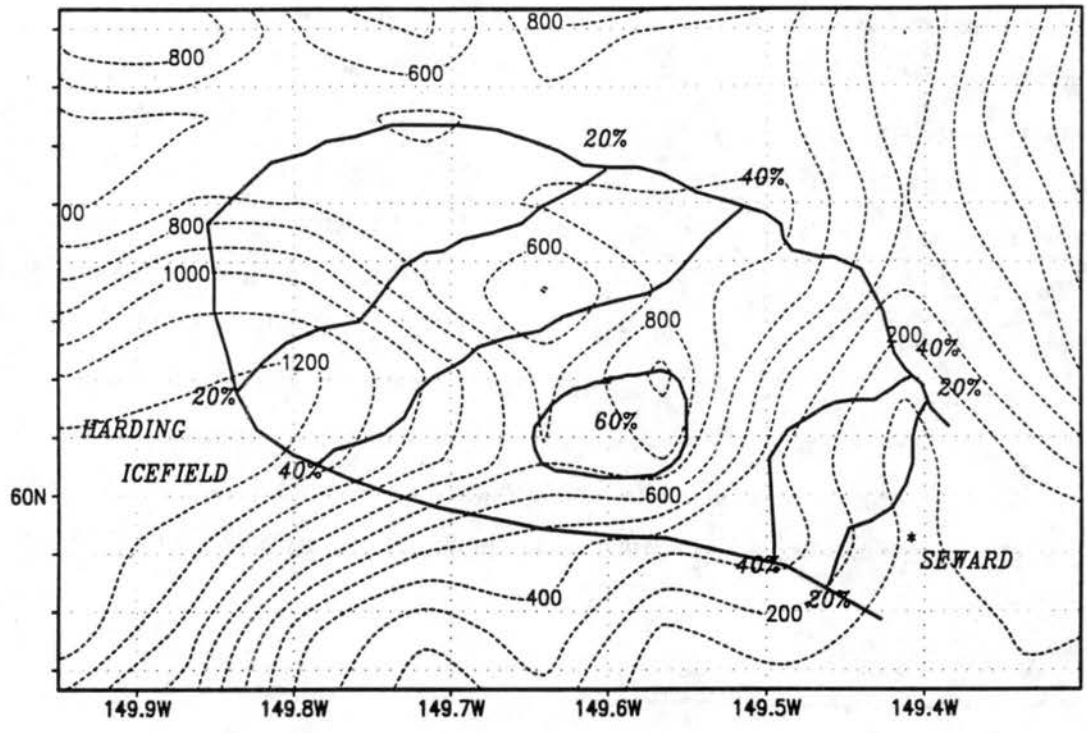

Figure 4.6: Continued. Probability of exceeding 20 mm.

It is worthwhile examining the influence that wind direction has on the generation of precipitation in the Resurrection Basin. Comparing three runs that were initialized with the same sounding except wind direction [180° (**k6**), 165° (**k29**), and 150° (**k16**)], indicates that the shift from 180° to 165° generated about 20% more basin wide precipitation, while the shift from 165° to 150° represented minimal changes in the precipitation. The primary area of increased precipitation was in the southwest, where the directional change enhanced upslope flow. This example illustrates the large sensitivity to wind direction *when the flow changes from a regime of downslope to upslope.* Once in a predominate upslope regime, small changes in wind direction may alter the areal distribution slightly, but the overall sensitivity is missing. It also shows that semi-interior basins like the Resurrection, are more sensitive to wind direction than basins on the windward slopes. However, this sensitivity is *not* uniform for all azimuthal wind directions.

One of the longstanding questions in mountain meteorology is: how does precipitation change with elevation? There is no unique answer to this question because of the complexity of the precipitation process. Using a polynomial regression equation of the third order, no satisfactory relationship was found for precipitation (from the **k16** run), versus elevation in the Resurrection Basin. This result is not too surprising since other factors such as distance from moisture source and slope aspect are also important independent variables (Hjermstad 1970). If the regression problem is solved using both elevation and distance from Resurrection Bay as independent variables, then a satisfactory relationship can be found (it is not practical to include slope aspect since model terrain at 5 km is still poorly resolved):

$$\mathbf{P}(\text{elevation,distance}) = -1.93 - (1.13\text{E-}3 \bullet \mathbf{elev}) + (6.33\text{E-}6 \bullet \mathbf{elev}^2) + (9.8\text{E-}9 \bullet \mathbf{elev}^3) + (2.79 \bullet \mathbf{dist}) - (4.66\text{E-}2 \bullet \mathbf{dist}^2) - (6.70\text{E-}4 \bullet \mathbf{dist}^3)$$

where precipitation (**P**) is in millimeters, elevation (**elev**) is measured in meters and distance (**dist**) in kilometers. As a first guess, the ratio between the mean basin elevation (652 m) and the mean basin distance (20.5 km), to the precipitation at Seward is 2.7. This means that if 50 mm is forecasted (or observed at Seward), over a 6 hour period, then the basin mean precipitation would be on the order of 135 mm. This could be used to evaluate the need for flood watches or flood warnings. In order to use this equation three criteria must be meet:

1. Wind direction should be from the Southeast (in the 165° to 130° range)
2. Wind speeds in the 950 mb to 600 mb levels should be on the order of 20 m s^{-1} (40 kts)
3. The lapse rate should be in the 4.5-6.5° C km^{-1} range.

This technique could be further refined by using a higher resolution terrain data set (≈2 km), and creating an ensemble suite based on the range of parameters listed above, then using the ensemble mean to establish a new regression equation.

Chapter 5

TERRAIN RESOLUTION

5.1-Three Dimensional Simulations

One of the fundamental elements of any model study is the determination of the grid interval which in turn determines the resolution of the model and the terrain. Model resolution is coarser than the grid interval, since it takes more than two points to identify an atmospheric wave (Pielke 1984). With regards to terrain resolution, from two consecutive grid points the slope can be determined but it still takes more than two points to determine the shape of the feature. The grid interval is important because in conjunction with the size of the domain, it determines the total number of model grid points and it also puts an upper limit to the length of the timestep. The time it takes to make a single model run is an important issue for ensemble forecasting and has been discussed in that context by Du *et al* (1997), Brooks *et al* (1995), and Hamil & Colucci (1997).

The current debate is whether to run a given model in a low-resolution ensemble configuration or produce a single higher-resolution simulation. Toth *et al* (1997) note that the benefits of ensemble forecasting for medium-range synoptic scale models is beyond question. However, for short range forecasting at sub-synoptic scales, the benefits of ensemble forecasting are not as evident. This is in large part due to the need for the models to resolve smaller scale features including the underlying terrain, since atmospheric features at these smaller scales are linked to both physiographic properties and the synoptic scale flow. The question of low-resolution ensemble versus single higher-resolution forecasts is limited ultimately by computer resources, but the type of phenomena to be modeled should not neglected in this decision. Tracton and Kalney (1993) suggest that due to the inherent non-

linear nature of the precipitation process, small uncertainties in initial conditions can lead to widely diverging solutions.

In this section, three different model configurations are used in order to test the model's sensitivity to terrain resolution. The control run is **k6**, which uses the same Δx, Δy of 5 km as presented in the previous chapters of this study. In addition, a 10 km (**k30**) and 15 km (**k31**) simulation were conducted using the same sounding as **k6**. The terrain data for these two additional simulations were derived from the 5 km terrain data set; the domain size for each run is approximately the same. Table 5.1 lists the pertinent model properties while Figure 5.1 displays model terrain for each simulation.

It is apparent from Figure 5.1 that the primary difference between the three model runs is the amount of terrain detail shown at the 5 km level. The difference in terms of mountain heights is not very significant, however the difference in the steepness of the slopes is significant. In the model set-up process, the modeler has to decide what scale is appropriate for the expected application. For example, if QPF's are needed for a number of smaller drainage basins, then the higher resolution terrain should be selected.

Table 5.1 Terrain Resolution

run	grid interval Δx, Δy (km)	grid points x, y, z	total # grid points	CPU time (sec)	wall clock run time (hrs)
k6	5	67, 66, 33	145,926	210	42.0
k30	10	34, 36, 33	40,392	153	22.9
k31	15	23, 26, 33	19,734	71	14.2

Table 5.1: Model properties for three different grid intervals. CPU time is the length of time it took the model to complete one timestep, and the wall clock run time is the total time it took the model to preform a 6 hour simulation.

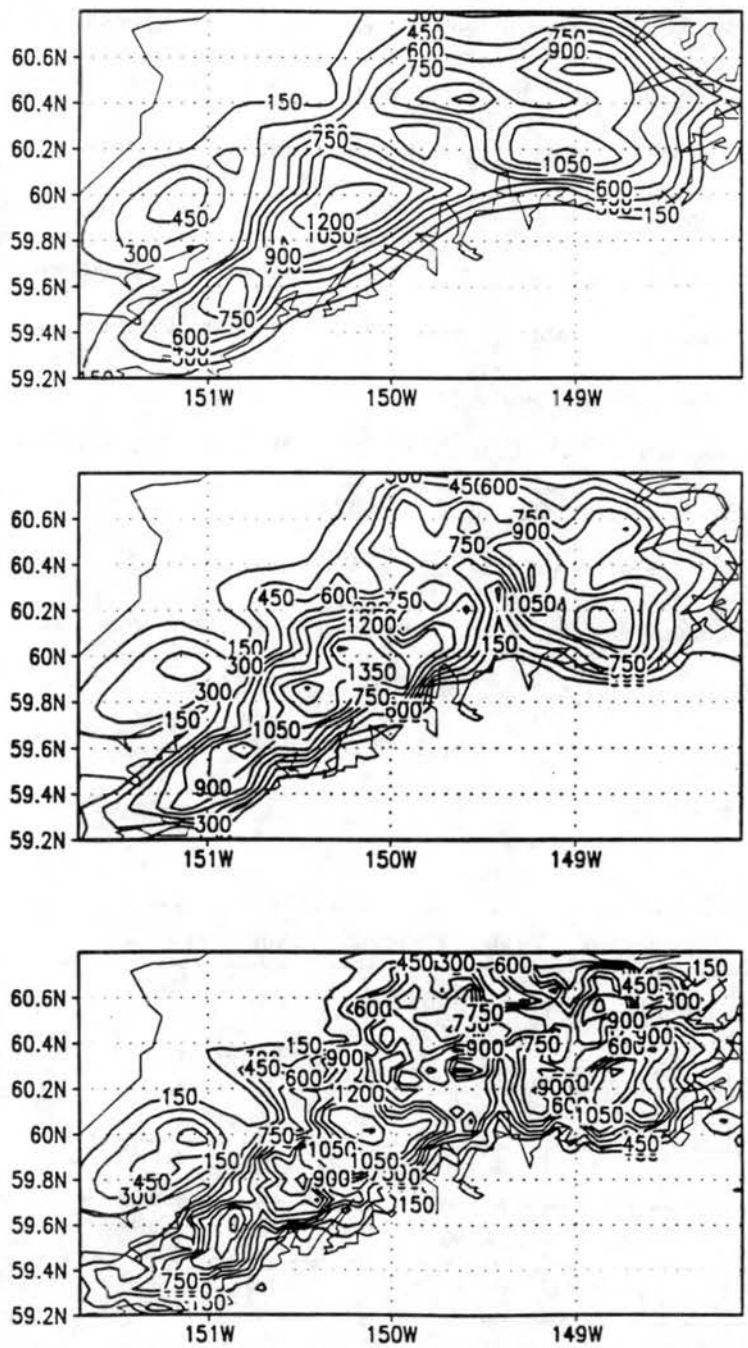

Figure 5.1: Zoom of model topography (contour interval 150 m) for; (top) 15 km, (mid) 10 km (btm) 5 km.

The length of time required to complete a given simulation is a function of a number of factors:

1. The total number of model grid points.
2. Complexity of parameterization selected. (For example; there are various options for radiation schemes, and microphysics, that require different amounts of CPU time).
3. The grid interval.

The primary model timestep (RAMS uses time splitting: i.e.- some processes run on the long timestep while some run at a fraction of that timestep), is dependent on the grid interval and steepness of the terrain. The primary constraint is that the model remain numerically stable. The most commonly used approximation for stability is the Courant number:

$$CR = U \Delta t / \Delta x$$

where **U** is the mean advection velocity, Δ**t** is the timestep, and Δ**x** the horizontal grid interval (Pielke 1984. section 10.1.1). The criteria for stability is that **CR** $\leq$ 1, and should in general be $\ll$1.

The "steepness of the slope" with regards to the timestep is not the rise over the run, but rather is given as the ratio of the change in terrain height between any two grid points and the vertical grid spacing. For the three runs discussed in this section, the timestep does not increase dramatically from **k6** to **k31** because of the previously mentioned requirement. The reduction in wall clock time is primarily due to a decrease in the total number of grid points for the coarser resolution simulation. However, if the vertical grid interval had also been increased in addition to the horizontal interval then the timestep could have been increased more dramatically.

Two methods of analysis were used to make comparisons of the amount of 6 hour total precipitation generated by each of the three simulations. First, the areas enclosed by the 5 mm, 10 mm, 15 mm, and 20 mm were compared; secondly, mean areal precipitation was calculated for four 900 km^2 regions. No matter which analysis is used the 5 km run produced considerably

more precipitation then either the 10 km or the 15 km runs (figure 5.2). The one exception was just upstream of the southern coastline, where all three runs had similar amounts.

In general, there was a larger precipitation difference between the 10 km and the 15 km runs than between the 5 km and 10 km runs. Comparison of the four 900 km^2 areas shows that precipitation was 26% larger for the 5 km run over the 10 km run, while the 10 km run was 33% larger than the 15 km run. In addition, the differences are the largest for the higher precipitation categories. **The conclusion is obvious: as the grid interval decreases and the terrain resolution increases, precipitation increases.**

Using a single high resolution terrain data set and grid intervals of 30 km and 15km, Katzfey (1995a) found that precipitation (rain) over the upper slopes of the Southern Alps increased as the grid interval decreased from 30 km to 15 km. At the same time the precipitation at low lying elevations and surrounding the mountain massif, decreased. **K6, k30,** and **k31,** however do not show this same trend of increasing peak precipitation at the expense of decreasing precipitation at lower elevations, in fact the area of the 10 mm contour almost doubles in size from the 15 km run to the 5 km run. The difference between the results presented in this section and Katzfey (1995a) could be due to the limitations of his DAR model: it was run in a hydrostatic mode and it lacked explicit microphysics.

The next question to be answered is: what is causing the significant differences in accumulated precipitation between **k6, k30**, and **k31** ? Examination of the **w**-component field reveals increases of 0.2-0.3 m s^{-1} over the steeper slopes between the 5 km and 10 km runs, and about 0.2 m s^{-1} for the 10 km over the 15 km run. It appears that the precipitation differences can be accounted for by the increase in slope steepness.

Hence one would expect model-generated precipitation to increase as the grid interval decreases, until some limit is reached. Poulos (1996) discusses the application of RAMS over steep terrain; the general criteria is that flow over steep slopes may be modeled properly if the terrain slope does not exceed 3-5 Δz across one Δx. This means that as steeper and steeper terrain is modeled, both the horizontal and vertical gird intervals have to be adjusted so that this criterion is not exceeded. This limits the size of the domain and increases the model run time.

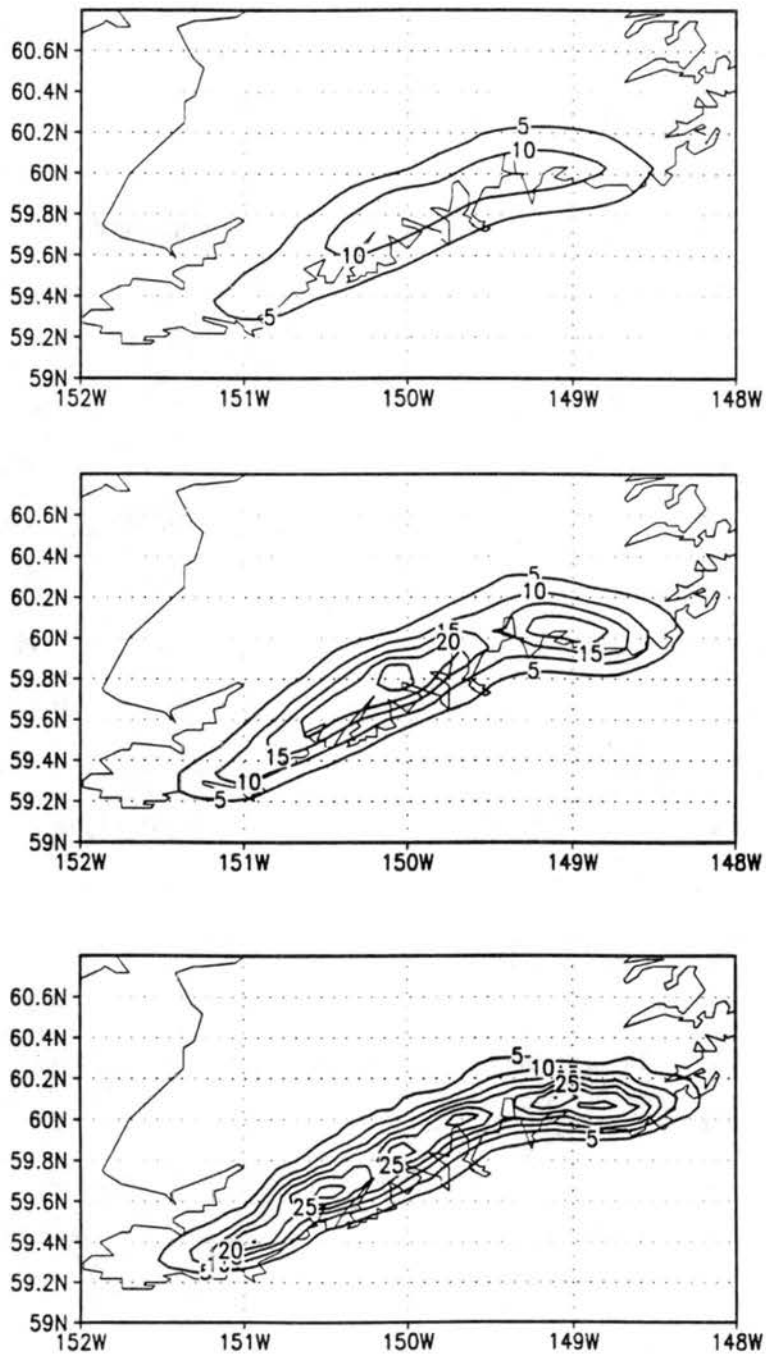

Figure 5.2: Zoom of total precipitation (contour interval of 5 mm) for: (top) 15 km (**k31**), (mid) 10 km (**k30**), (btm) 5 km (**k6**).

There has been no testing, up to this point in time, of RAMS sensitivity to slope steepness, especially in regards to the generation of precipitation. It is hypothesized that as the slopes increase well beyond 45°, that blocking, stagnation and flow reversal create a very complex and chaotic flow regime in proximity to that feature. The end result is that upstream flow is lifted earlier but at a decreased rate of ascent, which means that precipitation may be generated over a wider area but with decreased intensity.

It should be noted that the previously mentioned increase in precipitation in conjunction with a decreasing grid interval is restricted to areas with significant topographic variance. In other words there is nothing about flat terrain that would duplicate this process. In section 4.1, Du *et al* (1997) was noted for their work with an 80 km grid interval as well as a 40 km. Decreasing the grid interval from 80 km to 40 km over the central and eastern USA, does not increase the resolution of the terrain significantly, hence all else being equal, the 40 km run would only out perform the 80 km run if the model had been initialized with higher resolution (mesoscale) data or if the model is able to generate significant smaller scale precipitation features which can not be resolved with the 80 km grid interval. In other words, it has been demonstrated that a 80 km grid interval is adequate at resolving synoptic scale features, decreasing the grid interval is only cost effective if either the terrain resolution is increased substantially or if finer scale features are resolved.

Inspection of Figure 5.2 also shows that as the grid interval decreases the detail of the areal distribution increases. This increase in detail however, is still significantly less detailed than the topography itself. This is true in large part due to the advection of hydrometeors from their place of origin via the mean flow, and by the upstream/downstream influence that terrain has via blocking and gravity wave propagation. Examination of all of the simulations conducted in this study show that the areal distribution of precipitation is more of a function of the large scale topographic mass rather than individual peaks and valleys, at least for the topography of the Kenai Peninsula. This process appears to be a function of the atmospheric stability, as the lapse rate approaches its dry adiabatic value, the areal distribution of

precipitation shows increased variance (section 3.4). The question then arises: is it important for a mesoscale model to resolve fine-scale topographic features ?

Detailed observations of the areal distribution of precipitation in a mountainous environment are limited to a few cases, and it is not uncommon for two different sets of observations to show conflicting results. For example, using rainfall data collected in Southwest England, Pedgley (1970) suggested that airflow and precipitation did not closely follow the local topography, but rather the general shape of the mountain mass. Alpert and Shafir (1989), using a dense network of precipitation gages located over the Judean Hills of Israel, found a high correlation between small-scale topography and observed rainfall.

One thing we do know is that due to the interaction of thermodynamic and dynamic processes, the atmosphere becomes homogenized (the atmosphere shows less variance than the underlying terrain). This also applies to the precipitation process, where the simulations presented in this study indicate that when the atmosphere is very stable, the distribution of precipitation is a function of blocking, upslope flow, and gravity wave propagation and is not anchored to specific topographic features. When the atmosphere is unstable the mountains act as elevated heat sources that can trigger thermal convection, with the result that precipitation tends to be distributed in a semi-random fashion. It does appear that precipitation is the most closely anchored to the terrain when the atmospheric lapse rate is in the -5° C km^{-1} to -6° C km^{-1} range. We would then expect that fine-scale terrain features would be more important in this range of lapse rates.

In general, with all other factors being equal, the areal variance in precipitation should increase as the terrain resolution in a model increases, until some limit is reached at which any further increase in resolution is insignificant because of the homogenizing effect of the atmosphere. What that effective terrain resolution limit is, has not yet been established or fully explored.

Returning to the all important question of fine-scale topography, how important is it to a model run? Of course the answer to some degree depends on the intended application of the model output, but if we set that issue aside for the time being, there is some evidence to

suggest that the answer is scale independent. For example, if we consider a small hill that is 200 m high and place it on an otherwise flat landscape, we would probably expect that it will have a larger influence on the atmospheric flow and precipitation than if the same hill was positioned atop an already massive mountain. In the second case, the large mountain is already influencing the incoming flow in such a way that the additional influence of the 200 m peak is much smaller than the isolated hill.

A related question that is often discussed in mountain meteorology is why do valleys sometimes receive as much precipitation as the surrounding peaks and ridges and at other times much less? For a given mountain and valley configuration , there are a number of factors that should be considered:

1. Location of the valley with respect to the moisture source (coastal versus interior). The overall magnitude of precipitation whether it be on an event basis, seasonal or annual, depends on its distance from the moisture source(s).

2. Configuration of the surrounding terrain. If the terrain on the upstream side of a valley is significantly lower than the downstream terrain, then precipitation in the valley will tend to be larger than in the case when the upstream barrier is higher.

3. Orientation of the valley with respect to the flow. If the long axis of the valley is parallel to the flow, a limited amount of upslope flow may occur in the valley. Contrast this to flow over the shorter axis of the valley, where there is much less chance of any *in situ* upslope flow.

4. Width of the valley. Large intermontane valleys will tend to be drier in the sections that are adjacent to upstream barriers, and wetter in sections adjacent to downstream barriers. It should also be noted that in this types of large valleys, there may be local sources of moisture that could be essentially "recycled".

5. Depth of a valley is important because deep valleys tend to trap drier air, especially in the winter months. This means that hydrometeors falling through this dry air will experience enhanced evaporation or sublimation.

6. Atmospheric stability factors into this because the trapping of cooler air in a valley, as several modeling studies have demonstrated (Peterson *et al* 1991, Lee *et al* 1989), can alter the

"effective topography" that the incoming flow has to respond to.

Since these factors can change during an event or from one event to another, the amount of precipitation that is measured in a valley will also change to some degree.

The inclusion of fine-scale topography in a numerical model is a function of : 1) the intended application; 2) available computer resources, and; 3) the storm dynamics. Overall it appears that the topographic variance must be factored into this equation as well. In general then, for the particular topography of the Kenai Peninsula, grid intervals in the 2 km range are necessary for realistic terrain-atmospheric interaction.

5.2-Two Dimensional Simulations

This section further investigates the issue of terrain resolution and its effect on model generated precipitation. In this section, a 2D grid set-up is used to investigate the models response to grid intervals that range from 20 km down to 2 km, in increments of 2 km (Table 5.2).

The topographic profile selected was taken from a 2 km Kenai Peninsula terrain data set, and represents a typical north-south cross section. Elevations range from sea-level to 1688 m. Each of the subsequent terrain data files were constructed in such a fashion as to preserve the maximum height of the terrain. This has the effect that the slope angles are primarily a function of the grid interval, however, in some cases the slope angle changes less than 0.5° from one run to the next while in other runs it changes by as much as 2.7°.

The model set-up was similar to that used in the 3D cases described in earlier chapters. The top boundary was located at 14.6 km and, contained a five layer thick Rayleigh friction layer. A preliminary run was conducted to see the sensitivity of the 2D grid to a ten layer Rayleigh friction layer, but the results were identical to the five layer case. Despite being a 2D run, the Coriolis force was left on, which does influence the geostrophic winds (Meyers and Cotton 1992). The radiation and microphysics options were unchanged from the 3D cases.

Figure 5.3 shows a plot of **kp20-kp2**. Peak precipitation (after 6 hours of simulation time), was a maximum of 80 mm for **kp2** and 27 mm for **kp20**.

Table 5.2 2D Kenai Peninsula (kp) simulations				
run	max. precip (mm)	max. **W** ($m\ s^{-1}$)	max. slope (deg)	ave. slope (deg)
kp20	27	0.45	4.6	4.6
kp18	33	0.56	5.3	5.3
kp16	37	0.65	6.0	6.0
kp14	43	0.85	6.8	6.8
kp12	52	0.95	7.0	3.8
kp10	65	1.0	6.5	4.6
kp8	69	1.5	7.3	6.0
kp6	68	2.1	10.0	6.8
kp4	74	2.1	11.0	6.8
kp2	80	2.3	13.0	9.0

Table 5.2: Model configuration and precipitation for two-dimensional Kenai Peninsula runs. The number following **kp..** is the grid interval in kilometers. Max **W** is the maximum vertical velocity near the surface. The maximum slope (max.slope) is the steepest slope angle between any two grid points while the average slope (ave. slope) is calculate for the entire windward slope.

The plot is close to being linear but does not appear to reach any type of equilibrium value, as the grid intervals decrease. The volume of precipitation generated in these simulations however reveals quite a different picture than the peak precipitation, the volume for **kp20** is only about 5% less than **kp2.**

Analysis of the condensation and cloud mixing ratios for **kp20** and **kp2**, show that the primary areas of hydrometeor generation occur in a region that is some 500 to 1500 m above the terrain and directly over the steepest windward slope. When the terrain resolution is low, the model tends to shift updrafts, condensation, and hydrometeor formation, further upstream of the barrier, when compared to the cases where the terrain resolution is much higher.

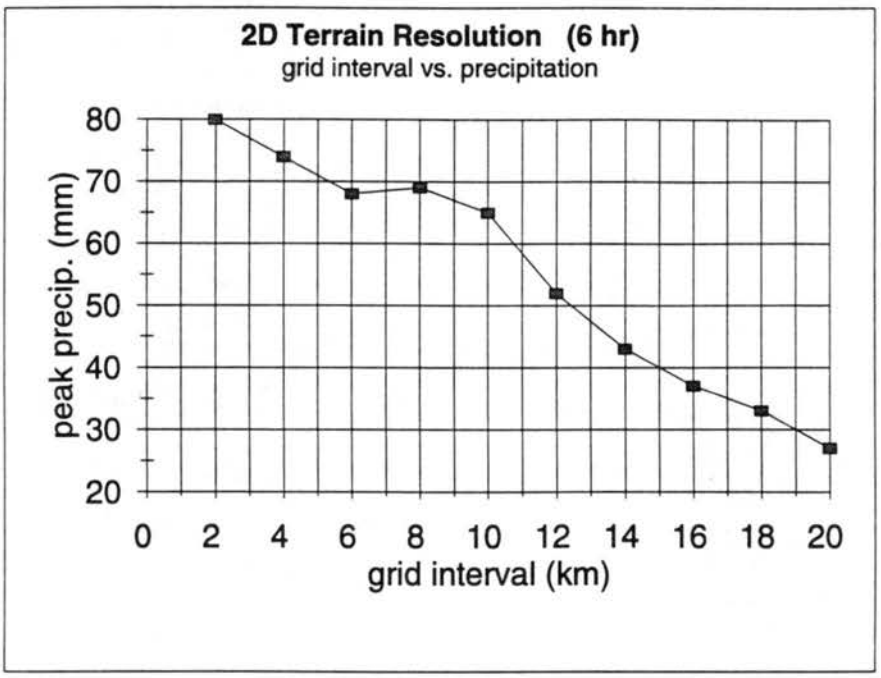

Figure 5.3: Maximum precipitation (mm) as a function of the grid interval (km) for **kp20-kp2**

The question we must then pose: are these results due to the change in grid interval or the change in slope angle? To facilitate an answer to this question, two more experiments are discussed: **Con1-4** uses an idealized mountain configuration with a constant slope, while the grid interval is allowed to change. In **ht1-5** the grid interval is fixed at 2 km and the mountain height changes from 1000 m to 3000 m in increments of 500 m.

5.3- Constant Slope Angle

The goal of this set of four simulations (**con1-4**), is to isolate the effect that a decrease in grid interval has on the amount of precipitation that the model generates. The model set-up is the same as in section 5.2, except the terrain is an idealized mountain with a height of 2000 m and a constant half-width, this fixes the slope at 11.3°. This slope angle is actually

quite steep if it is compared to most modeling studies that have investigated precipitation over a mountain environment (Richard *et al* 1987, Snook 1993, Thompson 1993, Katzfey 1995, Meyers 1995) however, it is considerably less steep than what one would encounter in nature. For comparison, slope angles for the mountains along the southern coastline of the Kenai Peninsula range from 20° to 30° in places. Another difference between these simulations and the **kp** runs is that a new sounding is used. In **con1-4** the surface temperature is set to 20° C and the atmosphere is saturated up to 6 km, the lapse rate is set to -5° C km^{-1}. What all this means is that the model produces copious amounts of precipitation, but since we are interested in the relative change in precipitation from one run to the next, this set-up will serve the purpose for which it is intended. This is an unrealistic moisture profile for just about any location, but the reason for this adjustment will be explained at the conclusion of this section. Table 5.3 lists the model results for grid intervals of 10, 5, 2, and 1 km.

Table 5.3 Constant Slope Simulations

run	grid interval (km)	max. precip. (mm)	volume precip.*
con1	10	140	1.0
con2	5	250	1.1
con3	2	282	1.1
con4	1	302	1.1

Table 5.3: Results of simulations **con1-4.** Where * indicates that the volume of precipitation has been normalized with the value from **con1**.

These results are similar to those discussed in the previous section. As the grid interval decreases, precipitation becomes more peaked over the mountain at the expense of precipitation at lower elevations. Inspection of the horizontal and vertical winds shows that a larger amount of blocking is occurring in **con1** than in **con4** , this creates stronger updrafts and of course the model produces more precipitation. These conclusions seem to be a result of model numerics and have no correspondence with any processes in the real atmosphere. This is to be expected in any model since the equations of motion are approximated on a finite-difference grid (or in a few cases on a finite-element grid). When the grid interval is large, disturbances (e.g.- blocking) propagate further upstream than in the runs where the grid interval is smaller. This results in a smoothing of the precipitation field. Are these results a consequence of the 2D nature of these simulations? The 3D simulations presented in section 5.1 did not indicate a decrease in precipitation at lower elevations as the grid interval decreased, however, in those simulations both the grid interval and the slope angles where varying. This is a topic that needs to be fully explored using high resolution 3D runs over steep terrain.

It was mentioned at the beginning of this section that the input sounding was changed so that the lower atmosphere was warmer and wetter than in the previous runs. The justification is that it was found that the vertical distribution of precipitation is as much a function of the actual temperature at given level as is the availability of moisture (Meyers and Cotton 1992). For example, if the upper slopes of a given mountain is near the freezing level, the precipitation gradient is much larger than if the freezing level is considerably higher than the top of the mountain. The explanation is that in the former case, mixed phase precipitation is occurring (e.g.- rain over the lower slopes and snow over the upper). Since snow (in a generic sense), has different properties than rain, especially when it comes to wind drift and temperature dependency, precipitation gradients are exaggerated if mixed phase precipitation occurs. Since the purpose of **con1-4** was to investigate grid interval dependency, while limiting other factors, the input sounding was changed to accommodate a freezing level that was well above the highest terrain.

5.4-Level of Maximum Precipitation

In this final series of simulations the objective was to consider any change in the level of maximum precipitation as a function of mountain height (**ht 1-5**), and the lapse rate (**ht 3 ,6 7**). These simulations differ from those presented in chapters 3 and 4 in that they are using a grid interval of 2 km in a two-dimensional configuration. In a strict sense the level of maximum precipitation could be divided into two categories: one for rain and the other for snow. Since the input sounding is quite warm, these simulations are limited to level of maximum rainfall.

As the height of the mountain increases from 1000 m to 3000 m by increments of 500m, for a grid interval fixed at 2 km, the level of maximum precipitation shifted one grid point upstream (to a lower elevation), in response to the increase in low-level blocking. This increase in blocking is to be expected since the Froude Number is a function of the inverse of the barrier height. As one would expect, the volume of precipitation increases some 6.6 times between a 1000 m and 3000 m high mountain.

In simulations where the lapse rate ranged from -5, -6 and -7° C km^{-1}, and the height of the mountain was held constant at 2000 m and the grid interval fixed at 2 km, the zone of maximum precipitation shifted one grid cell downstream, to a *higher* elevation. This was as a result of a 25% increase in the terrain updraft speed for the run using a lapse rate of -7° C km^{-1} compared to the -5° C km^{-1} run. This is in contrast to Alpert (1986), who suggested that as the lapse rate increases (surface temperature held constant), over a mountain of a fixed height, that the elevation at which precipitation is a maximum, *decreases* in response to a decrease in moisture. His analytical index model however, did not include the effects that the stability has on vertical velocities (section 3.4), which in some cases, more than compensates for the decrease in moisture at higher elevations.

With the current interest in global change, especially the apparent increase in surface temperatures at mid and high latitudes, it may be worth considering what effect a warmer and wetter boundary layer would have on precipitation in a region such as the Kenai Peninsula. If we just consider the orographic effect and neglect any change in position or intensity of

synoptic-scale features, then we would expect that lapse rates in the lowest 500 to 1000 m of the atmosphere would be slightly higher. In general we would expect an increase in precipitation at low and mid elevations over a windward slope, but whether that translates into increased precipitation over the upper slopes remains to be a question.

If the lapse rate above the boundary layer were to be increased then the additional moisture in the boundary layer has a greater chance of being distributed at higher elevations or advected to the interior of the mountain range. Miller (1963) found a 2.4° C rise in annual temperatures between the years of 1918 and 1953 for a number of coastal stations in Southeast Alaska. He assumed that this rise in surface temperatures could be extrapolated to elevations of around 1500 m, which he suggests were responsible for the shift in the level of maximum snowfall, of about 400 m over the Juneau Icefield. This is a topic that needs further work, but it holds considerable interest to hydrologists and glaciologists. The fundamental question that needs to be addressed is if sea-level temperatures rise, how do these effects translate to the middle atmosphere? There is probably a damping of this signal with height, but it would most likely have some type of influence at elevations under 2000 m.

Chapter 6

SUMMARY AND CONCLUSIONS

6.1-Summary

Kenai 5 produced heavy precipitation over the mountains along the southern coastline, but generated about one-half to one-third of the observed precipitation to the lee of this barrier. This was attributed to either the low resolution of the input data or to the model not generating smaller-scale features. At low elevations, the correlation between observations and model precipitation was moderately high. Unfortunately, there is little observed data at higher elevations to verify the model against, although the values produced seemed reasonable.

The uncertainty in initial conditions necessitates testing the models sensitivity to perturbed state variable such as temperature, wind speed and direction, as well as moisture. **Kenai 6** represented a wind speed increase of 4 m s^{-1}, which caused minimal increase in precipitation at lower elevations, but increased precipitation by 15-20% over the upper slopes. A third variable initialization run (**kenai 7**), was set-up in order to test the models sensitivity to sea surface temperatures as well as vegetation classification. The results indicated that these variables, with the given perturbations, played only a minor role in either the generation or distribution of precipitation. This result was not unexpected since this storm was dominated by large-scale moisture advection and strong flow into the southern coast of the Kenai Peninsula.

It was also shown that a maritime mountain range exhibits three distinct zones of orographic influence when the atmosphere is stable. The first zone is located upstream of the barrier where blocking generates low-level lifting which enhances condensation, in essence pre-conditioning the flow before it is forced up over the barrier. This upstream lifting can also

trigger potential instability or any other type of convective instability.

Zone two lies over the windward slopes of the barrier and extends to roughly the barrier crest. In this zone terrain forced updrafts are strongest above the steeper slopes, which are co-located with areas of precipitation generation. This zone is also the source of downstream propagating gravity waves. Zone three extends from the barrier crest to tens of kilometers downstream. Downsloping winds create the classic rain shadow effect of reduced precipitation. In general, what precipitation does fall out in this zone is primarily advected from zone two. In other words, the areal distribution of the precipitation in this third zone is often detached from the local terrain.

There are a number of exceptions to this conceptual model, namely if the windward barrier is not high enough to force the bulk of the available water vapor to condense, then the mean flow carries the supplemental water vapor to the next barrier where if local updrafts are significant enough to generate moisture convergence, hydrometeors are produced. Another example is if a broad valley is oriented parallel to the inflow, it is not uncommon for moisture to be advected a considerable distance up the valley before condensation occurs.

In Chapter 3 a series of experiments demonstrated the sensitivity of model-generated precipitation to the initial values of wind speed, wind direction, moisture, and atmospheric stability. Since it is not possible to determine the size of the uncertainty in observed fields in remote, data sparse locations, such as the Kenai Peninsula, intuition has to be used. In general, the model generated precipitation is quite sensitive to reasonably sized perturbations of the initial fields. These results show the non-linear nature of orographic precipitation, the coupling of dynamics, thermodynamics and microphysical processes.

There was an attempt to clarify the role which potential instability plays in the production of precipitation in extra-tropical maritime mountain ranges. The results were not conclusive but show that precipitation was reduced in a run that was more potential unstable than the control run. This does not mean that the release of some type of instability upstream of the barrier is not important in the orographic precipitation process, but since the stability is also altered, the dynamic response of flow forced upward as it crosses the barrier may be

weaker, creating a situation where precipitation is either reduced or the areal distribution is shifted. This is a topic that requires further investigation.

Factor separation was used to study the interaction among two state variables. In the first experiment it was shown that the response in terms of model-generated precipitation for a given wind speed perturbation is dependent on the lapse rate at which the perturbation is introduced. In the second experiment, wind speed and moisture fields were examined. When these perturbations were introduced separately, the total volume of precipitation increased. When combined however, these two perturbations indicated a slightly negative interaction. It was suggested that this result was due to the interaction of the dynamic forcing with thermodynamic constraints via latent heating effects.

In chapter 4 the concept of ensemble QPF forecasting was introduced. Since the precipitation process is the most complex of atmospheric phenomena, it is not surprising that reasonably small perturbations in initial conditions lead to a large dispersion in model precipitation. This means that some type of ensemble forecast is necessary. In circumstances where computer resources are limited, a modified ensemble may be a viable alternative to a 10+ member ensemble. For example, if the best analysis is used as a control run, two additional runs could be conducted using extreme perturbations. These extreme perturbations would be constructed based on detailed historical analyses of surface and rawinsonde data.

A detailed examination of the Resurrection River Basin revealed the poor relationship between precipitation and elevation alone. However, if the distance from the coast is included in this regression equation, a larger part of the variance is explained.

The selection of a horizontal grid interval is important because it determines how realistic the terrain is resolved. A series of 3D simulations using the terrain of the Kenai Peninsula, indicated that precipitation increased significantly when the grid interval decreased. Several follow-up simulations using 2D configurations also showed an increase in precipitation as Δx decreased. These effects were attributed to both the decrease in grid interval and the subsequent increase in slope angles. The general trend is for the volume of precipitation in these 2D simulations to be fairly constant as the grid interval decreases, but the distribution of

precipitation tends to peak over the steep windward slopes at the expense of precipitation upstream of the barrier. There is an indication that this trend starts to asymptotically reach a limit, for grid intervals in the one to two kilometer range.

It was also demonstrated that the distribution of precipitation is as much a function of the terrain configuration as the lapse rate. The zone of maximum precipitation is determined not only by the thermodynamic constraint of moisture availability but also by the dynamic response of air flow over the terrain (vertical motion). The height of any given mountain in relation to the freezing level also helps determine the distribution of precipitation.

6.2- Future Research

This study has attempted to answer a number of questions, in doing so it has generated some new questions, or it has been unable to satisfactorily answer some of the original questions. Areas of future research may include:

1. The upstream release of convective instabilities, how important is it in the distribution of precipitation over a mountain barrier? Is it less efficient in the generation of precipitation than classic upslope processes?

2. Considerable work in the future will involve QPF ensemble forecasting. The questions to be answered are: a) how to produce perturbations over mountainous regions where there is little historical or real-time data; b) what are the minimum number of ensemble members that can be used, and how is this a function of terrain resolution. It seems reasonable to assume that as the terrain resolution increases, the number of ensemble members needs to increase as the model becomes more sensitive to atmosphere-terrain interactions; c) Is a limited member ensemble forecast based on extreme perturbations feasible and will it show any utility?

3. Since mesoscale models have adjustable grids by definition, then the issue of what are appropriate grid intervals should be used when modeling precipitation over complex terrain is

a major consideration. a) should the grid interval be a function of the topographic variance? b) there is a need for some high resolution 3D simulations using grid intervals of 1-5 km over complex terrain, compare these new results to those presented in chapter 5.

4. Since observations of precipitation at higher elevations are lacking and will continue to be a problem, it is of some value to use high resolution numerical simulations to establish some type of relationships between observed precipitation at lower elevations and what is occurring at higher elevations (Gaudet and Cotton, in press 1998).

5. The results presented in this study have concentrated on warm season precipitation, how do they change for winter simulations? What role does wind drift and sublimation play in the distribution of snow over a mountainous region?

REFERENCES

Abbs, D. J., R. A. Pielke. 1987: Numerical simulations of orographic effects on NE Colorado snowstorms. *Meteorol. Atmos. Phys.* **37** 1-10

Ageta, Y. 1976: Characteristics of precipitation during monsoon season in Khumbu Himal. *Seppyo* 84-88

Alpert, P., 1986: Mesoscale indexing of the distribution of orographic precipitation over high mountains. *Jr. Clim. Appl. Met.* **25** 532-545

Alpert, P., H. Shafir. 1989: Mesoγ-scale distribution of orographic precipitation: numerical study and comparison with precipitation derived from radar measurements. *Jr. Appl. Met.* **28** 1105-1117

Alpert, P., H. Shafir. 1991: Role of detailed wind-topography interaction in orographic rainfall. *Q. J. Roy. Met. Soc.* **117** 421-426

Alpert, P., S. O. Krichak, T. N. Krishnamurti, U. Stein, M. Tsidulko. 1996: The relative roles of lateral boundaries, initial conditions, and topography in mesoscale simulations of lee cyclogenesis. *Jr. Appl. Met.* **35** 1091-1099

Bader, D. C. 1985: Mesoscale Boundary layer development over mountainous terrain. *Ph.D Dissertation. Dept. Atmos. Sci., Colorado St. Univ., Paper no.*396. 251pp

Bader, D. C., T. B. Mckee. 1992: Mesoscale boundary-layer evolution over complex terrain. Part II: factors controlling nocturnal boundary-layer structure. *Mon. Wea. Rev.* Vol.**120** No.**5** 802-815

Baines, P. G., K. P. Hoinka. 1985: Stratified flow over two-dimensional topography in fluid of infinite depth: a laboratory simulation. *Jr. Atmos. Sci.* Vol.**42** No.**15** 1614-1630

Banta, R. M. 1990: The role of mountain flows in making clouds. In *Atmospheric Processes Over Complex Terrain.* Ed- W. Blumen. American Met. Soc. Vol.**23** No.**45** Chapter 9 229-283

Barros, A. P., D. P. Lettenmaier. 1993: Dynamic modeling of the spatial distribution of precipitation in remote mountainous areas. *Mon. Wea. Rev.* **121** 1195-1214

Barry, R. G. 1992: *Mountain Weather and Climate.* 2nd edition. Routledge, London 402pp

Bergeron, T. 1965: On the low-level redistribution of atmospheric water caused by orography. *Suppl. Proc. Int. Conf. on Cloud Physics.* Tokyo and Sapporo. 96-100

Bradley, M. M., 1985: The numerical simulation of orographic storms. *Ph.D Dissertation. Univ. Illinois, Urbana-Champaign.* 261pp

Bonacina, L. C. W. 1945: Orographic rainfall and its place in the hydrology of the globe. *Q. J. Roy. Met. Soc.* **71** 41-55

Brooks, H. E., M. S. Tracton, D. J. Stensrud, G. DiMego, Z. Toth. 1995: Short-range ensemble forecasting: report from a workshop, 25-27 July 1994. *Bull. Am. Met. Soc.* Vol.**76** No.**9** 1617-1624

Browning, K. A., F. F. Hill., and C. W. Pardoe, 1974: Structure and mechanism of precipitation and the effect of orography in a wintertime warm sector. *Q. J. Roy. Met. Soc.* **100** 309-330

Browning, K. A., 1980: Structure, mechanism and prediction of orographically enhanced rain in Britain. In *Orographic Effects In Planetary Flows.* Global Atmos. Research Program. World Met. Org. No.**23** Chapter three.

Bruintjes, R. T., T. L. Clark, W. D. Hall. 1994: Interactions between topographic airflow and cloud/precipitation development during the passage of a winter storm in Arizona. *Jr. Atmos. Sci.* Vol.**51** No.**1** 48-67

Carruthers, D. J., T. W. Choularton. 1983: A model of the feeder-seeder mechanism of orographic rain including stratification and wind-drift effects. *Q. J. Roy. Met. Soc.* ***109*** *575-588*

Carruthers, D. J., J.C.R. Hunt. 1990: Fluid mechanics of airflow over hills: turbulence, fluxes and waves in the boundary layer. In *Atmosphereic Processes Over Complex Terrain.* Ed. W. Blumen. A.M.S. Vol. **23** No.**45** Chapter five.

Chein, F-C., C. F. Mass. 1997 Interaction of a warm-season frontal system with the coastal mountains of the Western United States. Part II: Evolution of a Puget Sound convergence zone. *Mon. Wea. Rev.* Vol.**125** No.**8** 1730-1752

Clark, T. L., W. R. Peltier. 1977: On the evolution and stability of finite-amplitude mountain waves. *Jr. Atmos. Sci.* **34** 1715-1730

Colton, D. E. 1976: Numerical simulation of the orographically induced precipitation distribution for use in a hydrologic analysis. *Jr. Appl. Met.* Vol.**15** No.**12** 1241-1251

Cotton, W. R., R. A. Anthes. 1989: *Storm and Cloud Dynamics*. Academic Press 870pp

Cram, J. M. 1990: Numerical simulation and analysis of the propagation of a prefrontal squall line. *Ph.D Dissertation. Dept. Atmos. Sci., Colorado St. Univ., Paper no.*471. pp.332

Davies, H.C. 1976: A lateral boundary formulation for multi-level prediction models. *Q. J. Roy. Met. Soc.* **102** 405-418

Dore, A. J., T. W. Choularton, D. Fowler, R. Storton-West. 1990: Field measurements of wet deposition in an extended region of complex topography. *Q. J. Roy. Met. Soc.* **116** 1193-1212

Dore, A. J., T. W. Choularton. 1992: A three-dimensional model of airflow and orographic rainfall enhancement. *Q. J. Roy. Met. Soc.* **118** 1041-1056

Dore, A. J., T. W. Choularton, R. Brown, R. M. Blackall. 1992: Orographic rainfall enhancement in the mountains of the Lake District and Snowdonia. *Atmos. Environ.* Vol.**26A** No.**3** 357-371

Douglas, C. K. M., J. Glasspoole. 1947: Heavy orographic rainfall in the British Isles. *Q. J. Roy. Met. Soc.* **73** 11-42

Du, J., S. L. Mullen, F. Sanders. 1997: Short-range ensemble forecasting of quantitative precipitation. *Mon. Wea. Rev.* **125** 2427-2459

Durran, D. R. 1986: Moutain waves. In *Mesoscale Meteorology and Forecasting*. Ed- P. S. Ray. American Met. Soc. Chapter 20

Durran. D. R. 1990: Mountain waves and downslope winds. In *Atmospheric Processes over Complex Terrain.* Ed- W. Blumen. American Met. Soc. Vol.**23** No.**45** Chapter 4

Elliott, R. D., R. W. Shaffer. 1962: The development of quantitative relationships between orographic precipitation and air-mass parameters for use in forecasting and cloud seeding evaluation. *Jr. Appl. Met.* **1** 218-228

Epstein, E.S. 1969: Stochastic dynamic prediction. *Tellus* **21** 739-759

Flood Report- ARNWS 1996: South Central Alaska Floods. September 19-October 2, 1995. National Weather Service, Alaska Region. Anchorage

Gaudet, B., W.R. Cotton. 1998: Statistical characteristics of a real-time precipitation forecasting model. submitted to: *Wea & Forecasting*

Georgelin, M., E. Richard, M. Petitdidier, A. Druilhet. 1994: Impact of subgrid-scale orography parameterization on the simulation of orographic flows. *Mon. Wea. Rev.* **122** 1509-1522

Hamill, T. M., S. J. Colucci 1997: Verification of ETA-RSM short-range ensemble forecast. *Mon. Wea. Rev.* **125** 1312-1327

Hantel, M., E. Reimer, P. Speth. 1984: ALPEX-diagnostics: quantitative synoptic over Europe. *Beitr. Phys. Atmos.* **57** 477-494

Henderson, R. D. 1993: Extreme storm rainfalls in the Southern Alps, New Zealand. In *Extreme Hydrologic Events: Precipitation, Floods and Droughts.* IAHS **213** 113-120

Hill, F. F., K. A. Browning, M. J. Bader, 1981: Radar and raingauge observations of orographic rain over south Wales. *Q. J. Roy. Met. Soc.* **107** 643-670

Higuchi, K., Y. Ageta, T. Yasunari, J. Inoue. 1982: Characteristics of precipitation during the monsoon season in high-mountain areas of the Nepal Himalaya. In *Hydological Aspects of Alpine and High Mountain Areas.* IAHS **138** 21-30

Hjermstad, L. M. 1970: The influence of meteorological parameters on the distribution of precipitation across central Colorado mountains. *Dept. Atmos. Sci., Colorado St. Univ. paper no.163* 71pp

Hobbs, P. V., R. Houze Jr., T. Matejka. 1975: The dynamical and microphysical structure of an occluded frontal system and its modification by orography. *Jr. Atmos. Sci.* **32** 1542-1562

Houghton, J. G. 1979: A model for orographic precipitation in the north Central Basin. *Mon. Wea. Rev.* **107** 1462-1475

Houtekamer, P. L., L. Lefaivre. 1997: Using ensemble forecasts for model validation. *Mon. Wea. Rev.* **125** 2416-2426

Kalnay, E., S.M.Tracton. 1993: Operational ensemble prediction at the National Meteorological Center: practical aspects. *Wea & Forecasting* Vol.**8** No.**3** 379-398

Katzfey, J. J. 1995a: Simulation of extreme precipitation events. Part I: sensitivity to orography and resolution. *Mon. Wea. Rev.* **123** 737-754

---------- 1995b: Simulation of extreme precipitation events. Part II: mechanisms of precipitation development. *Mon. Wea. Rev.* **123** 755-775

Klemp, J. B., D. K. Lilly. 1978: Numerical simulation of hydrostatic mountain waves. *Jr. Atmos. Sci.* **35** 78-107

Lee, T. J., R. A. Pielke, R. C. Kessler, J. Weaver. 1989: Influence of cold pools dowstream of mountain barriers on downslope winds and flushing. *Mon. Wea. Rev.* Vol.**117** No.**9** 2041-2058

Lorenz,E.N., 1965: A stduy of the predictability of a 28 variable atmosphere model. *Tellus* **17** 321-333

---------- 1969: The predictability of a flow which possesses many scales of motion. *Tellus* Vol.**21** No.**3** 289-307

Long, R. R. 1953: Some aspects of the flow of stratified fluids. Part I: a theoretical investigation. *Tellus* **5** 42-58

Mahrer, Y. R.A. Pielke. 1976: Numerical simulation of the air flow over Barbados. *Mon. Wea. Rev.* **104** 1392-1402

Marcus, M. G., R. H. Ragle. 1970: Snow accumulation in the Icefield Ranges, St. Elias Mountains. *Arct. Alp. Res.* **2** 277-292

Marwitz, J. D. 1980: Winter stroms over the San Juan Mountains. Part I: dynamical processes. *Jr. Appl. Met.* **19** 913-926

Mayr, G. J., T. B. Mckee. 1995: Observations of the evolution of orogenic blocking. *Mon. Wea. Rev.* **123** 1447-1464

Meyers, M. P. 1995: The impact of a two-moment cloud model on the microphysical structure of two precipitation events. *Ph.D Dissertation. Dept. Atmos. Sci. Colo. St. Univ.* paper no.575 165pp

Meyers, M. P., W. R. Cotton. 1992: Evaluation of the potential for Wintertime quantitative precipitation forecasting over mountainous terrain with an explicit cloud model. Part I: two dimensonal sensitivity experiments. *Jr. Appl. Met.* Vol.**31** No.**1** 26-50

Miller, M. M. 1963: *Tako Glacier Evaluation Study.* State of Alaska Deptartment of Highways. 200pp

Mullen,S.L., D.P.Baumhefner. 1989: The impact of initial condition uncertainty on numerical simulations of large-scale explosive cyclogenesis. *Mon. Wea. Rev* **117** 2800-2821

---------- 1994: Monte Carlo simulaitons of explosive cyclogenesis. *Mon. Wea. Rev.* **122** 1548-1567

Mureau, R., F. Molteni, and T. N. Palmer, 1993: Ensemble prediction using dynamically conditioned perturbations. *Q. J. Roy. Met. Soc.* **119** 299-323

Nickerson, E. C., E. Richard, R. Rossert, D. R. Smith. 1986: The numerical simulation of clouds, rain, and airflow over the Vosges and Black Forest mountains: A meso-β model with parameterized microphysics. *Mon. Wea. Rev.* **114** 398-414

Olafsson, H., P. Bougeault. 1996: Nonlinear flow past an elliptic mountain ridge. *Jr. Atmos. Sci.* Vol.**53** No.**17** 2465-2489

Parish, T. 1982: Barrier winds along the Sierra Nevada Mountains. *Jr. Appl. Meteor.* **21** 925-930

Parsons, D. B., P. V. Hobbs. 1983: The mesoscale and microscale structure and organization of clouds and precipitation in midlatitude cyclones: IX: some effects of orography on rainbands. *Jr. Atmos. Sci.* **40** 1930-1949

Passarelli Jr., R. E., H. Boehme. 1983: The orographic modulation of pre-warm front precipitation in southern New England. *Mon. Wea. Rev.* **111** 1062-1070

Pedgley, D. E. 1970: Heavy rainfalls over Snowdonia. *Weatherwise* **25** 340-350

Peterson,T. C., L. O. Grant, W. R. Cotton, D. C. Rogers. 1991: The effect of decoupled low-level flow on Winter orographic clouds and precipitation in the Yampa River Valley. *Jr. Appl. Met.* **30** 368-386

Pielke, R. A., 1984: *Mesoscale Modeling*. Academic Press, San Diego

Pierrehumbert, R. T. 1984: Linear results on the barrier effects of mesoscale mountains. *Jr. Atmos. Sci.* **41** 1356-1367

Pierrehumbert, R. T., B. Wyman. 1985: Upstream effects of mesoscale mountains. *Jr. Atmos. Sci.* Vol.**42** No.**10** 977-1003

Poulos, G. S. 1996: The interaction of katabatic winds and mountain waves. *Ph.D Dissertation. Dept. Atmos. Sci., Colorado St. Univ., Paper no.631* 299pp

Rauber, R. M. 1992: Microphysical structure and evolution of a central Sierra Nevada orographic cloud system. *Jr. Appl. Met.* **31** 3-24

Rhea, J. O. 1978: Orographic precipitation model for hydrometeorological use. *Ph.D Dissertation. Dept. Atmos. Sci., Colorado St. Univ., Paper no.*287 pp.198

Richard, E., N. Chaumerliac, J. F. Mahfouf. 1987: Numerical simulation of orographic enhancement of rain with a mesoscale model. *Jr. Clim. Appl. Met.* Vol.**26** No.**6** 661-669

Robichaud, A. J., G. L. Austin. 1988: On the modeling of warm orographic rain by the seeder-feeder mechanism. *Q. J. roy. Met. Soc.* **114** 967-988

Romero, R., C. Ramis, S. Alonso. 1997: Numerical simulation of an extreme rainfall event in Catalonia: role of orogrpahy and evaporation from the sea. *Q. J. Roy. Met. Soc.* Vol.**123** No.**539** 537-559

Sarker, R. P. 1966: A dynamical model of orographic rainfall. *Mon. Wea. Rev.* **94** 555-572

Sawyer, J. S. 1956: The physical and dynamical problems of orographic rain. *Weather* **11** 375-381

Schwartz, B. E., C. A. Doswell III., 1991: North American rawinsonde observations: problems, concerns, and a call to action. *Bull. Am. Met. Soc.* Vol. **72** No.**12** 1885-1896

Schwerdtfeger, T. 1975: The effect of the Antarctic Peninsula on the temperature regime of the Weddell Sea. *Mon. Wea. Rev.* **103** 45-51

Scorer, R. S. 1949: Theory of wves in the lee of mountains. *Q. J. Roy. Met. Soc.* **79** 41-56

---------- 1953: Theory of airflow over mountains. II: the flow over a ridge. *Q. J. Roy. Met. Soc.* **79** 70-85

Sinclair, M. R. 1994: A diagnostic model for estimating orographic precipitation. *Jr. Appl. Met.* **33** 1163-1175

Smagorinsky, J. 1963: General circulation experiments with the primitive equations. I: the basic experiment. *Mon. Wea. Rev.* **91** 99-164

Smith, R. B. 1979: The influence of mountains on the atmosphere. In *Advances In Geophysics.* Ed- B. Saltzman. **21** Academic Press, San Diego 87-230

Smith, R. B. 1982: A differential advection model of orographic rain. *Mon. Wea. Rev.* **110** pp.306-309

Smith, R. B. 1989a: Mechansims of orographic precipitation. *Meteor. Mag.* **118** 85-88

Smith, R. B. 1989b: Hydrostatic airflow over mountains. In *Advances in Geophysics.* **31** Academic Press 1-41

Smith, R. B. 1990: Why Can't stably stratified air rise over high ground ? In *Atmospheric Processes Over Complex Terrain.* Ed- W. Blumen. Amer. Met. Soc. Vol.**23** No.**45** Appendix to Chapter 5 105-107

Smolarkiewicz, P. K., R. Rotunno. 1990: Low Froude number flow past a three-dimensional obstacle. Part II: upwind flow reversal zone. *Jr. Atmos. Sci.* Vol.**47** No.**12** 1498-1511

Snook, J. S. 1993: An investigation of Colrado Front Range winter storms using a nonhydrostatic mesoscale numerical model designed for operatonal use. *Ph.D. Dissertation. Dept. Atmos. Sci., Colorado St. Univ., Paper no.*541 373pp

Stein, U., P. Alpert. 1993: Factor separation in numerical simulations. *Jr. Atmos. Sci.* Vol.**50** No.**14** 2107-2115

Strensrud, D. J., J. M. Fritsch. 1994a: Mesoscale convective systems in weakly forced large-scale environments. Part II: generation of a mesoscale initial condition. *Mon. Wea. Rev.* **122** 2068-2083

---------- 1994b: Mesoscale convective systems in weakly forced large-scale environments. Part III: numerical simulations and implications for operational forecasting. *Mon. Wea. Rev.* **122** 2084-2104

Thompson, G. 1993: Prototype real-time mesoscale prediction during 1991-1992 winter season and statistical verification of model data. *M.S. Thesis. Dept. Atmos. Sci., Colorado St. Univ., Paper no.*521. 105pp

Toth,Z., E. Kalnay., 1993: Ensemble forecasting at NMC: the generation of perturbations. *Bull. Am. Met. Soc.,* **74** 2317-2330

Toth, Z., E. Kalnay., S. M. Tracton., R. Wobus., and J. Irwin, 1997: A synoptic evaluation of NCEP ensemble. *Wea. Forecasting.,* **12** 140-153

Tracton, M. S., E. Kalnay. 1993: Operational ensemble prediction at the national meteorological center: practical aspects. *Wea. Forecasting.* **8** 379-398

Tremback, C. J. 1990: Numerical simulation of a mesoscale convective complex: model development and numerical results. *Ph.D. Dissertation, Colorado State University.* 247pp

Tremback, C. J., R.Kessler. 1985: A surface temperature and moisture parameterization for use in mesoscale numerical models. *Seventh conference on numerical weather prediction.* Montreal, Canada. Am. Met. Soc. 355-358

Walko, R.L., W.R.Cotton, M.P.Meyers, J.Y.Harrington 1995: New RAMS cloud microsphysics parameterization, Part I: the single-moment scheme. *Atmos. Research.* **38** 29-62

Wesley, D. A. 1991: An investigation of the effects of topography on Colorado Front Range winter storms. *Ph.D. Dissertation. Dept. Atmos. Sci., Colorado St. Univ., Paper no.*489 197pp

Wratt, D. S., R. N. Ridley, M. R. Sinclair, H. Larsen, S. M. Thompson, R. Henderson, G. L. Austin, S. G. Bradley, A. Auer, A. P. Struman, I. Owens, B. Fitzharris, B. F. Ryan, and J. F. Gayet. 1996: The New Zealand Southern Alps Experiment. *Bull. Am. Met. Soc.* Vol.**77** No.**4** 683-692

Young, G. S., R. A. Pielke. 1983: Application of terrain height variance spectra to mesoscale modeling. *Jr. Atmos. Sci.* **40** 2555-2560